Aalto University
School of Chemical
Technology

School of Chemical Technology

Degree Programme of Forest Products Technology

Risto Koivunen

INKJET-PRINTED HYDROPHOBIC PATTERNING OF POROUS SUBSTRATES FOR MICROFLUIDIC APPLICATIONS

Master's thesis for the degree of Master of Science in Technology submitted for inspection, Espoo, 16 April, 2014.

Supervisor **Professor Patrick Gane**

Instructor **M.Sc. Eveliina Jutila**

Aalto University
School of Chemical
Technology

Aalto University, P.O. BOX 11000, 00076 AALTO
www.aalto.fi

Abstract of master's thesis

Author Risto Koivunen

Title of thesis Inkjet-printed Hydrophobic Patterning of Porous Substrates for Microfluidic Applications

Department Department of Forest Products Technology

Professorship Paper and Printing Technology **Code of professorship** Puu-21

Thesis supervisor Prof. Patrick Gane

Thesis advisor M.Sc. Eveliina Jutila

Date 16.4.2014 **Number of pages** 184+17 **Language** English

Abstract

Paperfluidic devices are microfluidic devices patterned out of paper or other highly porous material. Liquid transport in paperfluidic devices is propelled either by surface wetting or interior capillary wicking. The direction of aqueous liquid flow on such devices is controlled by selective patterning of hydrophobic barriers on an otherwise hydrophilic base substrate. A variety of hydrophobic materials and printing methods have been lately demonstrated as feasible for producing such patterns. Unlike conventional graphic printing, hydrophobising ink has to penetrate the whole depth of the wicking substrate, in order to produce properly functioning leak-free barriers.

One major expected application area for paperfluidics in the future is in the field of lab-on-a-chip devices, intended to provide simple, transportable, disposable and self-sufficient analysis tools for medical diagnostics and environmental monitoring. On such devices, fluid samples flow along hydrophilic channels through assay zones, where they chemically interact with pre-applied reagents.

This study focused on the development of simple solvent-based hydrophobic inks for inkjet printing of microfluidic patterning on paper substrates. Hydrophobic inks were produced by dissolving alkyl ketene dimer (AKD), paraffin wax and low molecular weight polystyrene in p-xylene. Hydrophobic test patterns were created by inkjet printing these inks on two highly porous filter papers.

AKD ink was found to produce effective hydrophobic barriers but with poorly defined borders. Polystyrene ink produced well defined borders, but could only penetrate the full depth of the substrate on one paper. Channels 680 ± 80 µm wide and barriers 883 ± 91 µm wide could be produced with it. Adding polystyrene as a rheological modifier to AKD ink improved jetting frequency. Paraffin wax could not be dissolved in sufficient amounts to produce proper barriers.

Hydrophobic ink penetration into filter paper was found to take place as film flow rather than through complete filling of pores. Paper properties and ink viscosity were considered to play a role in providing ink with a quick access to the reverse side. Differences in border definition might be due to the well-known coffee stain effect and different interaction with the cellulose fibre surfaces.

Keywords Inkjet printing, Functional printing, Hydrophobic ink, Polystyrene, Alkyl ketene dimer, Microfluidics, Paperfluidics

Aalto-yliopisto
Kemian tekniikan korkeakoulu

Aalto-yliopisto, PL 11000, 00076 AALTO
www.aalto.fi

Diplomityön tiivistelmä

Tekijä Risto Koivunen		
Työn nimi Huokoisten materiaalien hydrofobinen kuviointi mustesuihkutulostuksella mikrofluidistisia sovelluksia varten		
Laitos Puunjalostustekniikan laitos		
Professuuri Paperi- ja painatustekniikka		**Professuurikoodi** Puu-21
Työn valvoja Prof. Patrick Gane		
Työn ohjaaja DI Eveliina Jutila		
Päivämäärä 16.4.2014	**Sivumäärä** 184+17	**Kieli** Englanti

Tiivistelmä

Paperifluidiset laitteet ovat mikrofluidisia laitteita, jotka muodostetaan hydrofobisesti kuvioimalla paperia tai muuta huokoista materiaalia. Tällaisissa laitteissa vesi virtaa spontaanisti pintajännityksen ja kapillaaripaineen vaikutuksesta samalla kun hydrofobiset seinämät ohjaavat virtausta hydrofiilisia kanavia pitkin. Virtauskuvioita voidaan valmistaa olemassa olevilla painatusmenetelmillä käyttämällä hydrofobista materiaalia sisältäviä musteita. Toisin kuin perinteisessä graafisessa painatuksessa, hydrofobisia virtauskuvioita valmistettaessa musteen täytyy tunkeutua paperiin koko sen syvyydeltä muodostaakseen toimivia seinämiä.

Tulevaisuudessa paperifluidistiikan odotetaan tarjoavan alustan yksinkertaisille, helposti kuljetettaville ja kertakäyttöisille testilaitteille muun muassa lääketieteellisessä diagnostiikassa ja ympäristön laadun tarkkailussa. Tällaisissa laitteissa nestemäiset näytteet virtaavat hydrofiilisia kanavia pitkin testialueille, joissa ne reagoivat valmistusvaiheessa lisättyjen kemikaalien kanssa.

Tässä tutkimuksessa keskityttiin tutkimaan yksinkertaisten liuotinpohjaisten mustesuihkumusteiden käyttöä virtauskuvioiden muodostamiseen paperille. Hydrofobiset musteet valmistettiin liuottamalla alkyyliketeenidimeeriä (AKD), parafiinia ja pienimolekyylimassaista polystyreenia p-ksyleeniin. Virtauskuviot muodostettiin tulostamalla musteita kahdelle eri suodatinpaperille.

AKD-pohjainen muste muodosti tehokkaita hydrofobisia esteitä, tosin esteiden reuna-alueet olivat epätarkkoja. Polystyreeni-pohjainen muste muodosti tarkkarajaisia kuvioita, mutta tunkeutui riittävästi paperin läpi vain toisella testatulla paperilla. Sillä voitiin kuitenkin valmistaa 680 ± 80 µm leveitä kanavia ja 883 ± 91 µm leveitä hydrofobisia seinämiä. Lisäksi pienen polystyreenimäärän lisääminen AKD-pohjaiseen musteeseen paransi syntyneen musteen tulostustaajuutta. Parafiini ei liuennut riittävissä määrin muodostaakseen tehokkaita esteitä paperille.

Hydrofobisten musteiden tunkeutuminen paperiin tapahtui pääasiallisesti pintavirtauksena kuitujen pintoja pitkin, näiden välisten huokosten täyttymisen sijaan. Paperin ominaisuudet ja musteen viskositeetti olivat merkittävässä osassa musteen tunkeutumissyvyyden kannalta. Erot hydrofobisten kuvioiden reuna-alueiden tarkkuudessa saattavat johtua hyvin tunnetusta kahvitahrailmiöstä ja hydrofobisoivien materiaalien erilaisesta vuorovaikutuksesta selluloosakuidun pinnan kanssa.

Avainsanat mustesuihkutulostus, funktionaalinen painatus, hydrofobinen muste, polystyreeni, alkyyliketeenidimeeri, mikrofluidistiikka, paperifluidistiikka

Foreword

This study was conducted in the Department of Forest Products Technology as part of the Functional Wicking Surfaces project, supported by Omya International AG.

This work would not have been possible without contributions from many other persons. Firstly, I would like to thank Professor Patrick Gane for providing me with this very exciting research topic, as well for coming up with plenty of ideas and questions as the study progressed, not to mention practical advice with writing in English. He also encouraged me to submit an Abstract based on this work to the IARIGAI 2014 conference.

I would also like to express my gratitude to Eveliina Jutila for plenty of practical advice, inspiration and interesting discussions during this work.

Various other staff members and researchers, too numerous to name here, have been most helpful in providing assistance on a wide variety of practical issues. Special mention has to be made of Timo Hartus, who helped to find most of the instruments used in this study and provided practical assistance with CAM 200, and of Michael Hummel, who provided practical assistance with the MCR-300 rheometer.

Chemigate Oy is acknowledged for donating the AKD sample used in this study.

Finally, a special mention has to be made of previous researchers in the field of paperfluidics. Coming from a variety of backgrounds, they have in a few years published a wealth of material, demonstrating how existing materials and technology can be combined to produce novel but simple devices.

Otaniemi 16.4.2014

Risto Koivunen

Table of Contents

List of symbols

η	Viscosity
θ	Contact angle
γ	Surface tension
ρ	Density
λ	Wavelength
ε	Porosity
ºC	Degree Celsius
c^*	Coil overlap concentration
Da	Dalton
k	Permeability
Oh	Ohnesorge number
Z	Inverse of Ohnesorge number

Abbreviations

2DPN	Two-dimensional Paper Network
AChE	Acetylcholinesterase
AKD	Alkyl Ketene Dimer
ALT	Alanine aminotransferase
ASA	Alkenyl succinic anhydride
AST	Aspartate aminotransferase
BSA	Bovine Serum Albumin
CMC	Carboxymethyl cellulose
DCSBD	Diffuse Coplanar Surface Barrier Discharge
IR	Infrared
LED	Light Emitting Diode
LFT	Lateral Flow Test
LoaC	Lab on a Chip
LoP	Lab-on-paper
microPAD	Microfluidic Paper-based Analytical Device
microTAS	Microfluidic Total Analysis Device
PDi	Polydispersity Index
PDMS	Poly(dimethylsiloxane)
PoNMBA	Poly(o-nitrobenzyl methacrylate)
PS	Polystyrene
PVAm	Poly(vinylamine)
PVOH	Polyvinyl alcohol
UV	Ultraviolet
VOC	Volatile Organic Compound

1 Introduction

1.1 Background

A lab-on-a-chip (LoaC) is a small, easily transportable microfluidic device designed to take in a tiny fluid sample and run a complete automated chemical, biological and/or medical analytical assay on it, consisting of one or more intermediate steps. Depending on the design, a single device may run one or more assays from the same sample in parallel. [1]

The early LoaC designs made use of traditional microfabrication materials and methods. Such devices tend to use glass, silicon-based materials and various polymers as the base chip construction, with photolithography as a common manufacturing method. In the manufacturing process, the base chip is patterned to contain channels that direct and control the flow of the fluid sample. [1] [2] [3]

The concept of using paper as a base substrate for modern lab-on-a-chip products was first introduced in a pioneering study published in 2007 by the Whitesides research group from Harvard university [4]. Though this study used filter paper as a substrate, the other materials and patterning methods used were typical for conventional microfabrication. Since then, a number of other studies have been published using a variety of other methods, including various conventional printing methods.

Paper makes a good platform for simple lab-on-a-chip devices due to being easily available, cheap, and disposable, as well as compatible with many chemical, biochemical and medical analytical methods [5]. Particularly important is the porous nature of paper, which allows it to absorb and transport liquid due to capillary forces [5] and makes it a natural filter [6]. Other advantages of paper include high surface-to-volume ratio, which provides plentiful surface area to bind reagents, as well as the white colour which provides an excellent background for colorimetric tests [7]. However, due to its nature, paper is not perfectly uniform, even within a single sheet [7]. Also the very nature of the paper manufacturing process results in paper having a fibre orientation that gives it somewhat differing properties in machine and cross-machine directions [8].

Paper-based LoaC devices can provide cheap, easy to use, portable, robust, equipment-free and easily disposable diagnostic tools. This makes them particularly suitable for home diagnostics, emergency care teams, remote areas, developing countries or other situations where full-scale laboratory equipment and personnel are not an option. [5] [9]

Paper-based analytical tools can be designed to be self-contained, or they can be combined with external instrumentation to help in the analysis [10]. Possible areas of application for paper-based lab-on-a-chip devices include at least medical and chemical diagnosis, food quality control and environmental monitoring [9].

Many authors consider developing countries as an area where paper-based lab-on-a-chip devices could have a particularly high impact. The World Healthcare Organisation (WHO) general guidelines for diagnostic devices in developing countries can be summarised with the simple mnemonic ASSURED: Affordable, Sensitive, Specific, User-friendly, Rapid and robust, Equipment-free, and Deliverable [11]. Paper-based devices have the potential for fulfilling all of these criteria.

Since modern paper-based lab-on-a-chip devices form a rather recent field of study, there is not yet an established vocabulary for such products. Rather, different authors use a vast variety of terms to describe them. Some of the commonly used terms include microfluidic paper-based analytical devices (alternatively abbreviated to microPAD or μPAD), paper-based microfluidic devices (alternatively shortened to paperfluidic devices), paper-based diagnostic devices, patterned paper devices and 2D paper networks (2DPNs) [7]. Other used terms also include lab-on-paper, system on a paper and bioactive paper [11]. From here on, the term *paperfluidic device* will be used in this study to describe any such item.

So far, modern paperfluidic device designs have been mainly restricted to laboratory prototypes. Only one design has been reported as having undergone extensive field testing; recently a liver function assay designed by Diagnostics for All, a US-based non-profit, was tested on 600 Vietnamese patients undergoing medication that could as a side-effect cause liver complications [12]. Getting actual commercial products on market will likely require several more years, due to a need to gain regulatory approval and optimise product for high-volume production. Past experience on other commercial point-of-care LoaC products has shown that newly established companies in this field usually require at least five years from their initial founding until they manage to get their first product approved [13]. While using the date of founding to estimate the total amount of time taken for product development and approval might be methodologically slightly questionable, since it is unlikely that actual product development work started at the same time, it has the benefit of being a date that is easily publicly accessible.

1.2 Research goals

This study had two main goals. The first was to provide an extensive literature review about the state of the art research within the field of paperfluidics. Particular emphasis was placed on hydrophobic patterning, studied in regard to base substrates (Chapter 3), patterning methods (Chapter 4), hydrophobising agents (Chapter 5) and patterning resolution (Chapter 6). These findings have been further concluded in Chapter 8. To provide a wider framework for this work, general features and applications for paperfluidics have also been described (Chapter 2), as well as theory and practice behind fluid transport in paperfluidic devices (Chapter 7).

The second goal, for the experimental research, was the development and characterisation of simple hydrophobic inkjet inks that can be used for patterning porous substrates. To this end, several inks were formulated and their performance tested on two different paper substrates. Particular attention was paid to the physical characteristics of the inks and to their jetting properties. Another important aspect studied was the dimensional limitation in resolution of channels and barriers that could be produced with these inks, as well as practical reliability of the produced barriers.

2 Paperfluidic devices

2.1 Structure

Paperfluidic devices operate by absorbing a liquid sample provided by a user and transporting this sample to various detection zones, where it interacts with reagents. The results of these reactions will provide information about the fluid properties that will be then displayed back to the user. Transportation of aqueous liquids is carried out in a network of hydrophilic capillary channels isolated by hydrophobic barriers. The purpose of such a channel network is to limit the needed amount of sample and reagent, to prevent possible leaking of reagents between the various detection zones and to provide means for controlling travel times inside the network. [5][10]

Paperfluidic devices can be divided into 1D, 2D or 3D devices, based on the number of dimensions in which the fluid will flow inside a device. This study concentrates mainly on the features of 2D and 3D devices.

In 1D devices, also known as lateral flow tests (LFT), fluid is carried in a single direction along a single channel. Since flow will be mono-directional, there is no need to pattern hydrophobic channel boundaries on the paper, as the edges of the paper itself will restrict flow. The simple nature of a 1D device largely restricts such a construction to tests that can be carried out in a single step, and to a single assay per test device. A typical paper-based 1D device is the commercially available pregnancy test kit. An example of a 1D paperfluidic device layout is shown in Figure 1. [14]

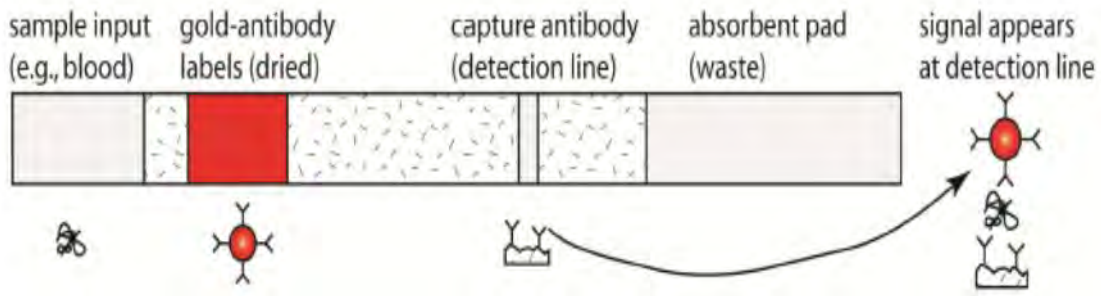

***Figure 1**. A typical 1D paperfluidic device layout. Fluid is wicked from the sample input zone on the left towards the detection line in the middle.* [14]

2D devices are designed to work around the limitations of the 1D device by transporting the liquid in a two-dimensional network of hydrophilic channels. This makes it possible to

introduce multiple steps, multiple assays and various functional features that can control the fluid flow. An example of a 2D paperfluidic device layout is shown in Figure 2. [14]

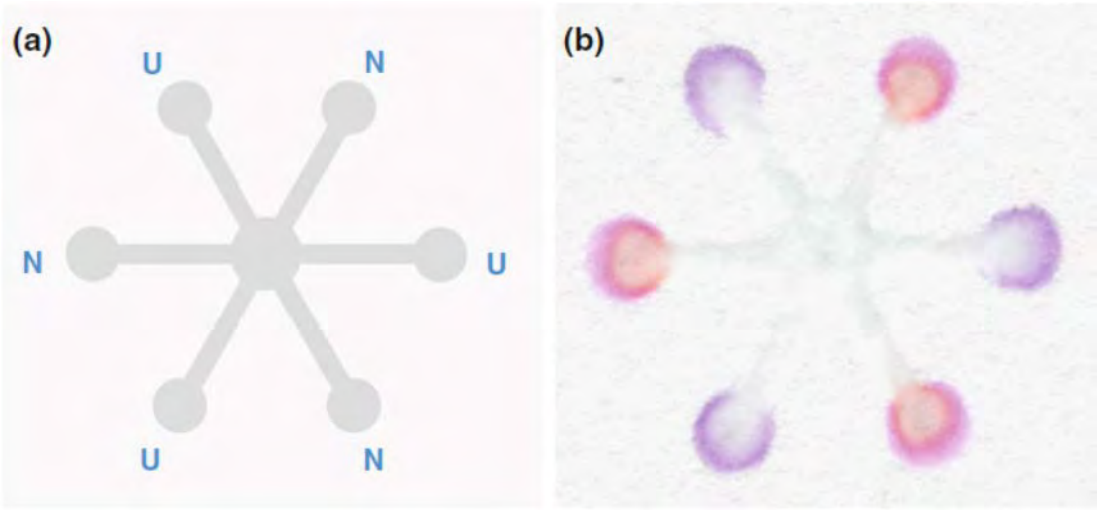

***Figure 2**. A simple 2D paperfluidic device layout. On the left (a) the device design displaying a central fluid intake location and multiple detection zones for uric acid (marked with U) and NO_2^- (marked with N). On the right (b) an actual device in action, with detection zones displaying colour changes.* [15]

3D devices are produced by layering multiple 2D devices on top of each other, separated by hydrophobic layers with holes in them. This will allow the fluid to flow not only horizontally inside the individual layers, but also vertically between them. This allows for a greater number of assays to be integrated into a single device than with ordinary 2D devices, while keeping the flow paths relatively short. It also enables some entirely new functional features that would not be possible with 2D devices, such as using different types of paper for different layers. An example of a 3D paperfluidic device layout is shown in Figure 3. [3][16]

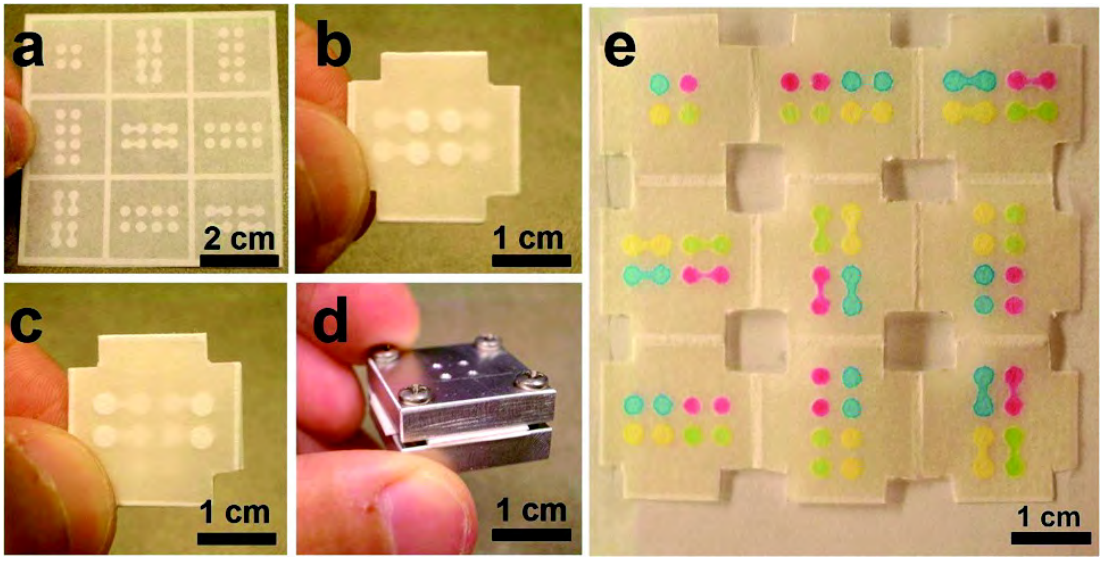

Figure 3. *A simple 3D paperfluidic device concept, assembled from a single sheet of paper using the art of origami or paper folding: (a) an unfolded sheet, (b) top view of a folded device, (c) bottom view of the folded device, (d) an aluminium clamp used to hold the folded device together, and (e) a device that has been used to channel coloured liquids, unfolded* [17].

Assembling 3D devices involves attaching the separate layers to each other. One way to do this is to use double-sided tape, with holes cut at appropriate positions to allow fluid transport between the layers [16]. Such tape will then also form a hydrophobic barrier between the paper layers. However, to ensure reliable transport through the holes in the tape, they need to be filled with a wicking material, such as a paste made of cellulose powder mixed with water. Another documented way of attaching the layers to each other is the use of spray adhesive, though in this case additional hydrophobised paper layers will be needed to provide barrier layers [18]. The used adhesive should be selected so that it does not seriously affect reagents or the wicking properties of the hydrophilic channels, and does not dissolve or lose adhesive properties when exposed to a specified liquid sample. Alternatively, adhesive can be applied selectively by screen printing, allowing one to leave hydrophilic areas uncovered and thus making it possible to use hydrophobic adhesive [19]. A third option involves using a simple mechanical clamp to hold the layers together; this also enables the user to disassemble a used device easily to provide access for analysing contents of the middle layers [17]. A fourth option is to use conventional mechanical bookbinding methods, such as stapling or stitching, to hold different paper layers together, though this

might result in partial loss of contact between paper layers if they buckle due to temperature and/or humidity changes [20].

SlipPAD design is a special case of 3D device. In such design, different layers are not physically attached to each other, but are rather left loose so that they can be slipped laterally in relation to each other. In this fashion, a user can first fill multiple intake zones on the top layer and then slip it laterally to bring all intake zones in contact with channels on a lower layer. This allows for simultaneous activation of different channels, which is more reliable than relying on a user to fill different application zones according to a pre-set time schedule. If needed, another lateral movement later on can again separate intake zones from the other functional areas of the device. [21]

Another method to introduce multiple samples to a device simultaneously is by adopting a folding design, where samples are initially placed on small individual pads or application zones on one half of the device, and these are then brought into contact with channels on the other half by folding the device. Such a design has been demonstrated using a transparent plastic casing to hold paperfluidic components [22].

Structurally, a 2D or 3D paperfluidic device consists of a base substrate (paper), a network of hydrophilic channels and hydrophobic barriers patterned on it, and one or more test stations containing reagents. It can also feature a coating on one or both sides, as well as additional components. From an end user point of view, the main features of a device are the intake zones, where the fluid sample is inserted, and the display zones where the results of the assays are eventually shown.

2.2 Reagents and applications

2.2.1 General

In order to be able to actually detect chemical or biological properties from the samples, a paperfluidic device needs to have chemical or biochemical reagents incorporated into the structure. The reagent is chemically reactive with certain substances in a way that provides an externally detectable signal, such as a colour change. Reagents can be damaged by high temperatures or UV-radiation; if these are present in the manufacturing process, the sensitive reagent should only be applied after those process steps.

One common immunodiagnostic assay, widely used as a demonstration in published paperfluidic studies, is the detection of glucose from a fluid sample, useful for monitoring blood sugar levels of diabetic patients or for detecting the presence of glucose in urine. This can be done by using potassium iodide and horseradish peroxidase/glucose oxidase solution as reagents. Presence of glucose results in enzymatic oxidation of iodide to iodine, which turns the previously clear reagent brown. [4] [23]

Another example of reagent use is in the detection of proteins in samples by tetrabromophenol blue. In the presence of protein, it ionises and binds to the protein. This results in a reagent colour change from yellow to blue. [4]

2.2.2 Bioagents as reagents

Many of the reagents used in biochemical reaction assays are referred to as bioagents. Typical bioagents used include enzymes, antibodies and nucleic acids. Biomolecules are susceptible to harsh conditions, such as swings in pH or temperature, or exposure to mechanical action or UV-radiation. Thus, they should be deposited onto paper with a suitably gentle method. Inkjet printing has been found to provide a deposition platform that is not too harsh for biomolecules, and allows for accurate deposition of small quantities via its non-contact transfer method. However, even inkjet printing can potentially damage some molecules, either through heat degradation in the case of thermal inkjet, or through compression in the case of piezoelectric inkjet. [24]

In case of proteins, their physical molecular structure has a significant impact on inkjet printability of suspensions. Proteins with globular geometries, such as enzymes, messenger and transport proteins, can be printed at significantly higher concentrations than fibrous scleroproteins, which are more affected by viscoelastic behaviour. For example, globular bovine serum albumin (BSA) is easily printable in concentrations of 10 % by weight or more, while fibrous collagen (I) solutions are unprintable in concentrations of 0.3-0.5 % by weight with the same printer. The common method of improving jettability by heating the ink to reduce viscosity can only be used to a limited extent, since proteins can become denatured at high temperatures. [25]

An experimental study on inkjet printing of glucose oxidase provides an example of the effects of piezo-electric inkjet printing of a reagent. In this study, mixtures of glucose oxidase, phosphate buffer solution and various levels of glycerol were successfully printed on silicon dioxide surfaces with a Dimatix material printer DMP-2800 (Fujifilm). Inclusion

of glycerol resulted in the jetted solutions having higher viscosity. Tested print parameters included the full range of print head drive voltage (0-40 V) and two different voltage waveforms. The tested waveforms were identically shaped, but differed in the pulse duration; the segments of the longer waveform were twice the duration of the shorter one. Testing glucose oxidase activity from the printed surfaces revealed that increasing the drive voltage, fluid viscosity level or pulse duration led to a decrease in the enzyme activity level. The authors of the study attributed these effects both to compressive stresses, caused by the initial piezo-electric impulse, and to shear stresses, caused by local flow rate differences inside the print head. [26]

Flexographic printing has been studied as a means of applying reagents to substrate surfaces in at least one published report. In this study, two different types of antibodies, anti-FITC (fluorescein isothiocyanate labelled) polyclonal serum and anti-sheep IgG (immunoglobulin T), were printed on acrylic coated polypropylene films with additional custom nitrocellulose coating on top, using a variety of ink compositions. Best results were achieved using an aqueous ink with 2.5 % by weight of high molecular polyvinyl alcohol as a rheology modifier, small amounts of carbonate pH buffer, and no surfactant. Antibody prints were found to remain stable for at least one month when stored at 4 ºC, though longer storage periods had not, as of yet, been tested. Authors suggested that the described method is also applicable to printing other types of bio-agents, such as enzymes, DNA, proteins, aptamers (oligonucleic acid or peptide molecules that bind to a specific target molecule) and cells, as well as for printing on paper substrate if used with higher volume anilox rollers. [27]

To provide easily analysable results, reagents in a detection zone should be properly immobilised on a substrate surface, so that they will not be carried away by liquid flow. For biomolecule immobilisation on cellulose surfaces, four main methods have been reported. First is physical immobilisation, based on van der Waals and electrostatic forces, which can be promoted through chemical treatments that affect surface charge. Second is covalent and affinity-based attachment, based on a chemical reaction between a reagent and a substrate, which can be promoted by chemical treatments that provide the surface with functional groups. Third is carrier immobilisation, based on attaching reagents to particles that will adhere to the substrate. The fourth method is entrapment, which involves coating reagents with porous, inorganic material that keeps them in place while allowing sample contents to reach them. [28]

2.2.3 Bioagent stability

To provide long shelf life for the final product, bioagents need to remain stable over extended periods in storage, possibly at elevated temperatures or whilst exposed to light. One way to promote bioagent stability is to modify a base substrate in such a fashion that it will be able to protect the bioagent from some aspects of environmental harm.

In an experimental study, storage stability of horseradish peroxide enzyme was improved by immobilisation on a silica surface. Firstly, mesoporous silica nanorods were functionalised with epoxy groups, onto which horseradish peroxide molecules were subsequently bound. The nanorods, so treated, were then applied to filter paper from aqueous suspension. Test results indicated that horseradish peroxide immobilised on the nanorods in this way displayed excellent storage stability after a week, both at room temperature and 37 ºC, with only minimal losses in enzymatic activity. By contrast, free horseradish peroxide applied to filter paper lost all of its activity within 16 h at room temperature and 4 hours at 37 ºC. Authors suggested that this improved thermal stability might be due to immobilisation preventing enzyme aggregation on surfaces, as well as due to multipoint covalent bonding providing rigidity to the enzyme structure, thus improving thermal stability. [29]

In another experimental study, porous silica sol-gel was used to improve storage life of acetylcholinesterase (AChE) enzyme, which can be used for the detection of toxic organophosphates and mycotoxins. In this work, a Dimatix material printer DMP-2800 (Fujifilm Dimatix) was used to deposit sol-gel solutions, a reagent solution containing AChE and 5-5’-dithiobis-(2-nitrobenzoic acid) (DTNB) and a solution containing poly(vinylamine) (PVAm). These were printed in a multi-layer structure, with PVAm solution forming the initial coating on paper, followed by a layer of sol-gel, a layer of AChE/DTNB and finally by another layer of sol-gel on top. The resulting sol-gel sandwich structure provided stability to AChE, with the enzyme activity level retained at over 95 % after having been stored for 2 months at 4 ºC. The PVAm layer was needed to ensure that reacted assays maintained their colour for later analysis by ensuring that the DTNB reaction product used for colorimetric analysis remained stable. Without the PVAm layer, reacted samples lost their colour within a day, while those with the PVAm layer stayed stable for at least 21 days. [30]

In a later study by the same research group, production of similar style assays using flexographic and gravure printing on filter paper was tested adopting an IGT F1 printability tester (IGT Testing Systems). Tested sol-gel solutions proved problematic for these printing

methods, displaying foaming, poor uniformity of printed pattern, and in the case of flexography poor ink transfer rate from the anilox roll and/or formation of ink residues on the anilox roll surfaces. On the other hand, solutions containing AChE, indoxyl acetate (IDA) or poly-L-arginine hydrochloride (PolyArg) provided acceptable printing results, though PolyArg suffered from foaming which similarly reduced print uniformity. [31]

2.2.4 Detection of microbes

Detection of microbes in samples may require some special considerations, since they might be too large to pass through a typical substrate porous network. In such a case, microbes contained in a sample would end up filtered and left on the surface of the sample application zone, a property which can then be turned to advantage. Such filtered microbial content could be either analysed immediately, or an intermediate microbe culturing step could take place on the substrate before a final analysis is carried out [32]. Many living micro-organisms are capable of propelling themselves in liquid. Thus, if a porous medium is of sufficient dimensions to allow micro-organisms to pass through, then living micro-organisms might not remain as purely passive passengers in a liquid sample. Micro-organisms have been known to swim in a particular direction based on stimuli such as gravity, light or oxygen gradient, leading to cell concentration differences within a liquid domain [33].

In an experimental study, detection of foodborne microbes was carried out on paper microspot devices manufactured on filter paper. These microspots, 7 mm in diameter, were surrounded by hydrophobic wax barriers, with one side of the device covered by packaging tape. Three different bacteria-detecting enzymes and colour changing reagents were applied to these microspots. To test the assay, bologna samples were inoculated with bacteria, allowed to dry for 3 h and swabbed. The swabs were then placed into reservoirs filled with nutrient containing solution, and these reservoirs were kept in a 37 ºC incubator to enrich the bacterial culture. When samples were taken from reservoirs and applied to microspot assays, presence of *Salmonella* Typhimurium could be detected from the sample after 8 hours of enrichment, *Escherichia coli* O157:H7 after 10 hours and *Listeria monocytogenes* after 12 hours, for samples swabbed from bologna inoculated with 10 colony-forming units per cm^2. [34]

As an alternative to analysing whole microbes, a lysis operation can be carried out as an initial step to break down microbial cellular structures. In an experimental study, pathogenic and non-pathogenic strains of *Escherichia coli* bacteria in aqueous samples were lysed with

B-PER (bacterial protein extraction reagent (Thermo Scientific)) so that bacterial presence could be detected with a paper-based lateral flow assay. Reagents used to detect the presence of bacteria were 5-bromo-4-chloro-3-indolyl-β-D-glucuronide sodium salt and chlorophenol red β-galactopyranoside. When combined with a pre-concentrated sample of bacteria formed by magnetic separation, bacterial levels of 5 colony-forming units per cm^3 of original sample could be detected, matching the regulatory limits for bathing water in Europe. According to the authors, sensitivity of the assay could be further improved by introducing a culturing period before lysis is carried out. Assay design itself in this case involved sandwiching enzymes between layers of porous silica sol-gel, resulting in good storage stability: only slight reduction in activity was observed for assays stored at room temperature for 2 months. [35]

Culturing of bacteria can take place within the paperfluidic device itself, presuming that suitable nutrients and moisture are present. In an example study, a culturing process was used to create a paperfluidic variant of the Kirby-Bauer antibiotic susceptibility test, normally carried out in an agar-filled Petri dish. In this assay, two spots on the diametrically opposite points of a circular test zone were treated with different antibiotics, while commercially available resazurin dye and bacteria-containing fluid were applied to the centre of the test zone. During an 18 hour culturing period the dye would change colour from blue to pink in those areas where bacterial culture developed, while the areas where the presence of antibiotics prevented growth would remain blue. Thus, should an antibiotic-containing area change colour, it would be an indication that the tested bacterial strain exhibits resistance to that antibiotic. [36]

2.2.5 Some other reagents and their applications

While the main interest with paperfluidic device design has so far been in immunodiagnostic assays, a number of working paperfluidic prototypes have been prepared for environmental analysis purposes. For example, presence of chromium can be detected colorimetrically through cerium-induced oxidation followed by reaction with 1,5-diphenylcarbazide [37]. For a more unconventional application, presence of ten different types of explosives, including TNT, can be detected fluorometrically using pyrene as reagent [38].

For monitoring water quality, the presence of reactive phosphate in water can be detected by using ammonium hepta-molybdate tetrahydrate, potassium-antimony(III)-tartrate hydrate and ascorbic acid as reagents, with only minimal amounts of reagents needed for a

paperfluidic assay compared to traditional methods [39]. Presence of seven different heavy metal ions (Co^{2+}, Cu^{2+}, Hg^{2+}, Cd^{2+}, Ni^{2+}, Zn^{2+}, Ag^{+}) in water can be detected fluorometrically with the use of di-2-picolyamine derivates and fluorophore [40].

Yet another possible field of application for paperfluidic devices is in the analysis of food and drink. For example, measurement of polyphenol, flavonoid and anthocyanin concentrations in wines has been demonstrated using paper microzone plates treated with a variety of reagents [41].

2.3 Analysis of bodily fluids

2.3.1 General

A particularly interesting application area for paperfluidic devices is in the analysis of various bodily fluids. The majority of the human body mass consists of aqueous fluids. Out of these, blood is a particularly important fluid for carrying out diagnostic analysis related to health. Also various fluids excreted by the body, such as urine, or secreted fluids, such as saliva, sweat and tears can be monitored for their contents. Paperfluidic assays designed for monitoring the health of human patients are likely to be based on analysis of the contents of one or more of these fluids.

2.3.2 Blood

Functions of blood in the human body include transportation, regulation and protection. As a transport medium blood carries oxygen, carbon dioxide, nutrients, hormones and waste products around the body. Regulation involves adjusting pH through buffer chemicals, influencing water content of cells, and adjusting temperature by absorbing and transferring heat. Protection against disease and infection is handled by white blood cells and various blood proteins. [42]

Whole blood consists of liquid blood plasma, and a family of cells and cell fragments collectively known as formed elements. Of these, blood plasma provides for about 55 % of the blood content, while formed elements provide the remaining 45 %. Blood has a slightly alkaline pH in a range from 7.35 to 7.45. [42]

Blood plasma is a liquid consisting of about 91.5 % water, 7 % of proteins and 1.5 % of other solutes. Blood proteins consist mainly of albumins, globulins and fibrinogens. Of particular importance are gamma globulins, also known as immunoglobulins or antibodies,

which are produced as immune responses to infections by foreign substances and organisms (antigens). These antibodies can disable antigens by binding to them. Other solutes carried in blood plasma include electrolytes, nutrients, enzymes, hormones, dissolved gases, and waste products. [42]

Formed elements consist of red blood cells, white blood cells and platelets. The main purpose of red blood cells or erythrocytes is transportation of oxygen and carbon dioxide. They are shaped as biconcave discs 7-8 µm in diameter. They have a strong and flexible membrane, which allows them to deform and squeeze through even the narrowest blood vessels of only 5-10 µm in diameter. White blood cells or leukocytes defend the body from infections. They can be divided into five different subtypes, with each of these having a different role. Depending on the type, they vary in size from 6 to 20 µm in diameter. Platelets or thrombocytes are cell fragments that break off from megakaryocytes in bone marrow. Their purpose is to stop bleeding from damaged blood vessels by forming platelet plugs. Platelets are irregularly disc-shaped and 2-4 µm in diameter. [42]

For assays made with blood as the test sample, it can be necessary to separate the blood plasma from the formed elements. A porous substrate with pore diameter below 2.5 µm can form a filter that will prevent the passage of red blood cells. On a substrate with larger pores, red blood cells will be able to pass through the pores due to their flexible nature. Due to their deformability, red blood cells can also pack rather tightly on the surface of a filtering porous structure, and thus form a filter cake that hinders the flow of the blood plasma into the substrate pores. Pre-treating a porous surface with agglutinating antibodies will cause red blood cells to group into multicellular aggregates that can be filtered out by a porous structure with larger pore diameter than required for filtering out independent red blood cells. [43]

Once the red blood cells have been filtered out, it becomes easier to conduct assays for the contents of the blood plasma, such as glucose. A colorimetric paperfluidic assay has been demonstrated for detecting blood plasma glucose levels in 50 - 200 $mg \cdot dl^{-1}$ (per 100 cm^3) range [43]. Also a paperfluidic device with screen-printed electrodes and two blood application zones for smoother flow has been demonstrated for electrochemical detection of blood plasma glucose levels [44].

Sickle cell disease, a hereditary disorder affecting the structure of haemoglobin in red blood cells, can be detected from blood samples using the filtering properties of paper. When a

small amount of haemoglobin solubility assay chemical is mixed with a blood sample from sickle cell disease patient, red blood cells in the sample will start to aggregate. When a drop of such blood sample is applied on a piece of porous paper, the aggregated red blood cells will form a filter cake on the paper surface, whereas the non-aggregated red blood cells of a healthy patient would be wicked inside the paper together with plasma away from the application zone. The shape and colour intensity of the resulting red dot on the paper is visibly different in the two cases. Besides the healthy patients and actual sickle cell disease patients, the test can also differentiate those patients who genetically carry the sickle cell trait, and while not affected by the symptoms of the disease themselves, they can pass it to their offspring. [45]

Human blood is divided into four different blood types (A, B, AB and O, all of which can be RhD negative or positive (Rhesus blood group, D antigen)), based on the type of antigens that are present on red blood cell surfaces and on the matching antibodies present in blood plasma. Correct blood type is critical for blood transfusions. An experimental paperfluidic device, based on agglutination of red blood cells by anti-bodies and vertical transport of non-agglutinated blood cells, has been demonstrated. When using the device, a 3 µl blood sample is applied to each of the four antibody-treated detection zones. After 20 s waiting time, two 50 µl doses of saline solution are used to wash each of the detection zones, flushing any non-agglutinated red blood cells through the paper pores and onto a separate absorbent paper sheet placed underneath. Agglutinated (clumped/glued together) red blood cells remain on the display zone surfaces to indicate the result, displayed in a textual format. [46]

The effect of paper properties on the transport of red blood cells has been studied in another research test series. Tested papers included experimental laboratory-made papers, as well as commercially available filter, blotting and towel papers. According to the results, thin papers with large pore size were most successful for separating between agglutinated and non-agglutinated red blood cells, by allowing the latter to easily move through the paper matrix. [47]

An experimental paperfluidic device for detection of malaria has been demonstrated. It is based on detection of antigen *Plasmodium falciparum* histidine rich protein 2 (PfHRP2) present in blood plasma. While the demonstrated assay could not handle whole blood samples, the authors suggested that it could be easily modified to do so by addition of commercially available filter pads to separate blood cells and plasma. [22]

Certain medical treatments can, as a side-effect, cause harm to the liver in humans. A paperfluidic device, based on detection of liver enzymes aspartate aminotransferase (AST) and alanine aminotransferase (ALT) in blood, has been designed to detect such side-effects early [19]. A variant of this device, testing only for ALT levels, has been subject to a field trial with 600 patients undergoing relevant medication [12].

2.3.3 Sweat

The purpose of sweat glands is to get rid of excess heat, water and carbon dioxide, especially during times of heavy exercise. Sweat consists mainly of water but also includes small quantities of salts, urea, uric acid, ammonia, amino acids, glucose and lactic acid. Apocrine sweat glands, located at hair follicles in certain parts of the body, secrete a more viscous form of sweat that also contains lipids and proteins. [42] [48]

No existing paperfluidic designs for analysis of sweat were found in this literature study.

2.3.4 Tears

Lacrimal glands around eyes secrete lacrimal fluid that protects, cleans, lubricates and moistens the eyeball. This solution consists of water, salts, mucus and the bactericidal enzyme lysozyme. Irritating substances or strong emotions can lead to excessive production of lacrimal fluid, resulting in tears. [48]

An experimental paperfluidic device for detecting dry eye syndrome has been demonstrated. In this test method, fluid from the eye will be wicked into a hydrophilic channel, treated with anthrocyanin to ease detection, and tear production volume will be measured based on the distance wicked. Volumes down to 0.2 µl were reported to be detectable. Authors suggested that it could be possible to functionalise the test further by integrating assays to analyse tear contents. [49]

2.3.5 Saliva

Saliva serves the purpose of aiding gustatory receptors (sense of taste) and to start the digestive process for food. Saliva consists of 99.5 % water and 0.5 % of solutes. These solutes include ions (sodium, potassium, chloride, bicarbonate, phosphate), digestive enzymes (lingual lipase, salivary amylase), bacteriolytic enzyme lysozyme, immunoglobulin A, and other organic substances including urea and uric acid. Saliva is slightly acidic (pH 6.35-6.85). [42]

An experimental paperfluidic device has been demonstrated for the monitoring of nitrite levels in saliva. Such a test could be used to monitor progress of haemodialysis for patients suffering from renal disease. This test was found to produce a good linear response in 25 - 250 µM range, thus providing a very handy tool for monitoring patients with renal disease, reported as having levels of 40 - 160 µM before treatment and 1 - 40 µM after 4 h treatment. [50]

2.3.6 Urine

Urine provides a means for the body to dispense of waste materials and foreign substances. It consists of around 95 % water, though depending on the body fluid level it can be more diluted or concentrated. Urine also contains urea, uric acid, creatinine (a breakdown product of creatine phosphate in muscle) and ions (sodium, chloride, potassium), accounting for the other 5 % or so. [42]

Various diseases can cause urine to have abnormal constituents, such as albumin (protein from blood plasma), glucose, red blood cells, ketone bodies, bilirubins (sometimes known as hematoidin) or urobilinogens. Urinary tract infections can be detected by the presence of bacteria, yeasts or protozoans in urine. [42]

Urine tests can also be used to detect the presence of alcohol or illegal drugs in the body, or the use of performance-enhancing drugs on athletes. Early pregnancy tests for women are based on the detection of human chorionic gonadotropin in urine, this being a hormone that starts to be excreted about 8 days after fertilisation. [42]

Detection of glucose and ketone from urine using a paperfluidic device has been demonstrated. In the presented test device, the detection limit for glucose was 2.8 mM; not quite sufficient to reach the 1.4 mM level which is usually considered to be an indicator of disease. No detection limits were reported for the acetoacetate ketone test, which could take up to 50 minutes to fully develop results. [50]

More successful detection of glucose in urine was reported in another study featuring paperfluidic devices manufactured by cutting. In this study, a detection limit of 0.5 mM was reported, with the detection signal increasing approximately linearly as a function of glucose concentration when said concentration was in the 0.5 - 10 mM range. Glucose assay also proved to be robust in the sense of being little affected by external factors. Simultaneously, the testing of bovine serum albumin (BSA) in the urine detection assay proved to be more

sensitive to external factors, such as humidity of the environment, though a detection limit of 2.5 µM was still reported as being reachable with this assay. [51]

2.4 Display zones and detection

The results of the assays need to be presented to the end user in some fashion. This can either be done by a simple visible signal on the device display zone, or it might require the use of some electrical device in obtaining the results. Overall, the methods of generating display results can be divided into two groups: optical and electrochemical methods.

Optical methods involve estimating or measuring the final colour of the assay sensor area, which will give an indication about the properties of the fluid sample. Such a measurement can be carried out either by the unaided human eye, or by an imaging system such as a digital camera or scanner, or by spectrophotometry. For use by a human observer, colour charts can be integrated with the device to help in interpreting the results. Variants of such optical methods include the use of UV illumination and subsequent observation of the fluorescence of the assay sensor area, or the measurement of light emitted by a chemical reaction in the display zone (chemiluminescence). [11]

Visual reading of test results can in some cases be improved by forming the reagents into a latent text or image that is converted into a visible form by a chemical reaction. Such a feature has been demonstrated for a blood type test, where the test result was represented to a user in textual format, e.g. as AB+ [46].

A significant challenge with optical methods relying on the unaided human eye is quantification of the results. Observed colour intensity is one possible approach, but it can vary based upon observer and illumination conditions. One alternative approach is distance-based measurement, where a display zone is shaped into a long channel, evenly treated with reagents. As a sample wicks along this channel, analytes contained within the sample react with the reagents, which change colour but remain fixed at their original spot. Thus, colour changes continue along the channel as long as unconsumed analyte remains in the sample, or until the end of the detection zone is reached. Analyte concentration can then be estimated based on the length of the display zone that changed colour. In an experimental study, distance-based measurement was tested for detection of nickel, glucose and glutathione concentrations on separate devices, and measured distance was found to match well with the logarithm of analyte concentration in tested samples. It is worth noting that this method is

reliant on colour changing components remaining fixed at their original spots rather than being transported by the liquid undergoing wicking. [52]

Another optical method, not based on colour measurement, is surface enhanced Raman spectroscopy (SERS), which has been demonstrated as a possible means for detecting low level concentrations of analytes on paperfluidic devices. In one such study, silver nanoparticles were printed on a detection zone to enhance sensitivity. Wicking and evaporation were then used to concentrate analytes on the detection zone, where they were measured with a portable spectrometer. [53]

Electrochemical detection methods are based upon the electrical properties of the assay, such as an electrical current created by a chemical reaction between sample and reagent, or a change in the electrical conductivity of a liquid. Simple electrical circuits and batteries can be printed on a paper substrate to help in such analyses, thus reducing the need for external analytical instruments. [11]

In an early study on the use of electrochemical detection on a paperfluidic device, simple screen printed carbon and silver electrodes were used to detect glucose, lactate and uric acid from inserted fluid samples [54]. An example of the printed electrodes is shown in Figure 4. Later on, electrodes for the electrochemical detection of glucose have been manufactured also with VOC-free inkjet printing, using a mixture of ethylene glycol and purified water as carriers [55]. In both studies an external reader was required to analyse the results.

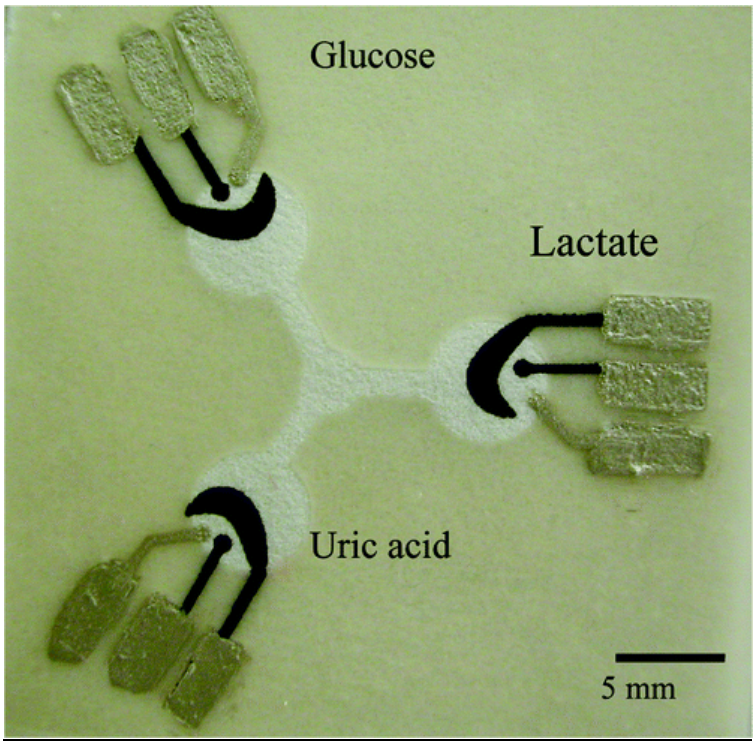

Figure 4. *Screen printed electrodes for electrochemical detection of glucose, lactate and uric acid. White patterns indicate hydrophilic regions, with a fluid intake area in the middle.* [54]

2.5 Valves

Various possible valve mechanisms have been introduced as a means to control liquid flow within hydrophilic channels. These valve mechanisms can be intended to delay flow, restrict a given flow direction or to provide the user with more control over flow routes.

Single-use fluidic valves on paperfluidic devices have been constructed by placing a narrow hydrophobic barrier between two hydrophilic areas, and applying a small amount of surfactant to one of these hydrophilic areas. When fluid arrives through a hydrophilic channel to the surfactant-treated area, the stored surfactant is released from the paper to the fluid surface and then adsorbed on the surface of the hydrophobic pores, turning the surface hydrophilic. This allows the fluid to pass through the previous hydrophobic barrier to the hydrophilic area on the other side. However, fluid arriving to the valve from the other (non-surfactant-treated) area would not have been able to pass through. Care should be taken with the amount of surfactant used for making valves, since excessive amounts of surfactant can cause the hydrophilising effect to spread unwantedly further downstream, and any

hydrophobic barriers located downstream need to be sufficiently wide in the direction of flow so as not to suffer any breaches by bridges formed from excess surfactant. Valve mechanisms can be used to add user-controlled trigger valves or automatically activated delay valves to fluidic circuits. [56]

Dissolvable barriers are another way of temporarily slowing down wicking rate. Such a barrier can be constructed by applying a section of suitable material, such as trehalose ($C_{12}H_{22}O_{11}$ (anhydride) also known as mycose or tremalose) disaccharide, to a hydrophilic channel. When the fluid front contacts a barrier, it needs to dissolve its way through, which temporarily slows down the fluid. However, since the dissolved barrier material afterwards becomes a part of the fluid sample, it can affect the flow properties also in dissolved form, by increasing fluid viscosity or by affecting fluid surface tension. Naturally, such material should be selected so as not to interfere with reactions between sample and assay reagents. [57]

In a later experiment by the same group, timed valves were manufactured on nitrocellulose membranes using sucrose as the valve material. To form these, solutions with 10-70 % of saturation level of sucrose in distilled water were prepared, applied to hydrophilic channels and left to dry. When liquid entered the channels, these valves were found to induce a delay that increased as a function of the sucrose saturation level, with delays ranging from a few seconds up to 53 minutes on the test strip. The delay effect was found to be primarily due to the viscosity increase as water wicked through a valve, dissolving the sugar, thereby generating a highly viscous leading wetting front that slowed down wicking speed. [58]

A particularly interesting variation of the dissolving valve concept is a design where dissolving time depends upon the contents of a sample to be analysed. In one experimental study, such a valve was constructed by locally treating a hydrophilic channel with a hydrophobic oligomer that would depolymerise into hydrophilic molecules when exposed to hydrogen peroxide contained in the sample. The time required for a sample to break through such a valve would depend on hydrogen peroxide concentration, and measuring this time could be used to quantify said concentration within the sample. By introducing also a similar untreated control channel, draining from the same application zone, the time difference for total travel between the two channels could be measured in order to eliminate partially the effect of external factors on wicking speed. A basic valve mechanism can be used for analysing the presence of a substance of interest on a test sample by exposing the sample to a reagent that would result in release of hydrogen peroxide when reacting with the substance

in question. For example, presence of an enzyme could be detected by first exposing a sample to an enzyme analyte that would react with an enzyme itself to release glucose, and then as a next step exposing the resultant glucose to glucose oxidase releasing hydrogen peroxide. All of these steps can be run in succession on a paperfluidic device. However, in order to detect only the presence of enzymes, a sample would need to be first exposed to catalase and glucose oxidase to scavenge any contained free glucose or hydrogen peroxide molecules. [59]

Another variant of the dissolving valve mechanism involves a design where a single application zone is connected via channels to multiple display zones, with a dissolving valve in each channel. By varying the amount of hydrophobic oligomer in each valve, the valves will have different breakthrough times for a given concentration of hydrogen peroxide. To operate such a device, a test sample is applied, a timer is started and the device is checked again after a fixed period of time to determine how many of the valves have been broken through. In an experimental study with such a device, the number of valves broken through after 10 minutes was found to match roughly with the hydrogen peroxide concentration within a given sample, i.e. time taken for a sample to pass through a valve could be considered proportional to the ratio between the amount of hydrophobic oligomer in the valve and the concentration of hydrogen peroxide in the sample. [60]

With 2D devices simple mechanical switches can be included in channel designs, allowing a user to open or close a section of channel at will. One such is a folding switch design, in which a switch is formed by making a cut-out tongue in a paper sheet. The cut out acts as a make or break in the wicking channel. By creating a fold axis passing through the attached end of the tongue cut-out, a hinge is constructed which can be operated to bring the tongue surface into or out of the wicking plane to open or close the channel [61]. In a sliding switch design, a switch region has been entirely cut off from a paper sheet and is activated by sliding it sideways until hydrophilic or hydrophobic regions of the switch match with those of the channel [62].

3D paperfluidic devices can be designed to provide users with a limited ability to program the device, rather than just using it straight off the shelf. This can be achieved by marking buttons on the top paper layer, with matching empty holes placed in the layer beneath it. This hole then forms a gap between two channels on different levels between which the fluid is not able to traverse. However, a user can push the button on the top layer with a suitable object (such as a ballpoint pen) to compress the top layer paper on that spot. This will close

the former gap and allow fluid to flow vertically between the layers. Since the buttons can be made quite small, a single device can feature quite many of them. According to an experimental study, the recommended diameter for such a button is 0.2 mm wider than the width of a matching hydrophilic channel beneath, while a 400 µm vertical gap between the layers was found to be sufficient to prevent accidental leaks across the gap. [63]

2.6 Other functional features

Besides the features mentioned previously, paperfluidic devices can sport a variety of other features that provide added functionality. Some of these will be explored in detail in this section.

Metering is the practice of slowing down local flow rates inside particular channels without affecting the actual dimensions of the channel in question. This can be achieved by treating a selected small region of a channel with a small amount of a hydrophobising agent, such as paraffin wax, creating a fluidic meter. The slowing down of the flow rate in this area is due to an increasing contact angle between water and the pore surfaces, and possibly due to decreasing pore volume. For metering purposes, a hydrophobic agent is used in such low amounts that it will not form an actual hydrophobic barrier inside the channel. Care should, however, be taken in regard to possible reactions between materials contained in intended fluid samples and the hydrophobising agent used for metering. [64]

Galvanic batteries can be integrated in the devices to provide power for simple in-built electrical devices. Such a battery can be constructed from deposited electrolytes, electrodes, salt bridges and simple conductive connections between galvanic cells and the electrical device. Such batteries integrated in paperfluidic devices are intended to remain inactive while dry, but introduction of fluid into the device will subsequently activate the battery and result in power being generated for the electrical device. Experimental batteries, for example, have been demonstrated as being able to provide current for a small UV LED light for 21 minutes at full power. [65]

2.7 Finishing

The open surface nature of a typical 2D paperfluidic device results in three problems. Firstly, the channels can be liable to contamination from external sources. Secondly, fluid wicking along a channel evaporates, thus reducing wicking speed and the total distance that the liquid will travel, and increasing the concentration of dissolved or suspended species in the sample.

Such a change in the fluid concentration level may also lead to an increase in the fluid viscosity, thus further slowing down wicking speed. Thirdly, while in use the device needs to be suspended in the air to avoid part of the fluid flowing into any surface that is in contact with the bottom of the device. A number of methods have been developed to cover one or both sides of a device with a protective surface coating. [66]

One simple method to isolate a wicking sample from the surrounding environment is to cover the device with regular plastic tape. This makes a good protective layer while the device is dry, but the adhesion can suffer when the channels are wet from the fluid sample. Also the adhesives from the tape can transfer to the paper over time, affecting adversely its hydrophilic properties. And when inlet or outlet holes for samples are needed, these have to be cut out and properly aligned with the device when attaching the tape. [66]

Hot lamination with thermally bonding polyester films has been demonstrated as an adhesive-free finishing option. Disadvantages of this method include compression of paper between laminating rollers, resulting in an effective loss of porosity, and high temperature at the laminating nip, which can affect reagents. Trying to reduce temperature resulted in small air bubbles being left between paper and polyester film, thus affecting wicking behaviour. Also, as in the case of plastic tape, inlet and outlet holes need to be cut in the laminating film. [51]

One novel way of producing a protective coating layer is to use electrophotography to print protective toner layers on paper. This provides for a stable thermally-bonded protective layer that can easily feature open inlet and outlet areas. Such a protective layer can also feature textual or other information. A study using an unmodified commercial Samsung CLP-620ND four-colour printer has been carried out to examine the properties of such toner layers. According to this study four consecutive toner layer printings on top of each other were needed to produce a coating that could be expected not to permit leakage of any fluid travelling in the channels. This result was found to be the same regardless of the toner colour used. The authors speculated that it should be possible to manufacture a specialised printer that could produce a sufficiently thick protective toner layer within a single print run. Since the protective properties were the same for all colours, yellow toner could be used to produce a semi-transparent layer on top of the paper, though it still negatively affected colorimetric analysis of the assay results. Use of clear, transparent toner, such as used to produce matt or gloss coatings on specialised commercial printers, would provide for a better toner material for coatings. Besides stopping leaks through the bottom, a protective layer was found to be

very effective in preventing evaporation, and thus speeding up the wicking process. A drawback of the toner coating process is the high temperature involved in the toner fusing step, since this can affect negatively any reagents necessarily pre-applied to the device. In the same study with toner coatings, also a Xerox Phaser 8560 wax printer was tested as a method for producing protective coatings. While a single wax layer was found to have protective properties equal to two toner layers, this method could not be used to produce multiple layers, since subsequent wax printings did not properly adhere to an existing wax coating. The authors, however, did not seem to consider the possibility of constructing a special wax printer that could produce a sufficiently thick layer with a single print. [66]

A somewhat more elegant method of producing a hydrophobic finishing was demonstrated in a study using UV-curable inkjet printing to produce hydrophobic channels. In this study, both hydrophobic barriers and hydrophobic finishing were combined into a single printing step. Barrier regions were printed with the printer set to 100 % coverage, while for the areas with only hydrophobic top surface desired 25 % coverage was used. The lower coverage resulted in lower volumes of hydrophobic agent being transferred to the substrate, and thus resulted in only the top layer becoming hydrophobic, while the bulk of the substrate beneath remained hydrophilic. With such a method, any reagents need to be applied before the top layer is printed. [67]

One-sided coating can be achieved by a variety of printing methods by printing on the reverse side of the paper with 100 % coverage. This works if the hydrophobic ink used is unable to penetrate through the depth of the paper, leaving the other side hydrophilic, while single printing with 100 % coverage is sufficient to turn the printed surface hydrophobic. A variant of this approach was demonstrated by printing a solid wax layer on the rear side of a device, followed by a brief heating that allowed wax to spread sufficiently to provide one-sided hydrophobicity, but not so much that it would have affected hydrophilic channels on the other side of the device [62].

3 Base substrates

3.1 General

The base substrate forms the basis of the paperfluidic device, upon which all functionality is imbedded. While the most commonly studied materials are various highly absorbent papers, the field is not strictly limited to paper only – any porous permeable matrix, or paper-like medium that can transport fluid through capillary wicking can be considered as a potential material for use as a paperfluidic device.

The porous medium consists of two interleaved elements. The first is a network of interconnected and immobile solid material. The second portion is a mostly interconnected network of non-solid material, called pores or voids. Individual pores are connected to each other through more narrow gaps, known as pore throats. The interconnected nature of the pores makes it possible for liquid or gaseous material to travel through the porous media. Permeability of a porous network depends on the level of connectivity between the individual pores and the cross-sectional area perpendicular to the flow direction of the constituting connecting channels. [68] [69]

Besides the liquid transportation properties, another important feature of a well-functioning substrate is the capacity to bind reagents. Pure cellulose-based papers, for example, tend to bind proteins, phages and DNA aptamers rather weakly [6]. These binding capabilities can be improved by a surface treatment of the substrate.

The protein-binding capability of cellulose can be improved by modifications of the surface chemistry. Adsorption of carboxymethyl cellulose (CMC) or chitosan on cellulose fibre surfaces has been shown to improve subsequent adsorption of bovine serum albumin (BSA) and human immunoglobulin G (hIgG) proteins on the treated cellulose surface. However, in both cases the adsorption rates of the proteins depended significantly also on the pH of the protein-containing solution. [70]

Polydopamine (PDA) has also been used to improve the capability of a substrate to immobilise biomolecules, such as enzymes. PDA solution can be inkjet printed onto detection zones, or other desired areas of a substrate, to improve local binding properties. [55]

A good paperfluidic substrate should feature a fast planar (*xy*) wicking rate for samples, should allow hydrophobising agents to penetrate to the full depth of the porous component(s) of the substrate in the vertical plane (*z*), and should be capable of handling any mechanical stresses present in the manufacturing process. For good analysability of colorimetric assays, the substrate should be white, with good colourfastness against aging and exposure to environmental factors. [71]

The thickness of a substrate plays a number of roles in paperfluidic device design. Together with porosity, it determines the maximum absorbable liquid volume per unit surface area. With opacity, it determines how much of the signal produced by reagents is visible to a user; on thick substrates, the signal produced by reagents deep within the substrate is not visible to the user, due to the bulk of the substrate limiting the amount of light that can penetrate into the depth of the substrate and return to the surface. [71]

However, wetting of a substrate can affect the opacity of that substrate. This can have an important effect when a liquid sample is applied to a paperfluidic device. However, such temporary effects are likely to be lost once the device has dried again. Retention of translucency, however, can be guaranteed when using non-volatile oils, fats or waxes as a component of the wicking liquid.

So far, the most commonly used substrates in paperfluidic device studies have been laboratory grade filter papers, though also a number of other materials have been tried. The rest of this chapter describes substrates documented in literature from earlier studies.

3.2 Filter paper

Filter papers are speciality papers designed to filter out solid material, such as dust, while allowing fluid (gas or liquid) to flow swiftly through the paper. For this purpose they need to have a high porosity and a controlled pore size distribution and pore connectivity, making them easily permeable towards fluid, while being simultaneously impermeable towards any contained particulate matter. Solid material is, thus, unable to pass through the pores, and accumulates either within the volume or at the surface of the paper. In case of surface accumulation, the solid material forms a layer known as filter cake, which by itself acts as an additional filter layer. Filter papers are used for a wide variety of applications, such as laboratory and diagnostic work, air conditioning, fuel and oil filters, and for various household purposes like coffee filters, tea bags or vacuum cleaner dust bags. [72]

So far, the most commonly reported substrate with paperfluidic studies is Whatman grade 1 filter paper (GE Healthcare). According to the information provided by the manufacturer, this paper is made of cotton cellulose, has a particle retention rating of 11 µm for liquid suspensions (at 98 % efficiency), and has a typical thickness of 180 µm and basis weight of 88 gm^{-2} [73]. Other filter papers reported for paperfluidics include Advantec 5C 185 mm (Advantec MFS), having 1 µm retention rating [74].

In addition to commercial filter papers, custom-made paper handsheets have been reported as substrates in one study. These handsheets were manufactured from ash-less filter paper pulp. The handsheets were reported to have a density of 0.67 $g \cdot cm^{-3}$, but unfortunately no details were provided by the authors about their thickness. [55]

Filter paper can be a problematic substrate for many traditional printing methods, due to high surface roughness, low surface and bulk strength and uneven pore size distribution, a problem even preventing adequate flexographic printability [31]. The most likely methods for successful printing are screen and inkjet, with the latter especially benefiting from its entirely non-contact nature with the substrate.

3.3 Nitrocellulose membrane

Nitrocellulose is a cellulose derivate manufactured by nitrating ordinary cellulose with nitric acid or some other nitrating agent. Nitrocellulose membrane (also known as NC membrane) is a paper-like substrate manufactured from pure nitrocellulose.

Nitrocellulose membrane has been successfully used as a base substrate in a study using wax printing. It was reported to have small (0.45 µm diameter) uniform pores, as well as a very smooth surface. Also it has been reported as being highly effective in immobilising proteins. On the other hand, nitrocellulose is highly flammable, with flash point of around 200 ºC, so care needs to be taken when using it with any patterning process that requires heating of the substrate. [75]

As an interesting feature, solvents used in printing may cause nitrocellulose membranes to become shrunken or compressed due to partial dissolution in the solvent and subsequent re-solidification upon drying. In a study using inkjet printing with dipropylene glycol methyl ether acetate as solvent, HF135MC100 nitrocellulose membrane (Nihon Millipore) was found to become significantly compressed along printed lines [76]. Such compression results in reduction of porosity and permeability, making it easier to manufacture effective barriers,

though it might also reduce mechanical strength of the substrate, possibly leading to runnability problems if used for roll-to-roll manufacturing.

3.4 Office copy paper

Office copy papers are intended primarily for use with electrophotographic printers and photocopy machines. They usually have a basis weight of 70-90 gm^{-2}**.** Use of office copy paper as a substrate for paperfluidic devices has been documented in three studies.

In a study using wax printing, conventional office copy paper was found to exhibit poor water absorption and flow properties. The authors of the study suggested that this could be circumvented by oxidising the substrate with oxygen plasma, or by adding surfactants to the fluid samples. [77]

In an early study with PDMS, office paper was reported to have been successfully patterned, though no mention was made about actual fluid transport properties [78]. In a second study using PDMS, surface sized office copy paper Optitext 80 gm^{-2} (Stora Enso) was tested and found to have 89º contact angle with water, though water penetration through the substrate was reported as having been moderately fast regardless, suggesting that the bulk of the paper had retained hydrophilic passages, while the surface sizing had resulted in a surface pinning mechanism [79].

3.5 Pigment coated paper

Pigment coated paper consists of a base paper which surface is coated with a layer of white pigment microparticles on top. Coating pigments are typically minerals, such as kaolin clay, talc, calcium carbonate or titanium dioxide. The weight median particle size of coating pigments is usually in the 0.5-1.5 µm range. Besides the pigments, the coating also consists of binder and small amounts of additives, amounting to about 5-20 % of the dry coating weight. The purpose of binder is to bind pigment particles to each other and to the base paper. Typical binders include starch, latex and polyvinyl alcohol (PVOH). [80]

The coating layer acts to smooth the base paper surface and form a new porous medium of its own on the paper surface. The purpose served by the coating is to improve the optical and print quality characteristics of paper, such as gloss, opacity and brightness. The coating also supports ink acceptance and promotes the ink setting process. Pigment coating also improves the printability and runnability of paper by increasing surface strength of the paper and

reducing linting and dusting. Coatings with very fine pore size also result in the virtual elimination of ink pigment and resin penetration into the substrate, thus leading into a more saturated print density and so improved image quality. Also, despite a higher initial speed of absorption, coating can reduce the ink vehicle uptake capacity due to the very fine pore structure, being in contrast to that of the more permeable base paper. [80]

Pigment coatings can also feature bioactive molecules as additives. In a laboratory study, two different laccase enzymes (copper containing oxidase) were successfully added to two different pigment coatings. The activity of laccase in coatings deteriorated over time, but all samples still displayed activity after 5½ months. As a side effect, addition of laccase slightly increased the hydrophilicity of the coatings. [81]

So far, there appears to be only one known study reporting the use of coated paper for paperfluidic devices, with poor results. The coated paper in question was a multilayer-coated woodfree grade LumiArt 250 gm^{-2} (Stora Enso), designed for sheet fed offset printing and featuring relatively low permeability to water and air. Printing this paper with PDMS and studying the results revealed that the ink did not penetrate into the bulk of the substrate, but instead formed a continuous film that covered the pigment coating. This is not a surprising result, since with high quality printing paper any material deposited by the ink is expected to be trapped on the substrate surface. This is in direct contrast to the needs of patterning paperfluidic devices. [79]

3.6 Other substrates

Besides the previously mentioned substrates, a number of other materials have been tested in prior reported studies. These include the following:

- newsprint and paper towels tested with PDMS hydrophobising agent by pen plotting, with the agent seen to have penetrated completely into both of these substrates [78],
- clean room paper C1 (Contec), consisting of 60 % cellulose and 40 % polyester, tested with flexographic printing [82],
- Steri-Pak LF indicator test sheets (SteriTec Products), of 700 µm thickness tested with PDMS [79],
- Technicloth non-woven wipers (ITW Texwipe) consisting of 55 % cellulose and 45 % polyester, tested with SU-8 photoresist and UV-curing cyclised polyisoprene derivative [16] [83] [84],

- household coffee filters and Kimwipes laboratory cleaning wipes (Kimberly-Clark) tested successfully, applied by photolithography using UV-curing cyclised polyisoprene derivative [84],
- paper napkins patterned by wax pencils, with poor performance unless fibre orientation was taken into account [62],
- silicone, wax and polymer coated speciality papers tested with laser treatment [85],
- hydroxypropyl cellulose methacrylate, patterned from dimethyl sulphoxide solutions through photolithography-induced cross-linking [86],
- silica gel plate, as used in thin layer chromatography, tested with permanent marker [87],
- electrospun synthetic nanofibre mats, used for lateral flow assays without hydrophobic patterning [88],
- hydrophobic cloth patterned by stitching hydrophilic thread on its surface [89], and
- cotton cloth tested with wax printing. To improve the hydrophilicity of the cloth, it was first chemically treated to remove impurities. [90]

4 Patterning methods

4.1 General

Patterning means the activity where the channel network is formed upon the base substrate by producing hydrophobic barriers and hydrophilic channels on it. A variety of technical methods are used for this purpose, drawing both from the fields of printing technology (inkjet, screen printing, flexography) and microfabrication (photolithography, plasma, laser). Besides hydrophobising agents, printing methods can be used to deposit also other analytical elements, such as reagents and electrically conductive materials, as well as conventional graphical content, onto a substrate.

There are two principal approaches involved in patterning substrates. The first method involves selective hydrophobisation of a hydrophilic substrate by forming local hydrophobic barriers out of hydrophobising agent. With this method, the formed barriers need to extend properly through the whole depth of the substrate in order to prevent leaks from the hydrophilic channels. The second approach involves first treating the whole substrate with hydrophobising agent to make it entirely hydrophobic, and then using selective dehydrophobisation to produce hydrophilic channels on it. When used for producing 2D paperfluidic devices, such hydrophilic channels do not need to extend through the whole depth of the substrate, they just need to be deep enough to be able to absorb and transport sufficient amounts of fluid sample. [5]

This chapter provides a technical overview of the main patterning methods reported in previously published studies. Inkjet printing is covered in greater detail than the rest, due to both its versatile nature in depositing many different kinds of materials and its importance in the experimental part of this work.

4.2 Inkjet printing

4.2.1 General

Inkjet printing is a form of non-impact printing where print heads are used to produce tiny individual droplets of ink that are then directly deposited by ejection from the head onto the printed surface. The formation of droplets can be induced either by heating the ink in the ink chamber (thermal inkjet) or by mechanically deforming the ink chamber (piezo-electric inkjet). Both of these operating principles are illustrated in Figure 5. Conventional inkjet inks consist of dye or pigment colorant, binder, liquid carriers and various additives such as

surfactants, humectants, dispersants, pH buffering agents, defoamers, biocides and corrosion inhibitors. [91] [92]

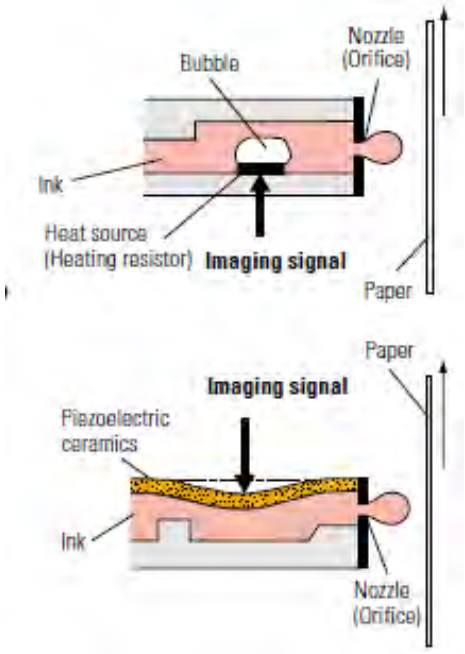

***Figure 5**. The concept of operation for thermal inkjet print head (upper) and piezo-electric inkjet print head (lower).* [91]

Besides ordinary inks that are liquid at room temperature, the inkjet printing process can also be used to print hot-melt or polymerising inks. Hot-melt inks, also known as solid, or phase-change inks, consist of material, such as wax, that is solid at room temperature but can be liquefied by heating at the print head and then propelled to the print substrate, where it quickly cools and solidifies. Polymerising inks contain liquid pre-polymer, i.e. monomer solution, together with perhaps a photo-initiator, cross-linker, siccative and/or catalyst. After the ink droplets have reached the substrate, they either polymerise relatively slowly through oxidation, or are subjected to external UV-light or an electron beam that initiates the polymerisation chain reaction, turning the previously liquid ink solid. [91]

In addition to its original uses in graphical production, inkjet technology has been more recently adopted for functional printing of many different types of devices. These include electrical elements, such as thin-film transistors, light-emitting diodes (LEDs), displays, solar cells, conductive elements and sensors. Other demonstrated applications include metal solder, sol-gel materials, magnetic inks, three-dimensional prototyping, DNA microarrays and pharmaceutical products with sustained release rates. [93] [94] [95]

Printing parameters that can be used to characterise inkjet inks include jettability and satellite droplet formation, drop velocity and maximum printing frequency. Furthermore, a good ink should not clog or dry at the nozzles in the print head.

4.2.2 Jettability and satellite droplets

Jettability covers a variety of characteristics used to describe the suitability of a particular ink formulation for inkjet printing. One aspect of jettability is the possibility to dispense ink from a print head in the first place: non-jetting liquids are simply those that cannot be forced to separate from a nozzle by a regular jetting pulse.

Another aspect of jettability is an ink's resistance to separation into satellite droplets after separating from the nozzle. As a drop breaks free from a nozzle, it is followed by a trailing filament, frequently termed ligament in inkjet printing, which eventually breaks free from the nozzle. From this point onwards there are two competing events taking place on the filament: surface tension driven axial collapse pulls the filament towards the primary drop body in order to merge with it, while simultaneously radial pinch-off tries to break the filament into a separate drop, different from the primary drop body. If the radial pinch-off takes place before the filament has fully collapsed axially, the filament forms one or more separate satellite droplets; whether this happens depends on both the physical properties of the fluid and on the ratio between filament length and radius. [96]

One method of modelling jettability of inkjet inks is the inverse (Z) of the Ohnesorge number (Oh), a dimensionless number defined as

$$Z = Oh^{-1} = (a\rho\gamma)^{½}\eta^{-1} \quad (1)$$

where a stands for the radius of the print head nozzle (characteristic dimension), η the ink viscosity, ρ its density and γ its surface tension. [97]

Jettability of inks with different values of Z has been studied experimentally. In a study conducted on particle-free Newtonian liquids, 8 different solutions with values of Z ranging from 1.43 to 17.32 were tested using a piezo-electric inkjet printer with 50 µm nozzle diameter. These solutions consisted of various mixtures of distilled water, ethylene glycol, diethylene glycol, ethyl alcohol and/or glycerol. Based on results, the authors of the study defined the good printability conditions for these fluids as being approximately set by the range $4 < Z < 14$. Tested fluids with higher values of Z than 14 displayed formation of

satellite droplets that did not merge with the primary drop, while for fluids with values of *Z* lower than 4 the jetted drops required excessively long periods of time for the filament connecting the droplet with the nozzle to break free, resulting in higher minimum stand-off distance between the nozzle and substrate. Fluids with low values of *Z* also featured higher positioning error, and lower maximum operating frequency, than fluids with higher values of *Z*. [97]

Studying jettability is further complicated in the case where the ink in question is a complex fluid that displays non-Newtonian behaviour under the conditions present in a print head. Fluids displaying shear thinning, such as aqueous poly(3,4-ethylenedioxythiophene): (polystyrene-sulphonate) (PEDOT:PSS) solution used for printed electronics, will display reduced viscosity under high shear rate conditions in the print head in contrast to measured viscosity under low shear rate conditions. Shear thickening liquids on the other hand will display increased viscosity in a print head. Viscoelastic liquids, such as many polymer solutions, display temporary increase in viscosity or even solidification after having been exposed to rapid application of external strain, such as the high-frequency pressure pulses present in piezoelectric print heads. They also undergo die-swell, an effect seen as expansion after a constricted flow region due to the induced normal force response, and this can be detrimental upon exiting the jet nozzle. [98]

In some cases, certain forms of non-Newtonian behaviour can be used to an advantage when formulating for ink rheology, since ideal viscosity for an inkjet ink is different during different phases of jetting. Upon initial ejection, and subsequent filament detachment, viscosity should be low in order to enable easy ejection and swift detachment. However, once a drop has been ejected higher viscosity becomes desirable, since it slows down ligament break-up and thus reduces satellite droplet formation. And once the ink drop reaches a substrate, desired viscosity may depend on application. [99]

4.2.3 Drop velocity

Drop velocity is an important factor in ensuring printing consistency, since individual drops with low velocity are more vulnerable to being deflected from their intended course by external factors, such as air draughts. Drop velocity is affected by fluid properties, drive amplitude at the print head and the nozzle exit diameter.

Every ink has an individual drive amplitude threshold for a given print head, with no drop ejected for signals under the threshold. This amplitude threshold value is heavily dependent

on the viscosity of the ink. Experimental tests with a variety of inks and piezo-electric print heads have shown that once the amplitude threshold has been exceeded, the drop velocity tends to increase linearly as a function of the drive amplitude. This rate of increase is largely independent of fluid viscosity, though for low viscosity fluids it is affected by the surface tension of the fluid. [100]

4.2.4 Jetting frequency

Jetting frequency refers to the number of drops produced by a single nozzle within a print head during one second. It is of great practical interest, since low maximum jetting frequencies can limit achievable production rates. Typical frequencies for print heads are in the range of several kHz.

Jetting frequency can also have an effect on other jetting characteristics of an ink. As the jetting frequency increases, the time interval between two consecutive drops gets shorter and there may not be sufficient time for the pressure variation from the previous impulse to have fully dissipated. If a system is adjusted to operate well under such high frequency conditions, this can lead to inconsistent initial drop formation after a nozzle has been idle for a while, unless a modulating pulse is used to maintain a pressure in the ink chamber while a nozzle is idle. [101]

In a study conducted with polyethylene oxide (PEO) in aqueous solution, the effect of jetting frequency on jettability was observed. A solution containing 0.01 % by weight of PEO with molecular weight of 700 kDa was jetted from a piezoelectric print head at various frequencies. Increasing the frequency led to reduced drop velocities when the frequency was in the 20-800 Hz range. At 1 000 Hz the jetting could only be sustained for less than a minute, and at higher frequencies jetting was not successful at all. For comparison, distilled water was successfully jetted with the same set-up at higher frequencies, with velocity decreasing as frequency was increased from 800 to 3 000 Hz, but increasing subsequently when frequency was increased to 4 000 Hz. [101]

4.2.5 Waveform

One important factor affecting jetting behaviour is the pulse signal waveform used to generate pressure changes in the print head. In the case of piezoelectric inkjet, a simple waveform can be characterised by pulse peak voltage, rise time (from rest voltage to peak voltage), dwell time (at peak voltage) and fall time (time to return to rest voltage). Complex

waveforms may involve a pulse dwelling at multiple voltages for various times, or multiple short pulses applied in quick succession. [102]

In one experimental study, effects of three different waveforms were tested on jetting characteristics of water-glycerol mixtures, containing 0, 20, 40, 60 and 70 % glycerol, using an MJ-AT-01 inkjet nozzle (MicroFab Technologies) for jetting. Tested waveforms were a simple single waveform, a double waveform (two pulses in quick succession) and a bipolar waveform (a positive voltage pulse followed by a negative voltage pulse). As a result, using the double waveform instead of the single waveform was found to prevent satellite droplet formation in low-viscosity solution, if the time interval between the two components of the double waveform was set appropriately; with too short time interval the components simply cancelled each other out and no drop was jetted. Also, using the bipolar waveform instead of the single waveform was found to improve jettability of higher-viscosity liquids: the solution containing 70 % glycerol, which could not be jetted with the single waveform, was successfully jetted with the bipolar waveform, though, depending on sharpness of rise and fall times, satellite droplet ejection tended to occur. [102]

4.2.6 Jetting of polymer solutions

Polymer solutions provide interesting possibilities for inkjet printing, either as rheological modifiers or materials for functional printing in their own right. Due to their macromolecular nature, they can exhibit significant viscoelastic behaviour or degradation in the print head.

When used for inkjet printing, the behaviour of polymer chains under stress can have a significant effect on the jettability of the polymer solution. This is not wholly dependent on the properties of the polymer chains, but also solvent-polymer interaction. Solvents are divided into good, bad and theta quality solvents depending on how a polymer molecule behaves in a dilute solution with solvent in question. In a good quality solvent, a polymer chain expands to maximise the number of segment-solvent contacts. In a poor quality solvent, a polymer chain tries to form contact with itself or other chains to minimise interaction with solvent, while also trying to reduce unfavourable contacts between certain polymer chain segments. In a theta solvent the effects of minimising both segment-solvent and inter-segment interactions balance each other, and the polymer chain is in its unperturbed condition. [103]

In a dilute solution, the polymer chains are mostly well separated from each other, and do not interact. As the polymer concentration in a solution is increased, the solution eventually

reaches a point where the polymer coils start to overlap. This is known as coil overlap concentration c^*, and solutions with higher concentration are considered to be semi-dilute. Reduced concentration c/c^* of a solution is the ratio between the actual concentration of a solution and the coil overlap concentration for a given polymer-solvent combination. [103]

The effect of the coil overlap concentration on the printability of polymers has been studied using cellulose ester solutions. Tested solutions consisted of 30.7 kDa molecular weight cellulose ester dissolved in γ-butyrolactone, with reduced concentrations ranging from 0.32 to 3.84. These solutions were jetted with a piezo-electric MicroJet dispensing device (Microfab) at differing voltages. Drop velocities for a given signal voltage were found to be relatively independent of concentration for reduced concentrations up to 1.28, but with the two solutions with highest reduced concentrations, of 2.52 and 3.84, velocities dropped significantly. Also, droplet ligament tail rupture time was reported to increase as a function of concentration. The authors of the study suggested that as the concentration of the solution exceeds c^*, the relaxation time of the polymer molecules starts to rise due to the extended polymer chains becoming entangled with each other. Furthermore, the authors suggested that in the case of cellulose ester, some of the intra-molecular hydrogen bonds might get broken upon chain extension, leading to temporary inter-molecular crosslinking as new hydrogen bonds are formed between the extended polymer chains. [104]

Polymers can also be liable to degradation due to the stresses induced in the print head. In an experimental study, polystyrene and polymethyl methacrylate (PMMA) were dissolved in various solvents. The resulting solutions were jetted using two different devices, a Dimatix DMP-2800 inkjet printer (Fujifilm Dimatix) and a MicroJet MJ-AB-01 drop-on-demand dispensing device (MicroFab). Molecular weights of the used polymers ranged from 123 to 2 000 kDa. As a result of the study, polymer degradation was found to depend on polymer molecular weight and polydispersity index (PDi), reduced concentration of the solution and strain rate at the nozzle tip. On the MicroJet print head with 50 µm nozzle diameter and estimated strain rate of 50 000 – 100 000 s^{-1}, no degradation was observed for polymers with PDi of 1.3 or less, while the two tested polymers with PDi of 1.8 and 1.9 displayed significant reduction in molecular weight and a shift in molecular weight distribution, but only for the solutions with low reduced concentrations. For higher reduced concentration solutions, no polymer degradation was observed. If the same solution was jetted multiple times in a row, significant degradation happened only on the first pass, with subsequent jetting having only minor effect. On the DMP-2800 print head, with 23 µm diameter nozzle,

strain rate was estimated as 200 000 – 300 000 s^{-1} and polymer degradation was found to be more severe; with PMMA, degradation was observed for molecular weights of 145 – 590 kDa, and with polystyrene for molecular weights of 290 – 770 kDa. The authors of the study suggested that the polymer degradation was due to the relationship between polymer chain extension and relaxation rates, and that the viscoelastic damping present with higher molecular weights and reduced concentrations helped to prevent degradation. Another group of researchers later analysed the results of this polymer degradation. According to them, halving of the molecular weight distribution was an indicator of central scission, which can only take place if a polymer chain is fully extended. Such an event could happen either at the nozzle exit or during subsequent ligament extension, where polymers are subjected to significant strain. For the tests with the DMP-2800 print head, strain involved in ligament extension was calculated to be insufficient to result in central scission, while that in nozzle exit was sufficiently high to cause it. However, according to the same calculations, there should have been also central scission in the MicroJet print head for some of the samples, in the case where full polymer extension would have taken place at the print head. Since no such behaviour was observed, the authors suggested that, with the MicroJet print head, polymers are not fully extended when arriving at the nozzle, due to a nozzle geometry which does not feature sudden contractions. [105] [106]

Polymers present in inks can also form an isolating skin around the ink drop during flight. In one example, polystyrene dissolved in toluene or butyl acetate was jetted with an Autodrop system (Microdrop technologies) with a 70 µm nozzle diameter onto glass plates at varying heights up to 25 mm. The diameter of the droplets after drying was measured and found to decrease as a function of increasing height. This behaviour was considered to be caused by evaporation taking place during the flight. At low polystyrene concentration evaporation of solvent was seen to continue to take place for the whole duration of the flight, but as starting polystyrene concentration was increased evaporation ceased at a certain point in flight, presumably due to skinning. For 2 % by weight polystyrene dissolved in toluene evaporation ceased after 11 mm flight, while for slower drying butyl acetate similar behaviour took place in 5 % by weight polystyrene solution after 14 mm of flight. It is worth noting that the observed droplets travelled at relatively slow speeds of approximately 1 ms^{-1} and the distances between print head and substrate were relatively long; with velocities and print head heights seen in typical inkjet printers, there would not be enough time for such skinning to take place with these solvents. [107]

4.2.7 Inkjet etching

Inkjet etching works in a reverse fashion compared to that of the more conventional inkjet patterning methods described so far. Instead of simply adding material onto the substrate, it works by displacing, removing or changing material on the surface.

An early research application of inkjet etching involved using solvent drops to etch a hole through an insulating thin polymer film on a printed transistor circuit board. A solvent drop on the film surface dissolved polymer, while solvent evaporation on the drop edge induced a flow of solvent-polymer solution from the centre of the drop to the edge. As the solvent dried, polymer was deposited at the edge and a hole was left in the centre. This hole could then be used to provide a vertical interconnection between different layers of the circuit board. [108]

By printing individual drops on a surface so close that they will merge together, more complex structures than holes can be produced. By printing a simple line of closely spaced drops, a groove can be etched on a surface. [109]

For paperfluidic device design, inkjet etching can be used to dehydrophobise areas of a hydrophobic substrate selectively, forming hydrophilic channels by transporting hydrophobising agent to the edges of the channel or by delivering surfactant or reagent to form a desired channel. This naturally requires that the hydrophobising agent is present in a dissolvable form. [110]

4.3 Screen printing

Screen printing is a printing method where the ink is forced into contact with the substrate through a screen, typically made of metal or plastic. The printing side of the screen is covered by a stencil that defines the pattern to be printed: non-imaging areas of the screen are blocked, while imaging areas are left open. On the reverse side ink is fed through the screen, typically using a squeegee device, or blade of varying flexibility, to provide an application pressure when using viscous ink. [91]

Flatbed printing is a very simple method of screen printing. In this method, the printing substrate is placed on a flat surface, while stencil and screen are suspended on a frame above it. To apply ink, the squeegee is moved horizontally while other elements stay stationary. The principle of flatbed screen printing is shown in Figure 6. [91]

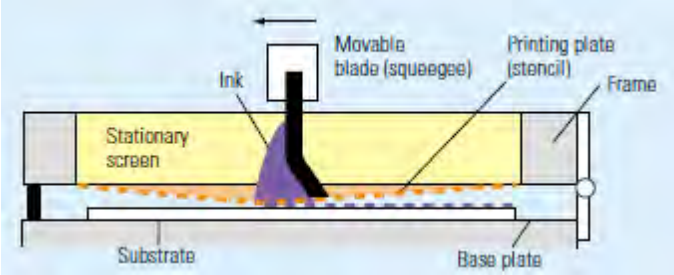

***Figure 6**. Flatbed screen printing.* [91]

On the other end of the scale, rotary screen printing provides a method suitable for high speed industrial applications. In this method the screen and stencil are formed into a rotating cylinder, with ink supply and squeegee placed stationary inside the cylinder. As the cylinder rotates on its fixed axis, ink is pushed through it onto a moving substrate on the other side. The principle of rotary screen printing is shown in Figure 7. [91]

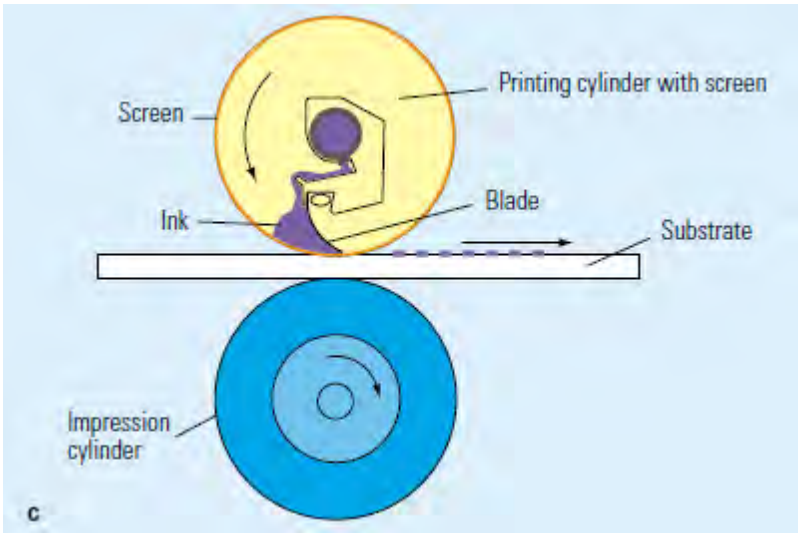

***Figure 7**. Rotary screen printing.* [91]

With screen printing, very thick ink layers can be printed on the substrate, layers 20-100 µm thick being quite normal. A very wide range of inks can be used with screen printing. Textile printing is a common application for screen printing. [91]

4.4 Flexography

Flexographic printing or flexography is a variant of the letterpress printing process, where the printing areas of a printing plate are raised above the non-printing areas. Anilox rollers, having a honeycomb-like structure of indented cells on a ceramic or hard-chromed metal

surface, are used to transfer ink from an ink supply to the printing plate. From the printing plate the ink is then transferred to the print substrate. Package printing is a common application for flexography. [91]

Flexographic printing plates are manufactured from a flexible and relatively soft material. Typical materials include vulcanised rubber and various photopolymers. Flexographic printing can be used with a wide variety of inks. [91]

So far, two reported studies have appeared in the literature concerning the use of flexography for producing paperfluidic devices. Both of these were carried out with laboratory test printing units. [82] [79]

4.5 Photolithography

Photolithography, also known as optical lithography, is a microfabrication manufacturing process. Conceptually it is essentially similar to traditional film photography: the base substrate is first covered by a photosensitive material (photoresist), after which it is exposed to UV-radiation through a photomask, and then the substrate is developed with chemical treatment to remove excess material and reveal the final pattern. Depending on the type of the resist used, the UV exposed areas become either more soluble (positive resist) or insoluble (negative resist) to the chemicals used in development. [111]

4.6 Plasma treatment

Plasma is ionised gas, i.e. gas in which the molecules have broken down into ions and electrons. It is sometimes referred to as the fourth state of matter, after solid, liquid and gas. In laboratory or industrial environment, low-temperature plasma can be created by applying a high electrical voltage to gas. Solid-plasma interactions can be divided into plasma etching or ablation (material is removed from the solid surface), plasma activation (the surface is chemically or physically modified by contact with plasma) and plasma coating (new material is deposited onto the solid surface). [112]

Plasma activation can lead to a change in the hydrophobic properties of a paper surface, but these are not necessarily permanent. The changes can be attributed to three potential causes: polar group attachment (permanent chemical change), polar group rotation (temporary rotation of existing polar groups on the surface) or plasma cleaning (temporary removal of impurities on the surface). [112]

Plasma treatment can take place either under vacuum or at normal atmospheric pressure. Maintaining a low pressure level is problematic for industrial application, due to the capital costs and need to run batch processes rather than continuous treatment. However, conventional corona discharge plasma treatment units tend to have a number of problems operating at atmospheric pressures, including having issues with paper dust. These problems can be circumvented by using instead Diffuse Coplanar Surface Barrier Discharge (DCSBD) plasma treatment. Such a plasma generation unit consists of two systems of parallel, strip-like electrodes, embedded in alumina. When a sinusoidal current with high-frequency (1-15 kHz) and high voltage (up to 10 kV) is applied to the electrodes, a plasma layer is generated from gas above the electrodes. The generated plasma layer is almost uniform and roughly 0.1 mm thick. [113] [114]

Conventional plasma treatment cannot be used to affect specific regions of a substrate selectively; rather, the whole area of the substrate passing through the plasma is exposed. However, the substrate can be covered by a photomask that leaves only selected areas exposed, resulting in a selective treatment that can be used for patterning [61]. Alternatively, in micro-plasma printing, local plasma discharges are generated selectively by metal needles moved closer to a substrate table to trigger discharges resulting from electrical potential difference between the needle and the table [115].

Plasma treatment can also be used to improve hydrophilic properties of a substrate if it has been affected by the use of antibodies and reagents that reduce its wettability. In a study using filter paper as a substrate, it was discovered that the addition of certain antibodies needed for a blood analysis test made the filter paper into a hydrophobic substrate. This effect could be reversed by subjecting the paper to vacuum plasma treatment. Ordinarily, such treatment would have deactivated the antibodies, making them useless for test purposes, but this effect was reduced to a manageable level by adding bovine serum albumin (BSA) as a protective agent to the antibodies. [116]

4.7 Laser treatment

A laser beam differs from ordinary discharge light sources by being highly coherent (i.e. emitted photons sharing single fixed wave phase) as well as monochromatic. Laser beams can also be focused to form small, intense spots. Lasers can produce either a continuous or pulsed beam. [117]

A laser beam consists of photons, with each photon carrying a discrete amount of energy. The energy *E* of a single photon is defined as:

$$E = \frac{\mathrm{hc}}{\lambda} \tag{2}$$

where h is Planck's constant, c is speed of light and λ is the wavelength of the light. [118]

For industrial application, a laser beam can be used to melt or ablate solid materials. It can also be used to modify surface properties of materials, through changes in surface roughness and surface oxidation. [117]

Recently, highly controlled low energy lasers have been used as tools in conservation of old paintings and papers. With painting conservation, the typical laser application is for the removal of aged material, such as varnish layers, while trying to avoid discolouration of the pigment layers underneath [119]. In paper conservation, laser light is used similarly to remove various contaminants from the paper surface, such as dirt and dust [120] or fungus-induced stains [121].

In a paper conservation study, lasers of 266, 355, 532, and 1 064 nm wavelengths were tested for cleaning cellulose paper. According to the results, at UV wavelengths (266 and 355 nm) laser beams damaged cellulose fibres by breaking the cellulose molecules into shorter chains. However, no damage was reported for the visible light (532 nm) or infrared (1 064 nm) laser beams. The penetration depth of the laser into the paper bulk increased with increasing wavelength, with the highest penetration estimated at 20-25 µm for 1 064 nm wavelength. [122]

Laser treatment has also been studied as a means of removing electrophotographic toner from paper as a tool for making the paper sheets re-useable. In a study using laser sources of various wavelengths, a laser beam at visible light frequency (532 nm) was successfully used to ablate toner from a paper surface without damaging the cellulose beneath, though it could result in damage to the coating layer of the single tested coated paper, Digital Color Elite Gloss (Xerox). Ultraviolet laser beams (193 and 355 nm) did not ablate toner, but damaged cellulose fibres through photo-oxidation reactions. Infrared laser beams (1 064 and 10 600 nm) ablated toner but also damaged cellulose fibre through photo-thermal degradation, causing visible yellowing. [123]

In a further study on laser-induced toner removal, a variety of laser sources with different wavelengths and pulse lengths were studied. According to this study, the ideal combination for avoiding damage to the tested wood-free copy paper was to adopt visible light wavelength (532 nm) combined with a 4 ns pulse length. Longer pulse lengths of 29 ns at the same wavelength led to fibre bonding/cohesion loss, while shorter pulse lengths of 10 ps resulted in slight yellowing of the paper. This difference between the varied pulse lengths can be explained by the differences in peak power and energy fluence (flux integrated over time) that were required to achieve good toner removal performance at various pulse lengths; short pulses required high peak power, while longer pulses required high energy fluence. 4 ns pulses provided a convenient middle ground, where good toner removal performance could be achieved with moderate peak power and energy fluence. [124]

One established industrial application of laser ablation is post-print marking. When used to mark printed pigment coated substrates, the laser beam tends to pass initially through the print layer, the energy instead getting absorbed by the coating layer beneath. This leads to the ablation of the coating organics and any print surface above it, leaving a visible light burn mark on the exposed coating layer. [125]

So far only one study appears to have been published on the use of laser treatment for patterning paperfluidic devices. This study was conducted on commercially available specially coated papers, and demonstrated that very good resolution could be achieved by a laser beam. However, the exact interactions between the laser beam and substrate were not fully studied. [85]

4.8 Other methods

A number of other methods have been demonstrated for small scale production of paperfluidic devices. These might not be useful for industrial scale production, but they can be handy for laboratory prototyping of test devices. Such methods include:

- old-fashioned pen plotter with custom built pens used to apply liquid PDMS [78],
- manual drawing, possibly with the help of stencils, has been demonstrated with wax pens [77], molten candle wax and paintbrush [62], permanent markers [87] [126] and micropipettes filled with polystyrene dissolved in toluene [127],
- contact stamping with custom-made poly-dimethylsiloxane (PDMS) stamp and commercial stone ink pad used to apply commercial indelible ink [128],

- wax patterns applied to substrates by dipping the partially masked substrate in molten wax [129], and
- paper cutting with a computer-controlled knife cutter [130], craft cutter [51] or laser cutter [57] used to produce 2D paperfluidic devices without use of hydrophobising agents – instead the air-substrate interface restricts the fluid flow to channels. Also die cutting could be used to produce such items [130].

5 Hydrophobising agents

5.1 General

With the exception of cutting, all patterning methods using an hydrophilic absorbent substrate are based on the use of a hydrophobising agent to produce hydrophobic barriers. Hydrophobising agents are chemicals that modify the surface chemistry of the substrate, either by physically adsorbing onto the substrate surface, or by chemically reacting with the substrate. In addition to the surface modification, in some cases such an agent can also prevent fluid transport by physically blocking the pores. [5]

Surface interaction between water and other materials is dominated by the polar nature of water molecules, with the two hydrogen atoms of the water molecule separated by an angle of 109º. Water molecules tend to form hydrogen bonds amongst themselves, with each water molecule bonded to four other molecules. When water comes in contact with surface of another material, the interaction is dependent on whether the polar water molecules can form bonds with the other material surface or not. Surfaces with hydroxyl or amine groups can form hydrogen bonds with water molecules, while polar compounds and charged surfaces allow the neighbouring water molecules to arrange themselves with the opposite charges aligned, making these surfaces hydrophilic. On the other hand, if the other surface is non-polar and incapable of forming hydrogen bonds, such as is case with hydrocarbons, the water molecules attempt to minimise their contact with the surface, and thus the surface is hydrophobic. [131]

If a single molecule features both hydrophilic and hydrophobic regions, it is considered to be amphiphilic. Such molecules can be useful as surfactants. [131]

The hydrophilic or hydrophobic nature of a smooth solid surface can be quantified by applying a drop of water on the surface and measuring the contact angle θ between the solid surface and the edge surface of the water drop. When $\theta < 90^{o}$ the solid surface is hydrophilic and water is said to wet the surface; in case of $\theta = 0^{o}$, water completely wets the surface. When $\theta > 90^{o}$ the solid surface is hydrophobic and no wetting takes place unless an external force is applied. [131]

Surfaces with a water contact angle larger than 150º and low contact angle hysteresis, i.e. difference between advancing and receding contact angles, are called superhydrophobic. Water drops very easily roll off from such surfaces, thus providing them with useful self-

cleaning properties [132]. Superhydrophobic paper has been demonstrated as a possible material for disposable labware [133].

With porous hydrophilic structures, the measurement of the contact angle can be tricky, as the water drop tends to get absorbed within the substrate very quickly – see section 7.2.

This chapter goes on to discuss hydrophobic agents described in previously published studies. These materials have been adapted from many different areas, including microfabrication materials, paper sizing agents, commercial polymers and various other sources.

5.2 SU-8 photoresist

SU-8 is an epoxy resin negative photoresist, typically used for photolithographic microfluidic applications in microfabrication. It is mechanically strong and transparent to visible light. It can be used for patterning using relatively thick applied layers (up to 2 mm) with vertical walls. It is also chemically stable. [134]

SU-8 photoresist has been tested for patterning 2D paperfluidic devices with two different variants of the photolithographic method and with inkjet printing.

In an early study by the Whitesides research group using SU-8 photoresist and photolithography, a rather complex manufacturing process was employed. First chromatographic paper was soaked in photo-resist, subsequently spun for 30 seconds, pre-baked for 5 minutes, exposed to UV light through a photomask for 10 seconds, baked again for 5 minutes, soaked in propylene glycol monomethyl ether acetate for 5 more minutes, and then washed with propanol. Finally, the paper was treated with oxygen plasma for 10 seconds to negate any hydrophobicity caused by resist remnants in the hydrophilic areas. No details were provided about the achievable resolution, other than a vague reference to *"well-defined, millimeter-sized channels*". [4]

In a later study by the same research group, paper was treated and patterned with SU-8 photoresist using a slightly simpler method named FLASH (Fast Lithographic Activation of Sheets). In this method, paper is first soaked in SU-8 and then dried to remove solvent. After this, the treated paper is sandwiched between an adhesive transparency sheet and black construction paper, and a pattern is printed on the transparency sheet using inkjet or electrophotographic printing. Then the paper is developed with UV-light exposure through

the patterned transparency sheet, either using a UV-lamp or natural sunlight. After this, the transparency sheet and construction paper are removed, and the treated paper is baked to polymerise the photoresist. Finally, the paper is rinsed with acetone and isopropyl alcohol to remove any soluble photoresist. With inkjet-printed patterns, UV-lamp exposure and chromatographic paper as substrate, an hydrophilic channel width of 256 ± 20 µm and an hydrophobic barrier width of 210 ± 30 µm were achievable. [83]

Inkjet printing provides a simpler means of patterning paper with SU-8. Inkjet printing has been studied in an experiment with a commercial T13 inkjet printer (Epson) used to apply inks made of different solutions of SU-8 and cyclopentane. In order to harden SU-8, printed substrates were heated on a hotplate for 5 minutes at 100 ºC, though UV-radiation is mentioned as an alternative possibility. Three different solution mixture concentration ratio levels (1:10, 2:10 and 3:10) of SU-8 were tested, with multiple barrier widths (0.5-5.0 mm) and with varying levels of over-printing (1, 2, 3, 5 and 10 times). Best results were achieved at a solution concentration mixture level of 1:10, with working hydrophobic barriers of 3 mm width being achievable with 3 rounds of printing, and 1 mm barrier width achievable with 5 rounds of printing. No working barriers were achieved with a single printing round, though 2:10 solution level did provide working barriers with 4 mm width, which could be produced with 2 printing rounds only. The study report, however, did not specify whether the reported barrier widths were nominal printed widths or final widths after hardening. [135]

5.3 Polydimethylsiloxane (PDMS)

Polydimethylsiloxane (PDMS), also known by the IUPAC name poly(oxydimethylsilanediyl), is a polysiloxane or silicone, i.e. a polymer based on silicon-oxygen chains. The basic molecular structure of PDMS is shown in Figure 8. Polysiloxanes are very stable and are highly hydrophobic, a property that can be exploited, for example, for applying water-repellent finishes to textiles. [136]

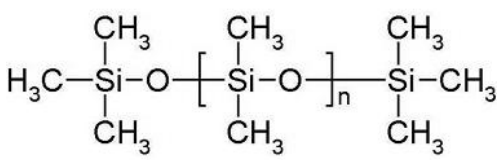

Figure 8. *The chemical structure of linear PDMS.*

Linear PDMS is manufactured from dimethyldichlorosilane. Linear PDMS is a liquid with low toxicity. It has high chemical and thermal stability. Under the influence of strong acids or bases PDMS can rearrange into cyclic molecules. Commercial applications of PDMS include rubbers, resins, water repellents, release agents and pharmaceuticals. [137]

Polydimethylsiloxane has a surface tension of 20.4 mN $\cdot m^{-1}$. PDMS chains tend to configure themselves on a surface so as to place the maximum possible number of methyl groups on the outside, resulting in highly hydrophobic surfaces. The properties of PDMS chains can be modified by replacing some of the methyl groups with other functional groups. [138]

While ordinary PDMS is liquid at room temperature, it can be hardened through cross-linking. Room temperature cross-linking can be achieved through inclusion of hydrolysable tetrafunctional silane or tetraethoxysilane. These will, respectively, result in emission of acetic acid or ethanol during the curing procedure. For high temperature curing applications partially vinyl substituted siloxane is used, with polymerisation initiated by a platinum salt catalyst at temperatures above 100 ºC. This will result in a high thermal and chemical stability. [139]

PDMS surfaces can be made hydrophilic by oxygen plasma treatment, though such effects tend to be only temporary, with PDMS reverting back to the hydrophobic state eventually. However, it has been experimentally demonstrated that briefly treating a plasma-exposed surface of PDMS with polyethylene glycol (PEG) or polyvinylpyrrolidone (PVP) can be sufficient to prevent or at least seriously slow down the reversion of the surface back to the hydrophobic state – several test surfaces so treated remained highly hydrophilic for at least six months after the treatment. [140]

Use of PDMS for patterning paperfluidic devices has been reported in two experiments, first with the use of a pen plotter [78], and later with both flexographic and inkjet printing [79].

In the pen plotter study by the Whitesides research group PDMS dissolved in hexane was used as an ink to fill custom-built plotter pens. This liquid successfully penetrated through the whole depth of the used test substrates. Resulting samples were cured for one hour at a temperature of 70 ºC. An achievable minimum width for working hydrophobic barriers was reported as being approximately 1 000 µm. [78]

In the second study by a research group from Åbo Akademi, PDMS with vinyl groups and small amounts of catalyst and crosslinker was used directly as a solvent-free ink for

flexography. The same ink was also diluted with xylene to produce an ink suitable for inkjet printing with a DMP-2800 materials printer (Dimatix). Printed samples were cured for 15 seconds in an oven at 150 ºC, though infrared drying was mentioned as an alternative and slightly faster (10 s) method. Various substrates were tested, with highly permeable uncoated substrates providing best ink penetration into the depth of the substrate. The contact angle between water and PDMS film printed on various substrates was found to vary somewhat depending on the substrate, ranging from 110º to 142º. These differences were presumed to be due to differences in the surface roughness of the printed film on various substrates. With flexographic printing, six printings were needed to produce a reliable hydrophobic barrier on the tested office copy paper, while with inkjet printing, a single printing was sufficient. This was reported to be due to the lower viscosity and surface tension of the ink used for inkjet ink, as well as due to an approximately 20 times higher volume of fluid transferred per print run. Inkjet printing was reported as being able to produce 700 µm wide hydrophilic channels, though no mention was given as to how this varied depending on the substrate used. According to the authors, both flexography and inkjet processes were considered to be effective methods for producing hydrophobic layers, with inkjet recommended for highly permeable substrates. [79]

5.4 Polystyrene

Polystyrene (PS) is a polymer of phenylethene (styrene). The basic structure of polystyrene is shown in Figure 9. It is a rigid plastic typically used for injection moulding of a vast variety of hard plastic consumer goods. Typical commercial polystyrenes have number-average molecular weights in the 50 000 – 150 000 range. Polystyrene has a good resistance to aqueous acids and bases, but can be vulnerable to hydrocarbon solvents. It is also somewhat brittle. [136]

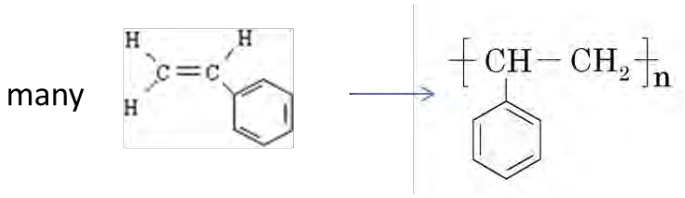

Figure 9. *The chemical structure of polystyrene.*

The hydrophobic properties of polystyrene can be affected by UV-radiation induced photo-oxidation or plasma treatment. In an experimental study, polystyrene films were exposed to

UV-light for 40 minutes and contact angles with water measured before and after. UV treatment resulted in the contact angle lowering from 96 ± 4º to 45 ± 4º. In the same study, a polystyrene film was also subjected to plasma treatment, lowering contact angle to under 10º. However, the permanence of these effects was not reported. [141]

In another experimental study, molecular level effects of UV-radiation induced photo-oxidation in polystyrene were analysed. In this work, thin polystyrene films were placed in a chamber filled with oxygen at 80 kPa and irradiated with mercury vapour lamps emitting mainly at 253.7 nm wavelength. In an analysis using a variety of spectroscopic methods, photo-oxidation was found to result in formation of at least hydroperoxides, carbonyl groups, hydroxyl groups, polymer chain scissions, carbon dioxide and water vapour. [142]

Polystyrene has been used to pattern paperfluidic devices, in one study, with manual drawing [127], in another with flexographic printing [82] and in at least two further studies using inkjet etching [110] [143].

In a study using a micropipette as a manual drawing instrument, polystyrene was dissolved in toluene and then used to pattern laboratory-made paper sheets of various thicknesses up to 273 µm. The tested solutions had polystyrene concentrations of 1, 2, 5, 10, 50 and 100 $g \cdot dm^{-3}$, respectively. A solution with 100 $g \cdot dm^{-3}$ concentration of polystyrene was reported as being sufficient for producing leak-free barriers on all of the tested paper substrates. However, when the same papers were coated with nano-fibrillated cellulose film on one side, and the pattern then drawn on the other side, the barrier was no longer entirely reliable, with water able to wick through after prolonged exposure – this was suggested to be due to hydrophilic gaps having remained between nano-fibrillated cellulose film and paper. [127]

In a study by VTT Technical Research Centre of Finland, flexography was used with an ink made out of 290 kDa molecular weight polystyrene dissolved in xylene or toluene. The test substrates used were chromatographic paper and clean-room paper, and hydrophobic barriers were successfully printed on both. However, to achieve sufficient barrier depth on the substrates at least two consequent printing runs were needed with one-sided printing. As an alternative approach, the reverse side of the paper could be printed with 100 % coverage, in which case single a print run was sufficient on the other side. With the methods used, the achieved minimum hydrophobic barrier width was 400 µm and minimum hydrophilic channel width 500 µm. [82]

In a study using inkjet etching, conducted by a research group from Keio University, Japan, filter paper was first soaked in a 1.0 wt% solution of polystyrene in toluene for 2 hours, and then dried at room temperature for 15 minutes. This made the paper hydrophobic. Inkjet etching was then carried out by a PicoJet-2000 printer (Microjet) modified to use toluene as ink substitute. A toluene droplet, thus applied, dissolved polystyrene in the area covered by the droplet, and as the droplet dried the dissolved polystyrene reformed on the edges of the droplet area in a coffee-stain fashion, leaving the centre of the droplet area free of polystyrene and thus again hydrophilic. This method produced hydrophilic channels of approximately 450 ± 50 µm in width. However, to produce reliably working hydrophilic channels, etching had to be repeated 10 times for the whole paper sheet, thus making the procedure, though elegant in concept, rather time consuming. [110]

In another later study by the same group, a similar approach was used with 1.8 wt% solution of polystyrene in toluene, with etching carried out 9 times instead of 10 in the previous case. In this study it was also found to be necessary to print the used immune-sensing inks on the hydrophobic surface before the etching of the hydrophilic patterns. This provided for sharper control and test lines than printing the inks on the hydrophilic channels, where they would have spread out more before drying. [143]

In this literature study, no mention was found of previous application of inkjet printing polystyrene for patterning paperfluidic devices. However, some studies have been previously carried out on the inkjet printing of polystyrene-solvent solutions for other purposes.

In a study using piezo-actuated AutoDrop micropipette (Microdrop GmbH) as an inkjet printer, monodisperse polystyrenes ranging in molecular weight from 64 000 to 2 530 000 Da were dissolved in various solvents to form inks. The maximum printable polymer concentration was found to be heavily dependent on the molecular weight of polystyrene used. With acetophenone used as solvent, the maximum printable concentration for the polystyrene with lowest molecular weight was approximately 5 % by weight, while for the polystyrene with highest molecular weight it was 0.025 % by weight. Authors suggested that this reduction in printability is due to elastic stresses taking place in the print head. [144]

Due to the viscoelastic character of polystyrene-solvent solutions, mere low shear rate viscosity measurement provides insufficient information about their jetting behaviour. In an experimental study, viscoelastic properties of polystyrene and diethyl phthalate solutions were measured with a piezoaxial vibrating rheometer at 5 kHz frequency in an effort to

model the effects of viscoelastic properties on jetting. Tested solutions consisted of mixtures of either 24 and 110 kDa polystyrene, or 75 and 210 kDa polystyrene, and had low shear rate viscosities in the 17.5-20.7 mPas range. Solutions were jetted using an XJ126-200 piezoelectric print head (Xaar) with drop velocity set to approximately 6 ms^{-1}. In rheometrical measurements, no viscoelastic behaviour was observed for the pure solvent, while for polystyrene solutions the measured elasticity ratio $G'/|G^*|$, where G' is the elastic modulus, G'' the viscous loss modulus, and G^* the complex modulus ($|G^*|^2 = G'^2+G''^2$), was found to rise almost linearly as a function of the concentration of the higher molecular weight polystyrene component in the solutions. Increasing elasticity ratio was also found to correlate with increasing drop detachment time and increasing drive amplitude needed to achieve the desired drop velocity. [145]

On the other hand, the impact and spreading of a polystyrene-containing drop on a substrate seems to be largely unaffected by the viscoelastic properties. In an experimental study, this was tested by dissolving effectively monodisperse polystyrene of 110, 210 and 488 kDa molecular weights in low concentrations (up to 0.2 % by weight) in diethyl phthalate and jetting the solutions with a Spectra SX3 print head (Fujifilm Dimatix) on indium tin oxide coated glass. The presence of even small amounts of polystyrene in the solutions was sufficient to produce long tailing filaments that resulted in satellite drop formation. However, the presence of polystyrene in solution had no significant effect on the impact or spreading behaviour, which was effectively the same for pure solvent and for all polystyrene-containing solutions. The authors suggested this to be due to the inertial forces dominating over elastic stress in the early phases of the impact, while solvent viscosity and surface tension dominated over the elastic stress at later phases. [146]

5.5 Wax

Use of wax for patterning paperfluidic devices has been widely studied with many different methods. Published studies cover simple drawing of patterns using a wax pen, wax crayon or lipstick [62] [77], dipping a masked substrate in molten wax [129], using a simple screen printing process with wax [147], using an etched copper sheet as wax-patterning master [148], laser treatment of a wax covered substrate [85] and several studies with hot-melt wax inkjet printing [38] [75] [77] [149]. With the exception of the dipping, all of these methods have one thing in common: wax is first applied to the substrate surface, and after this the substrate is heated for a few minutes so that the wax becomes liquid and penetrates into the bulk of the substrate.

In a study by a group of researchers from Chulalongkorn University, Thailand, on the use of wax dipping for prototyping paper areas that were to form hydrophilic channels were first covered by a simple metal mould, after which the whole mould was dipped in molten beeswax. With wax at 125 ºC dipping for one second was found to be sufficient to hydrophobise the exposed paper surfaces, while the areas protected by the mould remain hydrophilic. Once the wax on the dipped paper surface has cooled down, the metal mould can be removed for re-use and the microfluidic device is ready to receive reagents. Compared to other methods dealing with wax, this method has the advantage of needing only one quick manufacturing step. This method can be used to produce hydrophilic channels down to 639 ± 7 µm in width. [129]

Screen printing with wax has also been studied by the researchers from Chulalongkorn University. In this rather simple method, candle-making wax is manually rubbed onto the surface of the substrate through a screen printing stencil and screen. Afterwards wax-treated filter paper was heated on a hot plate at 100 ºC for 1 minute to allow wax to penetrate the whole depth of the substrate. This manufacturing process is illustrated in Figure 10. The heating resulted in significant line spreading of the wax, with the final barrier width for this method being estimated as

$$W_{RB} = 1.081\, W_{PB} + 1\,136.3\ \mu\text{m} \quad (3)$$

where W_{PB} stands for original printed barrier width and W_{RB} for the final result barrier width. The achieved minimum width for a working hydrophilic channel was 650 ± 71 µm, and for a working hydrophobic barrier 1 300 ± 104 µm. [147]

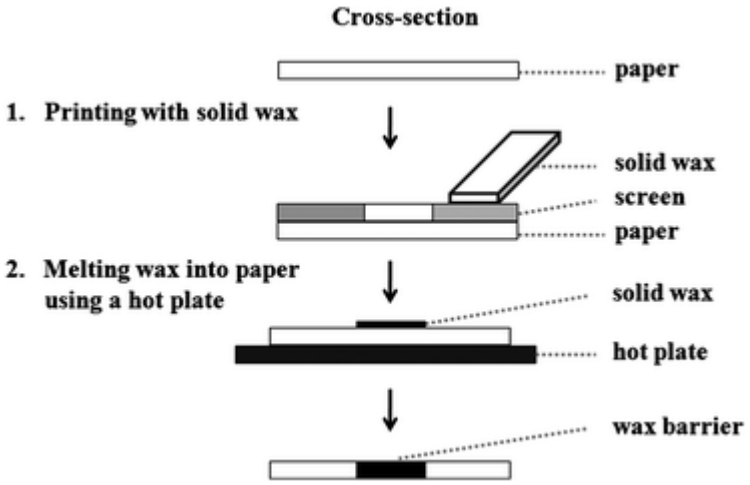

***Figure 10**. Screen printing patterns with wax*. [147]

Etched copper sheet has been used as a master for wax-patterning filter paper by a research group from Ningbo University, China. An etched copper sheet was manufactured by printing the pattern on a sheet of ordinary transfer paper, and then using a thermal transfer printer to transfer the pattern with carbon powder onto a 0.3 mm thick copper sheet. The copper sheet was then dipped in ferric trichloride solution, until the areas left uncovered by the carbon powder had been etched through. The resulting copper sheet patterning master was then finished by washing and drying. To pattern paper, the copper sheet master was covered with paraffin wax and placed upon a piece of filter paper. An electric iron was then placed upon the copper sheet master and heated to make the paraffin melt and penetrate into the filter paper to form hydrophobic barriers. The authors suggested using an oven as an alternative means of melting the paraffin wax. What the authors failed to mention in their report, is that the physical nature of the copper sheet restricts the pattern complexity that can be feasibly achieved with this method. [148]

Inkjet printing with hot-melt wax has been studied by several research groups. In a study carried out by the Whitesides research group, a commercial Phaser 8560N printer (Xerox) was used to print wax patterns on the paper surface. Initial printing of hydrophobic barriers was then followed by heating the paper on a hot plate at 150 ºC for 2 minutes to enable the wax to penetrate the whole depth of the paper. Due to the spreading of molten wax both laterally and horizontally, the barrier width was found to be different on the front face (where the barrier was initially printed) than on the rear face where it had reached by penetration, with the barrier on the front face being wider. The smallest functional hydrophobic barriers produced this way had a width of approximately 850 ± 50 µm, achieved by printing an initial pattern nominally 300 µm in width. The smallest working hydrophilic channels were found to be 561 ± 45 µm wide. The produced hydrophobic barriers were found to have no barrier effect on the flow of organic solvents, indicating that the barrier properties were due to changes in pore surface chemistry rather than from blocking of the pores. The authors of the study considered wax-printing to have potential for industrial manufacturing of assays, when combined with an oven for the heating step, and conventional inkjet printing for applying reagents needed for the assays. [149]

Another study using a similar printer to pattern substrates was carried out by researchers from the Chinese Academy of Sciences, and this study produced similar results. Furthermore, the heat stability of such patterned paper was tested. The wax-printed patterns were found to remain stable when stored at 60 ºC for 30 minutes. This was taken to indicate

that wax-printed products could be stored for extensive time periods in such conditions if necessary. [77]

In another study by the same research group from the Chinese Academy of Sciences, wax-printing was used to pattern a nitrocellulose membrane. The small pore size of the NC membrane was found to result in the forming of a reduced line spread compared to filter paper, with the line spread for one side of the barrier estimated at 86 µm for parallel-printed microchannels and 118 µm for vertically printed microchannels – note that this is for one side of the barrier only, with the total barrier width spread being twice as much. The barrier spread was found to be essentially the same regardless of the nominal barrier width. Hydrophilic channels down to 100 µm and hydrophobic barriers down to 260 µm could be produced, indicating superior resolution compared with the same method used on filter paper. Reasons for the differences in the spread of laterally and vertically aligned barriers were not discussed in the study, but they could be attributable to the difference in paper structure between machine and cross-machine directions. [75]

In a more recent study, a commercial ColorCube 8870 wax printer (FujiXerox) was used for patterning filter paper. In this study, printing with differently coloured waxes (cyan, magenta, yellow, black) was compared, and these waxes were found to vary in the extent of line spreading they displayed both after initial printing and after heating to spread the wax. Yellow wax was found to have the lowest spreading in both aspects, followed by cyan and black, with magenta having highest spreading. Interestingly, high spreading was found to correlate with low nominal width needed to produce working barriers, though no explanation was offered for this by the authors. This phenomenon might be explained either by differing wax properties or maybe by print head designed for depositing drops of different size for different waxes. Finally, the authors mentioned that the contents of these printer waxes are supposed to be polyethylene and fatty amine waxes (50 - 60 %), resin (10 - 20 %) and dye (up to 5 %), with exact compositions being proprietary information, though no source reference was provided for this information. [38]

In another study featuring a ColorCube 8870 printer (FujiXerox) and Whatman chromatography paper grade 1 (GE Healthcare), effects of both line width and heating conditions on wax penetration were evaluated. Line widths of 300 µm or more were found to be sufficient to form reliable hydrophobic barriers, with narrower lines resulting in insufficient depth penetration when heated. On the other hand, cross-sectional studies also revealed that in the case of the widest tested lines (900 and 100 µm in width) some wax still

remained deposited on the printed surface, forming a clearly visible bulge. Two different heating methods, an Ecotherm model 22 oven (Labotec) and a StableTemp DLM-51806-15 hot plate (Cole Parmer), were tested, with the hot plate found to provide better results due to direct contact with the paper. Various hot plate temperatures from 50 ºC to 250 ºC were also tested. For line widths of 300 µm or more, 100 ºC was found to be sufficient for a 1 minute treatment, with increasing temperatures providing no improvement of penetration. [150]

As an alternative to commercial wax printers, a research group from Nanjing University of Science and Technology (China) has constructed a simple custom wax-printing unit, consisting of a borosilicate glass tube, a piezoelectric actuator, heating coils to melt wax and a moving stage to hold a substrate. This system was used to jet paraffin wax, screened to remove solid particles, on filter paper. Printed samples were treated at 75 ºC for up to two minutes to re-melt the wax and to allow it to penetrate into the paper. [151]

5.6 Alkyl ketene dimer (AKD)

Alkyl ketene dimers (AKD) are waxy, water-insoluble solids that are used as paper sizing agents in paper production. AKD is derived from a mixture of palmitic (C16) and stearic (C18) fatty acids. Depending on the used fatty acid blend, the melting point can vary between 42 and 55 ºC. [152]

Sizing agents are paper chemicals that slow down or prevent penetration by wetting of polar liquid, usually water, into the final paper product. When used for internal sizing of paper, sizing agents are added to the slurry furnish as part of the paper machine wet-end chemistry. As the paper is dried, the sizing agent spreads over small regions of the fibre surfaces and bonds to them. This spot hydrophobising effect acts to pin the wetting front and so prevents the progress of the water into the bulk structure. [153]

AKD can react with cellulose hydroxyl groups and form β-keto esters on the cellulose surface, thus making cellulose hydrophobic. It can also react with water, forming a ketone that is no longer capable of reacting with cellulose. Both of these reactions are shown in Figure 11. When used as a sizing agent, AKD tends to spread quite evenly over the surface of cellulose. [154]

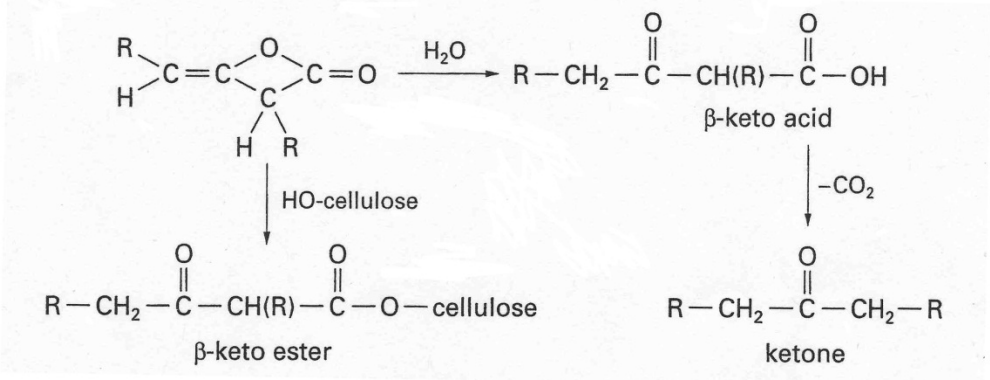

Figure 11. *AKD can react with cellulose to form β-keto ester, or with water to form β-keto acid, which spontaneously decarboxylates into ketone* [155].

The degree of hydrophobicity of AKD sized paper can be modified by plasma treatment. In a study using ambient atmospheric air and DCSBD plasma treatment on AKD sized paper, a quick 0.5 s treatment was sufficient to reduce the contact angle between paper and water from 120º to 55º. Longer 5 second exposure reduced the contact angle to 15º, while still leaving the reverse (untreated) side of the paper almost unaffected. [113]

Permanence of plasma treatment induced changes on AKD sized papers have been reported in another study, in which paper was treated with oxygen plasma at 75 Pa pressure. This study was conducted on cellulose-based paper, with approximately 10 % AKD and "*a few % of $CaCO_3$*". In this study just a 1 s exposure to plasma was sufficient to change the paper from hydrophobic to hydrophilic. Permanence of the treatment was tested by storing the paper for a month at room temperature, with no significant changes observable. According to the authors, the initial changes in the hydrophobicity were due to oxygen ions in the plasma reacting with surface AKD and causing its degradation during the first seconds of plasma treatment, while extended treatment led to the AKD in the bulk of the paper migrating to the surface and evaporating. However, for AKD (or actually β-keto esters) to be able to migrate in the substrate the bonds binding them to cellulose would first need to be broken. Thus, if any actual AKD migration from the bulk of the paper actually took place, it is more likely to have been AKD scavenged by the $CaCO_3$, in the case where it was precipitated calcium carbonate, or excess AKD associated with the bound ester sites, and held there by surface tension. [156]

Hydrophobic patterning of paperfluidic devices with AKD has been reported in several published studies by researchers at the Australian Pulp and Paper Institute, Monash

University. The first of these studies deals with selective plasma treatment of AKD treated paper [61], while the later ones deal with applying AKD selectively to the substrate by inkjet printing [15] [157] [158].

A plasma treatment study featured as substrate a filter paper that was dipped in a solution of AKD dissolved in analytical grade n-heptane in order to hydrophobise the paper entirely. After this treatment, the paper was dried and then placed in an oven at 100 ºC for 45 minutes to cure the AKD. Hydrophilic patterns were then created on the paper by exposing in a vacuum plasma reactor for 15 s under 60 Pa pressure with the paper covered by a metal photomask. The areas left uncovered by the mask, and thus exposed to the plasma, were reported to have become highly hydrophilic, though no explanation for the reasons behind this change were provided. Due to the nature of plasma treatment, plasma over-etching resulted in the paper having wider hydrophilic channels than patterned in the original photomask: 1 mm wide lines on the mask resulted in 1.5 mm wide channels on the paper. The authors reported that one of the advantages of this method is the possibility to integrate valves, switches and other simple mechanisms into the substrate – however that is not actually unique to this method, but applies equally to any other method where the substrate is initially fully hydrophobised followed by selective hydrophilic treatment. [61]

In the first study using inkjet printing, alkyl ketene dimer and similar alkenyl ketene dimer were dissolved in analytical grade n-heptane. The resulting solution, containing 2 % AKD by volume, was printed on filter paper using a commercial inkjet printer, and resulting samples were heated in an oven at 100 ºC for 8 minutes to cure the dimer. This resulted in printed areas having a contact angle of over 110º with water. The possibility of printing water-based sizing emulsion was also mentioned but not further explored – possibly due to spontaneous hydrolysis of AKD with water making such an emulsion inherently unstable. [15]

In a second inkjet study, 5 % by volume AKD-heptane solution was printed using a reconstructed commercial Pixma ip4500 inkjet printer (Canon). Using Whatman filter paper 4 as substrate, channels down to approximately 300 µm width could be printed. However, the channels were found to be non-uniform in their width: a channel of 500 µm nominal width was found to be actually 475 µm wide on the printing side and 667 µm wide on the reverse side. This was due to horizontal spreading and reduced vertical penetration at the edges of the barriers. [157]

In a third inkjet study, 3 % by volume AKD-heptane solution was printed using the same Pixma ip4500 printer. Kinematic viscosity of the solution was reported to have been 0.506 cSt ($0.506 \cdot 10^{-6}$ m^2s^{-1}) and surface tension 19.90 mNm^{-1} at 25 ºC. [158]

5.7 Acrylic polymers

Acrylic spray lacquer has been demonstrated as another simple and commercially available tool for selective hydrophobisation of filter paper. Such spray dries quickly to form a transparent and water-resistant coating. In an experimental study, filter paper was sandwiched between a magnetic sheet and a laser cut iron painting mask, and spray lacquer was applied to hydrophobise the areas left exposed by the mask. Both matte and glossy sprays were tested, with the glossy spray discovered to provide more uniform results. Also two different filter papers, with 11 µm and 20 - 25 µm particle retention ratings were tested, with the latter found to provide more uniform results. Finally, also paint lacquer applied by brush was tested, but was found to be unsuitable due to uncontrolled spreading of the lacquer on paper. [159]

Acrylic polymers have also been used for hydrophobic patterning with inkjet printing. In one experiment, a solution consisting of 20 % unspecified acrylic polymer in dipropylene glycol methyl ether acetate was printed with an SLT0505-HKF inkjet printer (SIJ Technologies) onto a nitrocellulose membrane. The minimum effective barrier width was found to be 120 µm. An interesting discovery, mentioned earlier elsewhere, and revealed by scanning electron microscope of printed cross-sections, was that the used solvent partially dissolved nitrocellulose, leading to a significant compression of the substrate on printed areas. [76]

5.8 UV-curing polymers

Polymerisation is a process where small molecules (monomers) link together to form much larger macromolecules (polymers). As the polymerisation process advances, the physical properties of the polymer molecules change as a function of increasing molecular mass. [136]

UV-curing inks used for printing are stable under ordinary conditions. However, when exposed to high energy ultraviolet light, the photoinitiators contained within the ink fragment into free radicals, which start a polymerisation process. This leads to the ink turning from liquid into solid as the polymer chain length increases. The advantage of such a printing

process is that there is no liquid carrier that would need to be evaporated, and thus no need to deal with solvent vapours. [160]

Use of UV-polymerising inkjet inks for patterning paperfluidic devices has been extensively studied by researchers from Keio University in a number of published studies. These were first demonstrated in a study using an unmodified EPSON PX-101 inkjet printer with refillable ink cartridges, Lightningcure LC-6 UV spot light source, filter paper with 1 µm pore size and polymerisable ink. The ink used consisted (by weight) of 59.5 % monomer (octadecyl acrylate), 25.5 % cross-linker (1,10-decanediol diacrylate) and 15 % photoinitiator (benzyldimethylketal). The selected pattern was simply printed onto the filter paper, after which the resulting print was subjected to UV-light at 600 $mWcm^{-2}$ intensity for 60 s to polymerise the ink. To ensure sufficient depth of barriers, one side of the paper was first printed with 100 % coverage, and then the desired pattern was printed on the other side. With the chosen method, 1 000 µm was determined to be the minimum width for a reliable hydrophobic barrier. [161] [74]

In a later report by the same research group, hydrophilic channels 272 ± 19 µm wide were achieved. Working hydrophobic barriers were achieved when nominally 200 µm thick barriers were printed, resulting in a final barrier width of 425 ± 26 µm. Testing the barrier properties with various liquids indicated that the hydrophobic effect produced was due to surface modification of the paper, rather than physical blocking of the pores. [67]

A UV-curing polymer mixture consisting of acryloxy-terminated siloxane polymer and acrylate based polymer, both commercially available and incorporating photoinitiators, has also been demonstrated as a possible patterning agent with photolithography. Approximately 30 $µl \cdot cm^{-2}$ (300 cm^3m^{-2}) of the polymer mixture were needed to saturate a filter paper completely. For patterning, a piece of filter paper saturated with polymer mixture was exposed through a photomask to 50 $mWcm^{-2}$ UV light for 1.1 s to initiate crosslinking of the two different polymers into a co-polymer. Finally, any non-crosslinked polymer was removed from paper by rinsing with acetone. Reported minimum working channel width was reported to be 90 µm, and minimum barrier width 250µm. [50]

Cyclised polyisoprene (SC) derivative diluted with xylene has been demonstrated as another UV-curing polymer suitable for photolithography in a study featuring microzone paper plates with paperfluidic properties. The manufacturing process involved soaking paper sheets in 10 % SC solution, drying them to evaporate the xylene solvent, exposing the sheets to UV light

through a photomask, and finally rinsing off the non-polymerised SC with xylene and methanol. Due to SC becoming opaque during the photopolymerisation process, mere UV exposure from one side was not sufficient to polymerise material through the whole depth of the sheet. Thus, each side needed to be exposed separately to UV light for 30 s. [84]

5.9 Silicone and polymer paper coatings

Hydrophobic silicone and polymer coated speciality papers have been reportedly made selectively hydrophilic by laser-induced surface chemistry changes. In a study using a commercial Professional series (Universal Laser System, Inc.) CO_2 laser cutting and engraving system, operating at a power level of 18 W and at maximum speed of 2 ms^{-1}, this method was successfully used to modify such papers. Laser treatment provides good resolution, with features of approximately 62 ± 1 µm width being possible. With silicone coated papers, laser treatment changed the contact angle between water and paper from 115º to 20º. However, while the surface could retain water, it did not provide for lateral diffusion of water. This could be circumvented by treating the paper with silica, which adhered to the hydrophilic channels, thus forming a pseudo coated channel product. Un-adhered silica was removed from hydrophobic regions simply by shaking the substrate after it had been dried. [85]

5.10 Trichlorosilane

Vinyl-terminated trichlorosilane has been used in one study to hydrophobise entirely a paper substrate, followed by selective hydrophilisation. This hydrophilisation was achieved by applying 6-mercapto-1-hexanol to the paper and exposing paper to UV-light through a photomask. This resulted in reaction between 6-mercapto-1-hexanol and the vinyl-groups of the trichlorosilane in the exposed areas, thus introducing hydrophilic hydroxyl groups to the surface to form hydrophilic channels. However, this whole manufacturing procedure was rather time-consuming. Firstly, the paper sheets were soaked in trichlorosilane solution for two hours, then rinsed with ethanol for 30 minutes and air-dried. After this 6-mercapto-1-hexanol was applied to the paper, and the paper and photomask were placed between glass plates and exposed with UV-light for 240 seconds. Finally, the sheets were again washed with ethanol and dried on a hotplate. [56]

In another study, commercially available octadecyltrichlorosilane (OTS) was used to hydrophobise filter papers, followed by selective dehydrophobisation by UV-light exposure. The manufacturing procedure involved soaking a filter paper sheet in 0.1 % by volume

solution of OTS in n-hexane for 5 minutes to bond OTS covalently with cellulose fibres, followed by rinsing with n-hexane and ethanol, and then drying the sheet under a stream of nitrogen gas. This resulted in the paper surface developing water contact angles of 125-130º. Finally, the paper sheet was placed under a quartz photomask and exposed to photogenerated ozone and 254 nm wavelength UV-light at 35 $mW \cdot cm^{-2}$ for 90 minutes, making the exposed areas again highly hydrophilic. This method could achieve working hydrophilic channel widths of 233 ± 30 µm and working hydrophobic barriers of 137 ± 21 µm. The generated patterns were very stable, remaining unaffected by either 6 month storage at room temperature, 24 h immersion in various organic solvents, or mechanical bending and folding. As a drawback of the material, the authors mention that OTS can react with water to produce flammable, toxic and/or corrosive gases, thus appropriate care needs to be taken during the manufacturing process, and the raw material should be stored away from high levels of moisture. Presumably OTS that has reacted with cellulose displays no such behaviour. [162]

5.11 Poly(o-nitrobenzyl methacrylate)

Poly(o-nitrobenzyl methacrylate) (PoNMBA) has been used as hydrophobising agent in a study that demonstrated a somewhat unconventional solvent-free method for patterning. In this work, initiated chemical vapour deposition in a custom designed reaction chamber was used to deposit a layer of PoNMBA on chromatography paper, resulting in the paper surface having water contact angles of 116-118º. For patterning purposes, the paper sheet was then exposed to handheld UV-light through a photomask for one hour, resulting in conversion of PoNMBA in exposed areas into poly(methacrylic acid) (PMMA). The paper sheet was then soaked in pH 8 solution for 15 minutes to remove PMMA, and afterwards air dried for one hour. This resulted in the exposed areas becoming again hydrophilic through the entire depth of the substrate. [163]

When combined with another hydrophobising agent to form the main hydrophobic barriers, PoNMBA can be used to pattern UV-sensitive valves controlling access into hydrophilic channels. For this end, a substrate is first treated with PoNMBA and then exposed through a photomask as above, leaving only the valve areas hydrophobic. Actual barriers are then constructed using another hydrophobising agent, such as wax. Valves can then be activated by exposing the device to UV light, with no photomask needed at this point. Exposure time needed to switch a valve would be one hour if using a similar UV-light source as in the previously mentioned study, though this could be speeded up by using a more powerful light source. [164]

The use of a UV-laser has not been mentioned as a patterning tool for PoNMBA-treated substrates, though it might result in significantly faster production times, and remove the need for using separate photomasks.

5.12 Other materials

Permanent markers have been successfully used as a rapid prototyping method to plot patterns manually on paper with the help of a guiding stencil. Permanent marker ink typically consists of a mixture of colorant, hydrophobic resin and solvent, typically ethanol. Upon contact with paper, the permanent marker ink dries rapidly, leaving a hydrophobic barrier. However, the resulting pattern can be vulnerable to exposure to organic solvents that can dissolve the resin. [126]

Commercial indelible ink, Lumocolor Permanent Universal Black Ink (Staedtler Mars GmbH), diluted with ethanol and n-propanol, has been reported to produce successful hydrophobic barriers, featuring contact stamping as an application method. Two other commercial indelible inks were also tested in the same study, but these could not produce sufficiently reliable hydrophobic barriers. [128]

An hydrophobic barrier, consisting of methylsilsequioxane formed by inkjetting a solution of methytrimethoxysilane and hydrochloric acid dissolved in ethyl alcohol, has been documented. However, no details were provided of the required barrier widths for this material needed to maintain integrity against penetration. [35]

Alkenyl succinic anhydride (ASA) is another common paper sizing agent. In a reported study, 10 % solution of ASA dissolved in hexanol was used to treat chromatographic paper hydrophobically using a commercial piezo-electric Workforce 30 inkjet printer (Epson). After printing, paper sheets were cured for 5 minutes at 175 ºC on a laboratory hot plate. [165]

Inkjet printing with a commercial printer using solvent-based ink has been used to produce hydrophilic patterns on the surface of superhydrophobised cartridge paper sheets. The remaining unprinted surface had a contact angle of approximately 156º, while the same surface printed with black ink, using 100 % coverage, had a contact angle of approximately 30º. For intermediate halftone levels, the contact angle decreased roughly linearly as a function of coverage. The experiment in question was conducted using a commercial Stylus SX105 printer (Epson), applying commercial solvent-based inks designed for this printer

supplied by the same manufacturer. Also, the purpose of the study was to produce an open air paperfluidic device, where the fluid would travel on patterns on the paper surface, rather than through wicking within the bulk of the paper. However, with a more porous paper, a similar approach might work for selective dehydrophobising of pore surfaces. [166]

6 Patterning resolution

Two commonly used parameters for characterising the resolution of different patterning techniques are minimum working channel width and barrier width. However, there are also other parameters that can be used to characterise paperfluidic patterning methods, such as barrier spread (difference between nominal printed and final barrier width) and barrier edge roughness.

Minimum working channel width indicates the narrowest average channel width where fluid is still able to flow. Channels narrower than this have localised sections where fluid is not able to pass, due to some of the hydrophobising agent used to produce barriers having spread too much and locally blocking the channel. Minimum working channel width can be experimentally tested by printing a simple 2D paperfluidic device containing an application zone and a number of channels of different nominal widths leading away from it. A small amount of coloured liquid, sufficient to saturate the complete test wicking area, is dropped on the application zone, after which the wicking of liquid into the radiating channels is visually tracked to indicate the narrowest channel where the fluid travels to the end of the channel. Afterwards the real widths of the channels can be measured by microscope imaging.

Minimum working barrier width indicates the narrowest barrier that can reliably stop liquid from passing through it. Barriers narrower than this contain localised sections that let fluid leak through it. Minimum working barrier width can be experimentally tested with a setup that is rather similar to that used for measuring minimum channel width: a paperfluidic device with an application zone and a number of channels leading out of it is printed. However, instead of allowing liquid to travel freely from the application zone to the channels, barriers of different nominal widths are printed between the application zone and the channels. Examples of such test designs are shown in Figure 12. Again, to test the design, coloured liquid is applied to the application zone and the channels are visually observed; if liquid passes through a barrier into the channel beyond, then that barrier is deemed not working. The narrowest barrier that consistently does not let liquid through is defined as having the minimum working barrier width. Once again, the real width can be measured with a microscope imaging system. The difference between measured and nominal barrier width can then be used to calculate barrier spread in the manufacturing process.

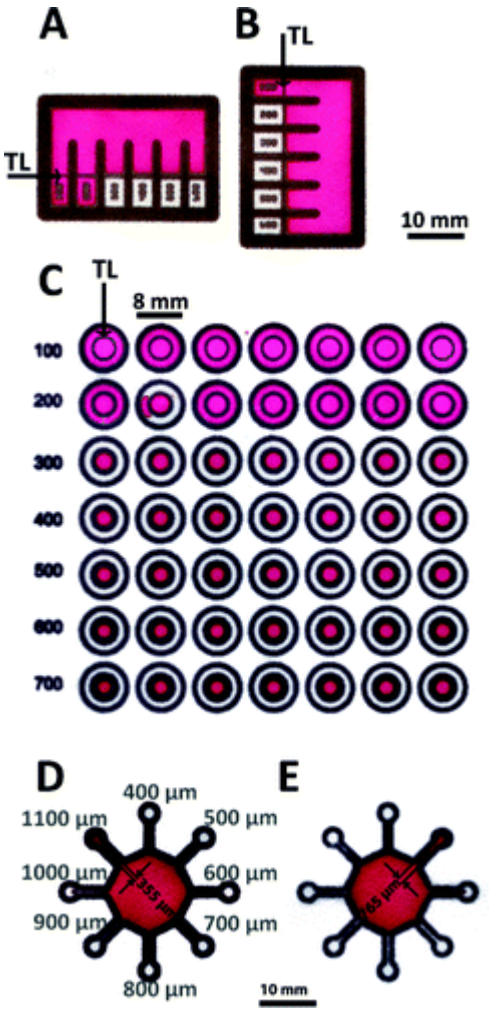

Figure 12. *Various test patterns for measuring resolution: (a) horizontal barriers, (b) vertical barriers, (c) circular barriers, (d) and (e) hydrophilic channels at various angles*. [149]

Minimum working barrier and channel widths play a number of controlling roles in the design of a paperfluidic device. Firstly, they determine the amount of parallel channels that can fit within a given substrate area. Secondly, barrier width affects the volume of hydrophobising agent that needs to be applied to produce a barrier. Thirdly, channel width affects the minimum amount of fluid sample that is required to travel through a channel. Fourthly, minimum channel width also plays a role in determining how many times a channel can be narrowed down to speed up lateral wicking.

Minimum working channel and barrier widths are affected by the choice of hydrophobising agent, patterning method and base substrate. Values reported in different studies for these have been collected in Table 1. However, these values should be viewed critically, since, so

far, there is no exact established standard for testing these properties, and thus the testing set-ups can vary slightly from one study to another. More importantly, some of the studies report nominal rather than actual widths, while other studies feature multiple different substrates but fail to specify for which substrate the reported value was measured. Finally, in some cases the barriers and channels may have different widths depending on whether they are measured from the front (printed) or reverse side of a substrate. In any case, these values provide a general impression about dimensions readily achievable with paperfluidics. Compared to sophisticated microfabrication methods, which can easily produce channel widths measured in tens of µms, paperfluidic channels may appear large and crude. However, they are not intended to compete in fine detail, but in simplicity and affordability.

Table 1. Patterning resolutions reported in studies. Channel and barrier widths indicate the width of narrowest working channel/barrier. Dash (-) indicates that no value was reported.

Hydrophobic agent	**Patterning method**	**Substrate**	**Channel width** / µm	**Barrier width** / µm	**Source**
SU-8	Photolithography	Chromatography paper	256 ± 20	210 ± 30	[83]
SU-8	Inkjet	Filter paper	-	1 000	[135]
PDMS	Plotting	Various	-	1 000	[78]
PDMS	Flexography	Various	-	-	[79]
PDMS	Inkjet	Various	700	-	[79]
Polystyrene	Inkjet etching	Filter paper	450 ± 50	-	[110]
Polystyrene	Flexography	Chromatography paper	500	400	[82]
Wax	Dipping	Filter paper	639 ± 7	-	[129]
Wax	Screen printing	Filter paper	650 ± 71	1 300 ± 104	[147]
Wax	Inkjet	Chromatography paper	561 ± 45	850 ± 50	[149]
Wax	Inkjet	Nitrocellulose	100	260	[75]
AKD	Plasma treatment	Filter paper	1 500	-	[61]
AKD	Inkjet	Filter paper	300	-	[157]
UV-curing polymer	Inkjet	Filter paper	272 ± 19	425 ± 26	[67]
UV-curing polymer	Photolithography	Filter paper	90	250	[50]
Octadecyltri-chlorosilane	Photolithography	Filter paper	233 ± 30	137 ± 21	[162]
Acrylic polymer	Inkjet	Nitrocellulose	-	120	[76]
Silicone coating	Laser treatment	Silicone paper	62 ± 1	-	[85]

7 Fluid transport in paperfluidic devices

7.1 General

The primary mechanism adopted for liquid transport in a paperfluidic device is through wicking caused by capillary pressure within pores. For a liquid to be wicked by a substrate, the liquid needs to be capable of wetting the substrate surface, meaning that the contact angle between the liquid and substrate needs to be less than 90º.

The rate of liquid wicking in a porous medium is affected by physical properties of both transported liquid and the transporting medium. Unless the device is isolated from the environment, evaporation of the liquid may take place, with the rate of evaporation depending on external factors of temperature and vapour pressure (humidity in the case of water). Besides evaporation, there can also be other dynamic phenomena taking place in the medium itself during wicking, such as swelling of the medium through liquid absorption or de-bonding of the substrate matrix in the presence of the liquid. The wicking liquid on the other hand may experience a change in viscosity due to evaporation-induced or substrate adsorption-induced changes in solution concentration.

This chapter sets out to cover in closer detail the theory and experimental work related to wicking in porous media. This is of twofold interest in paperfluidics. Firstly, it can help to explain how a hydrophobic ink penetrates into a substrate to form hydrophobic barriers. Secondly, it can explain how a liquid sample wicks along a hydrophilic channel, and what factors can be identified to explain differences in wicking speed between different substrates.

7.2 Fluid properties

Viscosity η is the property of a gas or liquid which acts resist flow, comparable to internal friction. For fluids, viscosity usually decreases as a function of temperature. For example, pure water has viscosity of 1.00 mPas at 20 ºC and 0.47 at 60 ºC. For solutions, relative viscosity η_r of the solution is defined as the ratio of the viscosity of the solution to the viscosity of pure solvent. [167]

Surface tension or energy γ of a fluid defines the resistance of the fluid towards extension of surface area, expressed in terms of the energy required to initiate extension of the surface per unit surface area. Alternatively, surface tension can also be expressed as the force needed to extend the length of an interface contact line between the liquid and another material, such as

air or its own vapour, or a solid. In an equilibrium situation, a fluid has a tendency to minimise its surface to a point of minimum free surface energy. Surface energy or tension decreases as a function of temperature. For example, pure water has surface tension of 72.75 $mN \cdot m^{-1}$ at 20 ºC and 66.18 $mN \cdot m^{-1}$ at 60 ºC. Surface tension of water can be lowered by the addition of surfactants, which tend to place themselves at the surface interface of such a solution. [131] [167]

Contact angle θ of a liquid placed on a solid surface depends on the properties and interactions of the solid, liquid and gas present at the triple interface of the three phases [131]. As an alternative to trying to measure actual contact angle visually, effective or equivalent contact angle can be calculated [168]. Measuring actual contact angle on porous substrates can be difficult, and for a wetting liquid undergoing absorption it is in fact impossible to describe theoretically without a complete knowledge of the geometrical porous structure, something generally unknown except in model cases.

The apparent contact angle on a rough non-permeable surface is different from the contact angle measured on a smooth surface made out of the same material. This behaviour is modelled by the Wenzel equation, which applies if the roughness is completely wetted by the liquid:

$$\cos\theta_w = r_w \cos\theta_Y \tag{4}$$

where θ_w is the contact angle for the rough surface, θ_Y is the contact angle for the smooth surface and r_w is the roughness of the surface, defined as the ratio of the actual surface area to its planar projection. For a smooth surface, $r_w = 1$. [169]

For a heterogenic surface, consisting of materials of different contact angles, an overall apparent contact angle can be predicted with the Cassie equation:

$$\cos\theta = \sum_i x_i \cos\theta_{Yi} \tag{5}$$

where x_i is the surface area fraction of the material with contact angle θ_{Yi}. [170] [171]

7.3 Substrate properties

Pore size is usually determined by pore radius *r*. Real world porous media usually contain a variety of pores of different effective radii, which can be characterised with a pore size distribution curve, defined usually by porosimetry as the volume of pores having a given

measured size. For simple modelling purposes, such a medium can also be characterised by an effective or equivalent pore radius that tries to represent the overall effect of the combined pore distribution [168]. Pore aspect ratio *l/r* is defined as the ratio of pore length, *l*, to pore radius, based on the assumption that the pores are of cylindrical shape [172].

Porosity, ε (or frequently ϕ), is a dimensionless number indicating the pore volume fraction of a medium. The rest of the medium consists of solid material. Saturation level of a fluid in a medium defines the pore volume fraction of the medium that can be filled with the fluid. [68]

For a porous substrate with known basis weight, b, thickness, τ, and density of solid phase, ρ_{solid}, porosity, ε, can be calculated as

$$\varepsilon = 1 - \frac{b}{\tau \cdot \rho_{\text{solid}}} \tag{6}$$

and in the case of dry cellulose τ_{solid} is 1 540 kg·m^{-3}. [31]

A variety of methods exist for measuring pore radius and porosity of a medium. In digital volumetric imaging (DVI), pores of a medium are first filled with hardening resin, after which cross-sections of the medium are cut, photographed and digitally analysed to determine the relative surface areas of resin-filled pores and original solid material, as well as radii of the pores. In non-destructive X-ray microtomography, radiation is passed through a substrate at varying angles and local absorption coefficients measured to construct 2-D cross-sections. In magnetic resonance imaging (MRI) the substrate is first submerged in water, and the signal from water-filled pores is measured to construct an image. [173]

Permeability, k, represents the area of a sample, of unit length, through which unit flux (1 m^3 of liquid per second) of incompressible liquid of unit viscosity can pass under laminar flow in response to the application of unit of pressure difference as defined by Darcy's law, discussed later in Eq. (10). It is affected not only by the pore properties and porosity of the medium, but also by the level of connectivity between individual pores. Methods for measuring permeability usually involve using external pressure to force a liquid or gas through a medium and measuring flow rate. Permeability of a medium is not necessarily uniform in all dimensions. For example, in a medium consisting of long, orientated fibres the permeability can differ significantly depending on whether the flow is parallel to the fibres, or at an angle to them. This also applies in a medium where the fibres are semi-orientated,

such as paper, where a difference exists between machine-direction and cross-machine-direction permeability. [173] [174] [175]

Permeability of a porous medium can be dynamically affected by the fluid flow within the medium itself. Flow of a particulate suspension through a porous medium can lead to reduction in permeability of the medium, due to individual particles getting deposited on the pore surfaces, or larger particles plugging narrow pore connecting throats [37]. Another dynamic effect that can take place is swelling, where solid material, such as cellulose fibres, forming part of a porous medium, absorbs fluid and swells, thus reducing the porosity and permeability of the medium [176]. However, surrounding environment permitting, swelling can also result in an increase in the total volume of the medium [175]. Penetration of water into fibres can also cause breakdown of intra- and interfibre hydrogen bonds, leading to dimensional changes in fibres and fibre-fibre debonding, respectively [177].

Due to the nature of the porous medium, liquid or gas will not be able to travel in a straight line, instead weaving a path through the pores. Thus the actual travelled path length through a complex porous medium between two points in that porous medium is longer than a straight line drawn between them. The relationship between the length of the real travelled path and a straight path through the medium is tortuosity τ. [68]

The Kozeny-Carman equation, based on modelling laminar flow in granular particle beds, tries to predict permeability of a medium based on its physical characteristics. Permeability from this equation can be written as:

$$k = \frac{\rho g \varepsilon^3}{\eta C_{kc} S_0^2 (1+\varepsilon)} \tag{7}$$

where ρ is liquid density, g is acceleration due to gravity, S_0 is specific surface area per unit volume of particles and C_{kc} is the Kozeny-Carman empirical coefficient, usually taken to be equal to 5. This equation is based on an assumption that particles are relatively compact, and does not work for modelling a medium consisting of platy particles. [178]

7.4 Rate of wicking

Wicking is fluid transport taking place due to capillary pressure created by a difference in surface energies between dry and wet surfaces, based on mutual attraction of molecules in

the respective solid and liquid phases. Capillary pressure, p_c, acting across the liquid-air meniscus within a cylindrical capillary tube is defined by the Young-Laplace equation as

$$p_c = \frac{-2\gamma_{LV}\cos\theta}{r} \tag{8}$$

where r is capillary radius, γ_{LV} the liquid-vapour surface tension, and θ the liquid-solid contact angle. [179]

The rate of travel of a fluid front in a uniform cylindrical capillary, under capillary pressure, is modelled by the Lucas-Washburn (L-W) equation, which is derived from the balance of the Laplace capillary pressure with the flow rate given by the Poiseuille equation

$$\begin{aligned} &\frac{dV}{dt} = \frac{\pi r^2 dl}{dt} = \frac{\pi r^4 \Delta P}{8\eta l} = \frac{\pi r^4}{8\eta l}\left(\frac{2\gamma_{LV}\cos\theta}{r}\right) \\ &\Rightarrow l\frac{dl}{dt} = \left(\frac{r\gamma_{LV}\cos\theta}{4\eta}\right) \\ &\Rightarrow l^2 = \frac{r\gamma_{LV}\cos\theta}{2\eta}t \end{aligned} \tag{9}$$

where l is the distance travelled in time t, and r is the radius of the capillary. The factor $t\gamma_{LV}\cos\theta/2\eta$ is called the coefficient of penetrance for a given combination of fluid and capillary material, where γ_{LV} is the liquid-vapour surface tension, θ the contact angle of the liquid, of viscosity η, on a flat substrate surface. The Lucas-Washburn equation can also be used to represent the rate of flow in a porous medium, if said medium is considered to consist of a bundle of small, uniform parallel capillaries contributing in effect to a single equivalent hydraulic capillary having the same liquid flow property. [180]

The Lucas-Washburn equation neglects a number of real world phenomena that can affect flow in capillaries, especially during short contact times and/or where geometry changes rapidly within a structure. Improved versions of the equation that take into account such factors as momentum changes during acceleration of the liquid, depending on the density of the liquid, as well as external forces, such as gravity and pressure, and the properties of any displaced gas, have been developed.

An experimental study conducted in micro-gravity conditions, created with 4.7 s free-fall in a drop tower, has demonstrated that the initial wicking speeds in capillaries do not match up

with the Lucas-Washburn equation. Rather, the authors suggested that initial wicking behaviour can be time-wise split into three different regions. In the first region, wicking speed is dominated by inertial forces and the distance travelled is roughly proportional to square of time. In the second region, wicking speed is dominated by convective forces and distance travelled is roughly linearly proportional with time. In the third region, wicking speed becomes dominated by viscous forces and the distance travelled starts to follow Lucas-Washburn flow where distance travelled is proportional to the square root of time. The duration of the first two regions was found to depend on the fluid properties, though in general being relatively short. [181]

In a real porous medium, pores are likely to be of varying sizes. A modified version of the Lucas-Washburn equation that treats a porous medium as a bundle of parallel capillaries of varying radii has been presented by Marmur. In this model, vertical rise in a porous medium is initially driven by the pores with large radius, while the final rise height is determined by the pores of smallest radius. [182]

On the other hand, the inertial flow model, based on the Bosanquet equation [183], suggests that initial wicking happens differently to what is described by the Lucas-Washburn equation. A pore size selection occurs on the short timescale related to the volume of liquid being accelerated: the larger the pore, the greater the inertial retardation of the liquid entering it and so there is a delay compared with a finer pore. Additionally, under the highest acceleration, the liquid front moves independently of viscosity, i.e. it behaves under plug flow until the viscous drag eventually establishes itself. According to this model, wicked distance l is expressed as

$$l^2 = \frac{2\gamma \cos\theta t^2}{r\rho} \tag{10}$$

on condition that the regime at each stage is short lived, i.e. prior to viscous flow, such that

$$\frac{8\eta t}{\rho r^2} \ll 1 \tag{11}$$

applies in the case where there is no external pressure present. Further, it is suggested that inertial flow takes place whenever wicking liquid is accelerated, also within the bulk structure, such as when entering from a pore into a narrower pore throat. Thus, in a real world porous medium, consisting of an array of pores and pore throats of varying

dimensions, the wicking liquid is subjected to inertial flow time and time again as it passes from one pore to another. [184]

Another way of modelling liquid absorption into a porous medium involves minimising the Gibbs free energy. For a single cylindrical capillary, Gibbs energy ΔG can be defines as

$$\Delta G = -\pi d h \gamma_{\mathrm{LV}} \cos\theta \tag{12}$$

where d and h are diameter and length of the capillary, respectively. For a system of multiple independent capillaries of varying dimensions, total Gibbs energy is the sum of Gibbs energies for all capillaries. Specific Gibbs energy for a given sample of a porous medium is the total Gibbs energy of all capillaries contained, divided by the mass of the sample. [185]

In practice, porous media, therefore, being more complex than can be modelled with any parallel capillary model, require a consideration of their three-dimensional structure consisting of pores of varying dimensions, connected to each other through narrower pore throats of equally varying dimensions. Also, the pores and pore throats are not necessarily circular, as assumed in the Lucas-Washburn equation, but can actually be more angular in their dimensions. Such structure can be more accurately modelled as a pore network, where the pores are represented by the nodes of the network and pore throats by the connections between the nodes. Such network models can be used for numerical simulation of fluid flows. Also during liquid flow in networks, parts of the gas phase can actually become trapped inside the spreading fluid, due to local variations in wicking rates. [186]

Since a pore network consists of a continuous series of pores and pore throats, a wicking liquid is subjected to a series of accelerations as it enters from wider pores into narrower pore throats, and decelerations when vice versa. This makes the inertial effect more significant than in a single long capillary, where acceleration only takes place once in the beginning of flow. The practical effects of this were demonstrated in an experimental study, where fluid wicking into ground calcium carbonate (GCC) tablets was measured. As a result, a difference was found in wicking behaviour between tablets made out of finely and coarsely ground material that could not be explained by the Lucas-Washburn equation. [187]

In a pore network study on liquid wicking, pore aspect ratio was found to have an effect on the time required to fill pores when using Bosanquet flow as a model. The ideal aspect ratio, to reach fastest wicking rate, varied as a function of pore length, with longer pores requiring higher aspect ratios. [172]

All bulk liquid flow models in filling capillaries discussed so far assume a clear and sharp advancing fluid front. However, an alternative model of liquid front spreading is that of film flow, where the liquid and gas fronts gradually overlap. In this model, the liquid front can flow along the walls of the pores, while the central areas of pores remain filled with gas which eventually gets displaced by liquid. In an experimental study with paper samples, liquid spreading was measured by applying drops of caesium iodide in aqueous solution on a sample, followed by immediate freezing of the sample with liquid nitrogen to immobilise the liquid. The frozen samples were then studied with cryo-scanning electronic microscope to observe the spreading behaviour. Analysis of the images indicated that the initial spreading of the fluid front was through bulk liquid film flow advancing along channels formed by fibre overlaps, followed later on by the filling of the actual pores. [188]

During liquid transport in hydrophilic channels, the basic principle of the Lucas-Washburn equation (distance travelled is a function of the square root of time) can be applied over those much longer distances than the actual pore size range in the medium itself, and while the fluid travels along a channel of constant cross-sectional area. In a case where the channel widens, though, the travel speed of the liquid front will slow down due to the resistance to flow through the prior narrower region. On the other hand if the channel narrows down, the fluid front will gain speed initially, but once the viscous drag through the narrower channel is established then a re-widening to the original width will manifest a slower speed than was originally the case. For the purposes of measuring travelled distance along the narrower channel, the time is effectively reset to zero when the fluid enters the narrow channel. This can be used as a tool to reduce travel times in channels. Thus, for a channel consisting of an initial wider section, and later narrower section, the minimum travel time is achieved when both sections are of equal length. [189]

In the case of fully wetted, saturated porous media, incompressible fluid transport in such a saturated medium can be modelled with Darcy's law

$$\frac{\mathrm{d}V}{\mathrm{d}t} = -\frac{kA\Delta p}{\eta L} \tag{13}$$

where k is the Darcy permeability of a sample of cross-sectional area A to a liquid flowing under a pressure difference across the sample length L of $-\Delta p$. [189]

One method for measuring flow rates in paper networks involves treating the liquid with chemical whose optical properties can be locally altered either chemically or by concentration change to produce visible bands in the fluid. This provides the possibility to track the movement of the liquid from several different positions, rather than just the edge of the liquid front. In a fluorophoric approach, fluorescence bands can be produced by introducing photolysis-reactive fluorophores into the liquid, and then using a narrow slit to expose a section of the flowing liquid to a photoflash unit. In an electrochemical approach, pH sensitive dye is added to the liquid, and a pulsed voltage source is used to apply a small electrical current that locally changes the pH of the liquid, thus producing visible coloured bands. [190]

7.5 External forces

Besides unaided capillary wicking, paperfluidic devices can also feature application of an external force to adjust transport rate – usually to retard it. In one exemplification, strips of paper were attached to a plastic disc that was spun at varying angular velocities with frequencies up to 6 000 min^{-1} to generate a range of centrifugal force. Liquid samples were then applied to the paper strips on the end closer to the outer edge of the disc. When the disc was spun, two opposite forces applied simultaneously to the liquid samples: capillary pressure pulling them towards the centre and centrifugal pressure drawing them back. Combined, this results in a pressure difference ΔP defined as

$$\Delta P = P_{\mathrm{c}} - \rho\omega^2 \left(r_{\mathrm{pap}} - \frac{h}{2}\right) h \qquad (14)$$

where P_{c} is capillary pressure, ω is angular velocity of the rotating disc, h is wicking distance and r_{pap} is the rotational radius of the rotating system as measured from the end of the paper strip to the disc centre. Since the centrifugal pressure grows as the liquid mass uptake into the paper increases ($\sim\rho h$, with centre of gravity at $h/2$), it is possible, depending on angular velocity, to reach an equilibrium state where the two pressures balance each other out and no further liquid transport will take place. Furthermore, if the angular velocity is increased sufficiently, it becomes possible to draw the liquid front backwards, though at least with filter paper strips once wetted areas will still remain partially wetted even if the main bulk of liquid is drawn back. [191]

Besides affecting fluid flow, spinning can introduce other functionalities to paperfluidic devices. In a study of this, rapid spinning was used to separate blood plasma centrifugally

from blood cells on a non-porous application zone before angular velocity was reduced in order to allow blood plasma to reach paper strips positioned inside the liquid radius [192]. Furthermore, spinning has also been used to route fluid in a junction through application of the coriolis effect, the well-known vortex effect of liquid being drawn through an orifice perpendicular to the axis of rotation of the experiment, dependent on the direction of rotation [192]. A later study also demonstrated valves of hydrophobic barrier material that could be activated by applying a spinning motion: the liquid sample would be loaded close to the centre of a disc, which would then be spun so rapidly that the centrifugal and capillary pressures combined would be enough to force liquid through the valve [193].

Transport of ionised particles in paperfluidic devices can be speeded up electrokinetically through application of an electric field. This was demonstrated using a simple single-channel paperfluidic design which was enhanced by addition of pencil-drawn electrodes at both ends of the channel. These electrodes were then connected to a DC power source with copper wires and conductive silver paste, and aqueous KCl solution applied to wet the whole length of the channel. To determine effects of the electrical field, aqueous KCl solution dyed with rhodamine-B was applied additionally to one end of the channel and the power source was switched on. The electrical field increased diffusion speed of dye along the channel, with the effect dependent on applied voltage. The authors suggested that similar phenomena could be used, for example, for mixing or separation of analytes on a device, or for trapping of electrically responsive biomolecules. [194]

Another demonstrated means of applying external force to adjust fluid flow is through surface acoustic waves (SAW). In an example study, a piezoelectric device was used to apply SAW to one end of a pre-wetted channel on a paperfluidic device. Application of SAW resulted in a rapid evaporation of water at the applied end of the channel, resulting in an even flow of liquid along the channel from the sample application zone to the other end. [195]

7.6 Evaporation and finishing

In practice, the transport rate can be affected by fluid evaporation from the channel surface. This can be limited by covering the channels with a finishing that prevents water evaporation. Some methods for preventing this were presented earlier in section 2.5.

On a porous surface, consisting of a mixture of solid material and small pores filled to the brim with liquid having a flat meniscus, the rate of evaporation has been somewhat surprisingly found to be effectively equivalent to an identically sized surface fully covered with liquid, on the assumption that the pores themselves are sufficiently small and closely spaced. However, such a model surface is not necessarily representative of a fluid front wicking within a porous medium, since the moving liquid front does not have a flat meniscus. Especially in the case of film flows along pore walls, or fingering movement along corners of angular pores, the liquid front can have significantly greater surface area. [196]

Combined effects of wicking, evaporation and gravity have been tested on small, porous sheets of twilled steel weave suspended vertically, in an attempt to model a possible wicking-based propellant management system for use in spacecraft. Tested sheets were 50 mm high, 10 - 18 mm wide and 149 µm in depth. The test chamber was provided with an aperture that could be adjusted to increase or decrease air flow, and so evaporation rate. Wicking height was measured either visually or by measuring the mass of liquid absorbed by the sheet. The following model was derived from the Lucas-Washburn equation to predict the amount of time required for a liquid of density ρ and viscosity η passing through a medium of permeability k, porosity ε and equivalent capillary radius r to wick a vertical distance, h, when effects of capillary pressure, gravity and evaporation were all accounted for

$$t = \frac{1}{2c}\left[-\ln\left(\frac{-ch^2-bh+a}{a}\right)\right] - \frac{b}{2c\sqrt{-\psi}}\ln\frac{\left(-2ch-b-\sqrt{-\psi}\right)\left(-b+\sqrt{-\psi}\right)}{\left(-2ch-b+\sqrt{-\psi}\right)\left(-b-\sqrt{-\psi}\right)} \tag{15}$$

where

$$a = \frac{2\gamma\cos\theta k}{\varepsilon\eta r} \tag{16}$$

$$b = \frac{\rho g k}{\varepsilon\eta} \tag{17}$$

$$c = \frac{\dot{m}_e(W+T)}{\rho W T \varepsilon} \tag{18}$$

$$\psi = -4ac - b^2 \tag{19}$$

and g is acceleration due to gravity, W is sheet width, T is sheet thickness and $\dot{m}_e$ is rate of evaporation in terms of $kg \cdot m^{-2}s^{-1}$. [197]

When predictions calculated by the above model were compared with experimental results, the shapes of the curves were found to match well, but the measured results were found to be consistently around 20 % lower than predicted values, which the authors could not reliably explain [197]. In their critical commentary of the study, another group of researchers pointed out that the measured results were based on the assumption of complete pore saturation by a wetting fluid, while 10 - 20 % under-saturation due to evaporation would have been a more realistic assumption [198]. When combined with deriving wicked height from absorbed fluid mass, this would lead to estimated wicking heights that would be lower than the real values.

In a previously mentioned study on toner coating of paperfluidic devices, the practical effects of reducing evaporation were measured. Three different device designs were tested: an uncoated, a coated with four toner layers and one coated with six toner layers. Wicking was measured along 80 mm long and 2 mm wide channels for 30 minutes. When devices were placed into a glass chamber with 100 % relative humidity, water wicked at approximately the same speed on all three types of devices, almost reaching the end of the channel in 30 minutes. When placed at 53 % relative humidity (test temperature not specified), water initially wicked at approximately the same speed on all the three types of devices for the first 5 minutes, but after this point the wicking rates started to segregate; travelling a distance of 50 mm took 25 minutes on the uncoated device, 17 minutes on the device with four toner layers, and 15 minutes on the device with six toner layers. Varying the local thickness of toner coatings was suggested by the authors as a possible means of adjusting wicking rates. [66]

Coating a device is not automatically guaranteed to increase wicking speed. In a study featuring thermally laminated paperfluidic devices, the laminating procedure was found to slow down wicking speed significantly when compared to a similar non-laminated device. The authors of the study attributed this difference to three different factors: compression of paper during the laminating procedure resulting in reduced effective pore size, partial filling of surface pores during the laminating procedure, and increased back pressure due to contained air being unable to evacuate from the pore network. However, the authors may have failed to spot a possible systematic error when measuring wicking speed for the non-laminated devices: these were placed on glass microscope slides, rather than suspended in the air, thus generating a possible capillary effect between the paper and glass slide acting to

speed up the wicking. However, such an error would likely not be sufficient to explain the scale of differences encountered. [51]

The surface roughness of a substrate can be used to develop a capillary effect between a porous medium and a separate covering film to promote wicking speed. This was demonstrated in one set-up using pieces of filter paper sandwiched between two pieces of flexible plastic film. This arrangement was found to improve wicking speed across filter paper significantly. Where a 7 cm vertical rise on plain filter paper alone required over 2 000 s, on sandwiched filter paper the same distance only required < 150 s. This speeded wicking was partially due to capillary pressure pulling the flexible film closer to the paper, and thus pushing liquid located between the two surfaces onwards. The vertical rise of the liquid in this set-up was found to match the form

$$h(t) \sim \phi \left(\frac{\gamma^2 t}{\eta \rho g}\right)^{1/3} \tag{20}$$

where g is acceleration due to gravity and ϕ is drainage coefficient, defined as

$$\phi = \frac{2\delta}{2\delta + \varepsilon L} \tag{21}$$

where δ is the distance between paper and covering film and ε is porosity of the paper of thickness L. Three different plastic films, of varying contact angles with water, were tested, but the contact angle was found to have little effect on the wicking speed. Potential application for such film coating speeded up wicking was demonstrated on a paperfluidic device consisting of two parallel channels, of which one was coated with film for faster local wicking. Further, the wicking speed could also be adjusted by changing thickness or porosity of the chosen paper. [199]

Due to its porous nature, paper has a large surface area, which can significantly increase the rate of evaporation, especially if the amount of liquid on paper is below the pore saturation level. Also, if a paperfluidic device is hydrophilic through its whole depth, water can evaporate from both sides of the paper, increasing evaporation further. While in many cases fast evaporation may be a problematic feature on paperfluidic devices, sometimes it can be used to advantage. In a study featuring microzone paper plates, such a fast evaporation rate was described as being good for fast concentration of analytes in test zones. [84]

8 Conclusions of literature study

8.1 General conclusions on hydrophobic patterning

2D and 3D paperfluidic devices form a relatively new field of study, with no significantly successful commercial applications produced so far. It is an inherently multidisciplinary area, drawing researchers and methodologies from a variety of fields, including chemistry, pharmaceutics and biomedical sciences, microfabrication, paper science and printing technology. Also the materials and methods used have been largely based on pragmatic attempts to utilise and modify already existing easily available technology, rather than trying to engineer new solutions from scratch. While the field of paperfluidics itself is quite vast, the main focus of this study is on fabrication of hydrophilic-hydrophobic patterns on porous substrates. Therefore, this chapter draws conclusions mainly by discussing these aspects.

Paperfluidic analytical devices show great promise for helping mankind, and great ingenuity has been shown in many of the studies related to them. However, when it comes to substrates, production methods and hydrophobising agents, there is still work to be done before an optimised industrial scale production environment can be set up to churn out cost-effective paperfluidic devices in massive volumes.

Also the analytical methods for paperfluidic experiments have not taken full advantage of all of the methods provided by many other fields of modern scientific and technological endeavour. The emphasis of research seems to have put little effort toward trying to analyse the exact effects of changes in surface chemistry caused by various patterning methods. Similarly, the actual penetration depths of hydrophobising treatments under different conditions have not been studied – such information would be important for attempts to engineer substrates specifically for paperfluidic device production.

When compared to regular printing applications, functional printing methods used for patterning paperfluidic devices face one major challenge: rather than producing a pattern close to the substrate surface for good print quality, they need to extend through the whole depth of the substrate. Otherwise a fluid sample will be able to leak through the gaps and out of the channels.

One attempt to ease this problem is to print the reverse side of a substrate with a pattern of 100 % coverage, thus making the whole reverse side hydrophobic up to a certain depth. This will restrict the depth that the printed pattern needs to penetrate on the front face, and also

prevents any fluid leaks through the bottom of the substrate. It also limits the fluid volume that hydrophilic channels will be able to absorb and transport, due to their shallower depth, though this is not necessarily a disadvantage, since it helps to reduce sample volumes. For production of 3D devices such a structure may be beneficial, since fewer substrate layers will be needed overall to produce a complete device, though in this case the reverse side needs to feature additional *z*-plane channels to allow fluid transport between different layers.

Another approach is to impregnate the substrate totally with hydrophobic agent, and then to turn some of the areas selectively once again hydrophilic. Such a hydrophobising step could be even carried out already at a paper manufacturing plant, by hydrophobising paper with sizing agent, or at a specialised paper converting plant, by spraying or otherwise impregnating the substrate with a desired hydrophobising agent. Thus, the substrate would only need to be selectively dehydrophobised at the actual paperfluidic device manufacturing plant. However, methods reported to date (plasma treatment, laser treatment, inkjet etching, photolithography) are not easily applicable to quick and simple industrial scale production. Furthermore, also these kinds of methods may result in relatively shallow channel depths. Such shallow channels can be advantageous due to requiring smaller sample volumes, but they may also be more vulnerable to the effects of evaporation, especially in hot or dry environments, unless isolated properly.

8.2 Conclusions on manufacturing methods

No conventional printing technology used so far has proved to be the perfect tool for producing paperfluidic devices. Inkjet printing shows great promise, since it can be used to print not only hydrophobic patterns, but also the actual reagents used for the assays. However, documented patterning inks either contain solvents, or require UV-light or heat for curing – all of which can be potentially harmful to the assay reagents. This issue could be circumvented by separating the printing of the reagents from the printing of the patterns, with the reagent printing happening as the last step. On the positive side, inkjet can be used to print very low viscosity inks, which will be able to penetrate quickly into a substrate. However, inkjet is not well suited to printing viscous inks, which might be required for constructing some elements, such as carbon electrodes.

Besides applying hydrophobising agents, reagents and ordinary printing inks to a substrate, printing technologies also provide great potential for producing selective surface coatings on substrates. So far, this has only been tested with inkjet printing and electrophotography,

though it could be carried out also by other printing methods. In this role, poor penetration of the coating into the substrate is actually an advantage, so methods that are poor for hydrophobic patterning can be great for finishing.

Hybrid printing lines, where flexographic, screen printing and/or inkjet units are all combined in a series, could be used to employ each printing method in an area most suitable for it. For example, inkjet could be used to deposit hydrophobic barriers and reagents, screen printing used to add electrodes, and finally flexography used to add in a thin protective coating layer on desired areas.

Use of laser or micro-plasma treatment for patterning paperfluidic devices has been little studied so far. There might be great promise to be found in this technology, since laser can provide very precise patterning, and depending on the beam intensity it can be used in many different ways to modify a substrate. Also, from a logistical point of view, there would be no need to handle hydrophobising materials in the paperfluidic device production environment, presuming that the base substrate has already been hydrophobised at a paper production line and only needs to be selectively de-hydrophobised on a paperfluidic device production line.

8.3 Conclusions on hydrophobising agents

So far no hydrophobising agent has proved to be the perfect barrier material from a manufacturing point of view. Most of the materials described require a UV or heat treatment step to cure properly. While readily available industrial solutions exist for such purposes, the hydrophobising agent should not require too long treatment times in an actual high speed industrial production environment. There are probably lots of potential hydrophobising agents that have not even been tested yet.

Also, hydrophobising agents generally tend to not be water-soluble, necessitating use of organic solvents in ink formulations. Thus, production lines need to be designed to handle solvent vapours, like many conventional printing lines. Evaporation of solvent also sets a limit to penetration depth that can be achieved with a solvent-based ink.

In case a feasible water-based hydrophobising ink could be formulated, there might yet be runnability issues when such an ink would be used on a roll-to-roll production environment. Achieving full penetration depth on a substrate requires applying a significant amount of ink, and water contained in this ink could affect the mechanical strength of the paper by breaking

hydrogen bonds connecting cellulose fibres. Special substrate with enhanced wet strength properties might be necessary to handle printing with such inks.

Wax is a material that has shown great promise for patterning paperfluidic devices. However, it too requires a significant heating period to penetrate properly into a substrate, and during this phase, it suffers from significant barrier spread. Also, in a web-fed production environment some of the molten wax might transport from the substrate to rolls, where accumulating residual wax might lead to runnability issues and inaccuracy of later patterning. On the other hand, ability to control heating time also allows a level of control over penetration depth. Thus, for laboratory research purposes and small scale prototype production, hot-melt wax inkjet printing is likely the most promising method available at the moment. It is a mature, easy-to-use technology for home and office printing, with commercial printers and supplies readily available at reasonable prices.

8.4 Conclusions on base substrates

Little effort has been so far been given toward new substrates specifically designed for paperfluidic applications. Instead, experiments have so far concentrated on testing substrates that are commercially available. Actually, only two publications encountered in this literature search have even raised a voice as to suggest what features such an engineered substrate should have.

The porous structure design of a substrate can provide other useful property tools for a device besides that of basic capillary wicking of a fluid. The filtering ability of the pores has proved to be a valuable property on several blood analysis devices, where it can be used to separate red blood cells from blood plasma or to test blood type by filtering red blood cells that have agglutinated by contact with antibodies. Such filtering properties might prove to be useful in other kinds of applications, such as detection of some micro-organisms in a sample.

Speciality pigment coatings could provide a potential new substrate for paperfluidic applications. A pigment coating of desired depth could be applied on top of a base paper, and isolated from that paper by a barrier layer that could prevent vertical wicking. This could provide the device with the robustness of a thicker device, while restricting the channel depth and the depth that the hydrophobising ink needs to penetrate to generate barriers. Also, speciality surface chemistry designed coating pigments might provide a better surface for attaching certain types of reagents that might have trouble binding with regular cellulose

substrates. Coatings could also provide better spatial resolution for patterning of substrates. Alternatively, if regular cellulose substrate would be considered sufficient for fluid transportation, pigment coatings could still be selectively applied to detection zones, e.g. by screen printing. This would allow for local improvement of reagent binding properties in those regions where it would be needed.

9 Introduction to experimental part

The aim of the experimental part of this study was to characterise physical properties and jettability of various hydrophobic inks, and to compare their performance in producing hydrophobic patterns on porous substrates. For this purpose, four different hydrophobic inks were designed and prepared from readily available materials and tested on two different filter papers.

A variety of patterns were printed on the filter papers using the inks. Dyed water was then allowed to wick into hydrophilic regions under various test conditions to outline the patterns and to test barrier properties of hydrophobic patterns. Finally, the printed samples were dried and imaged with a scanner, followed by a software analysis of the scanned images.

The experimental part starts with a description of the chosen materials (Chapter 10), followed by descriptions of the main equipment employed (Chapter 11) and test methods developed and applied (Chapter 12). Several items of the test equipment are used for multiple test methods. These chapters are followed by a description of results (Chapter 13) and a discussion around them (Chapter 14), with some of the results also detailed in appendices to form a complete record. Finally, the main outcomes (Chapter 15) and arising suggestions for future work are presented (Chapter 16).

Keeping true to the pragmatic tradition of paperfluidic research, good use was made of what materials and equipment were readily available or easily accessible. It would have been of interest to diversify the material range further by also testing, for example, polydimethylsiloxane (PDMS)-based ink, but unfortunately readily available PDMS-product with a suitable viscosity range for jetting and quick curing time could not be found with the moderate time and effort available.

Regarding methods, paperfluidics is at the moment a rather young and small field of study, with practitioners drawn from many fields. Thus, there are no established standards so far for evaluating performance and properties of paperfluidic devices. Due to this, some of the test methods used in the present study, while drawing inspiration from prior studies, are novel and therefore unique. Great effort has, therefore, been taken to describe them in sufficient detail to be repeatable by other experimenters, as well as providing some suggestions on certain features that maybe could have been better done in a different fashion.

Besides the large sampling scale experiments, described in detail, small series of pilot tests were carried out to evaluate feasibility of most of the test arrangements before engaging in the large sampling scale experiments. Except for a few special cases, results of these preliminary tests are not described in this work.

10 Materials

10.1 Hydrophobising agents and solvent

Three different hydrophobising agents were used for preparing the inks used in this study: polystyrene (PS), alkyl ketene dimer (AKD) and paraffin wax.

Polystyrene (Sigma-Aldrich, product number 331651) had an average molecular weight of 35 kDa and density of 1.06 $kg \cdot dm^{-3}$ according to information provided by the manufacturer. No information about polydispersity index was provided. The material itself was provided as small, transparent pellets that could be easily cut into even smaller pieces if needed. The literature study had indicated that molecular weight plays an important role in jettability of polystyrene solutions [145]. This particular polystyrene product was chosen for having particularly low molecular weight. The initial intention had been to use a higher molecular weight polystyrene product, as done in a previous study using flexography [82], until the importance of low molecular weight for jettability was discovered. Using small molecular weight polystyrene also means that there is no danger of polymer degradation in the print head, which has been reported to happen under similar printer conditions for polystyrene of 290 kDa or higher molecular weight [105].

Alkyl ketene dimer (AKD) was taken as grade commercially used as a sizing agent Basoplast 88 (BASF). No insightful technical details of this product were available from the manufacturer. The material itself was provided as small, dry pellets of off-white colour. Obtaining AKD in pure solid form proved slightly challenging, since it was not available from ordinary laboratory chemical suppliers, and for industrial use it is normally delivered as a liquid emulsion.

Paraffin wax was laboratory grade (Sigma-Aldrich), with a melting point of 54-56 °C. No further technical details were available from the manufacturer. The material itself was provided as large, semi-transparent chunks that could be carved into smaller pieces with a knife as needed.

The chosen solvent used for manufacturing all inks, based primarily on viscosity and surface tension requirements in application as well as prior art showing it to be suitable for flexographic printing of hydrophobic patterning ink [82], was laboratory grade p-xylene C_8H_{10} (Fluka, Acros Organics) with at least 98 % purity. p-Xylene or para-xylene (CAS number 106-42-3) is a colourless, flammable liquid, insoluble in water, with molecular

structure as shown in Figure 13. At 20 °C pure p-xylene has density of 861.1 $kg \cdot m^{-3}$, with a viscosity of 0.648 mPa·s and surface tension of 28.37 $mN \cdot m^{-1}$. It has a melting point of 13.2 °C, boiling point of 138.35 °C and flash point of 27 °C. The odour threshold of p-xylene is 0.62 ppm. [200]

Figure 13. *The chemical structure of p-xylene.*

10.2 Substrates

Two commercially widely available filter papers, Whatman 1 and Whatman 4 (both GE Healthcare), were chosen as substrates for this study. Both of these were manufactured from cotton cellulose. The filter papers were provided as circular discs, of 150 mm diameter for Whatman 1 and 185 mm diameter for Whatman 4. Using different sized discs helped to avoid accidentally mixing up the different papers.

One drawback of using discs rather sheets was that there was no easy way to figure out machine-direction, especially since it would have needed to be determined for each sheet separately. Therefore, no effort was taken to determine machine- or cross-machine-direction. This means that printed patterns were entirely randomly aligned in regards to machine-direction. Also no effort was taken to investigate whether there might have been a difference in permeability between machine- and cross-machine-directions.

Information about technical properties of these papers, as provided by the manufacturer, is shown in Table 2. Porosity was not directly provided by the manufacturer, but has been calculated based on other data as per equation 6.

Table 2. Filter paper properties [73].

Filter paper	**Whatman 1**	**Whatman 4**
Thickness (µm)	180	205
Basis weight ($g\ m^{-2}$)	88	96
Particle retention (µm)	11	20-25
Air flow permeability (s/100 cm^3/in^2)	10.5	3.7
Porosity	68 %	70 %

Prior to printing or testing, the filter papers were stored for at least overnight (>16 h) in a laboratory room with nominal temperature of 23 °C and nominal relative humidity of 50 %. Prior to printing they were quartered to provide pieces of suitable size to hold one printed test pattern each.

10.3 Dyed water

Since the printed patterns, once dry, were almost invisible to the naked eye, dyed water was needed to outline hydrophilic regions. Two different forms of dyed water, magenta and cyan in colour, were prepared for this study.

Magenta dyed water was prepared by mixing 10 % by weight of commercial carmine food colorant (Dr. Oetker) with distilled water. This food colorant was provided as an aqueous solution containing unspecified amounts of dye, citric acid and potassium sorbate. Exact chemical composition of the dye was not available.

Cyan dyed water was prepared by mixing 0.2 % by weight of nickel(II) phthalocyanine-tetrasulphonic acid tetrasodium salt (Sigma-Aldrich), provided as dry powder, with distilled water.

No surface tension or viscosity was measured for either of these dyed waters. Also, possible chromatographic separation of dyes from water during wicking was not formally evaluated, though in experimental studies no significant separation could be observed.

11 Equipment

11.1 Modular compact rheometer MCR-300

The modular compact rheometer MCR-300 (Physica Messtechnik GmbH) was used to characterise the viscosity behaviour of the inks. This rheometer provides a variety of measurement geometries, but in this study only one of these was used: this consisted of a flat Peltier element and a flat, rotating spindle, with the liquid sample to be tested sandwiched between these two parallel plate surfaces. This geometry leaves the tested sample slightly exposed to air around the edges, which might lead to issues with evaporation under certain conditions. However, no significant evaporation could be observed to take place during the relatively short measurements conducted in this study.

Viscosity measurement with MCR-300 is based upon rotating the top plate spindle at a specific speed, resulting in a laminar shear within the liquid. Torque required for a specific rotation speed is measured by the rheometer. Torque and rotation speed are then converted into shear stress and shear rate, and the actual viscosity is calculated from these. [201]

The MCR-300 equipment allows the user to measure viscosity under a wide variety of shear rates, dependent on the chosen spindle. Besides measurements at constant shear rates, viscosity can also be measured as a function of increasing or decreasing shear rate. Temperature of the Peltier element, upon which a test sample is placed, can be adjusted from -30 °C to 150 °C in order to test effect of temperature upon viscosity.

11.2 Contact angle meter CAM 200

The contact angle meter CAM 200 (KSV Instruments) used in this study is based on taking digital images of liquid drops and using image analysis to calculate contact angles from those images. This allows for measuring liquid surface tension or contact angle between surface and liquid. These can then be used to further derive surface free energy data.

Liquid surface tension is measured with a pendant drop experiment. In this method, a small drop is carefully squeezed out of a syringe or pipette tip so that it is left hanging from the tip. This hanging (pendant) drop is then imaged, and image analysis software is used to analyse drop size and shape. Surface tension is then calculated as

$$\gamma = \frac{\Delta \rho g r}{\beta} \tag{22}$$

where $\Delta\rho$ is the difference in density between measured liquid and surrounding fluid (air), g is gravitational constant, r is radius of drop curvature at apex and β is a computational shape factor. [202]

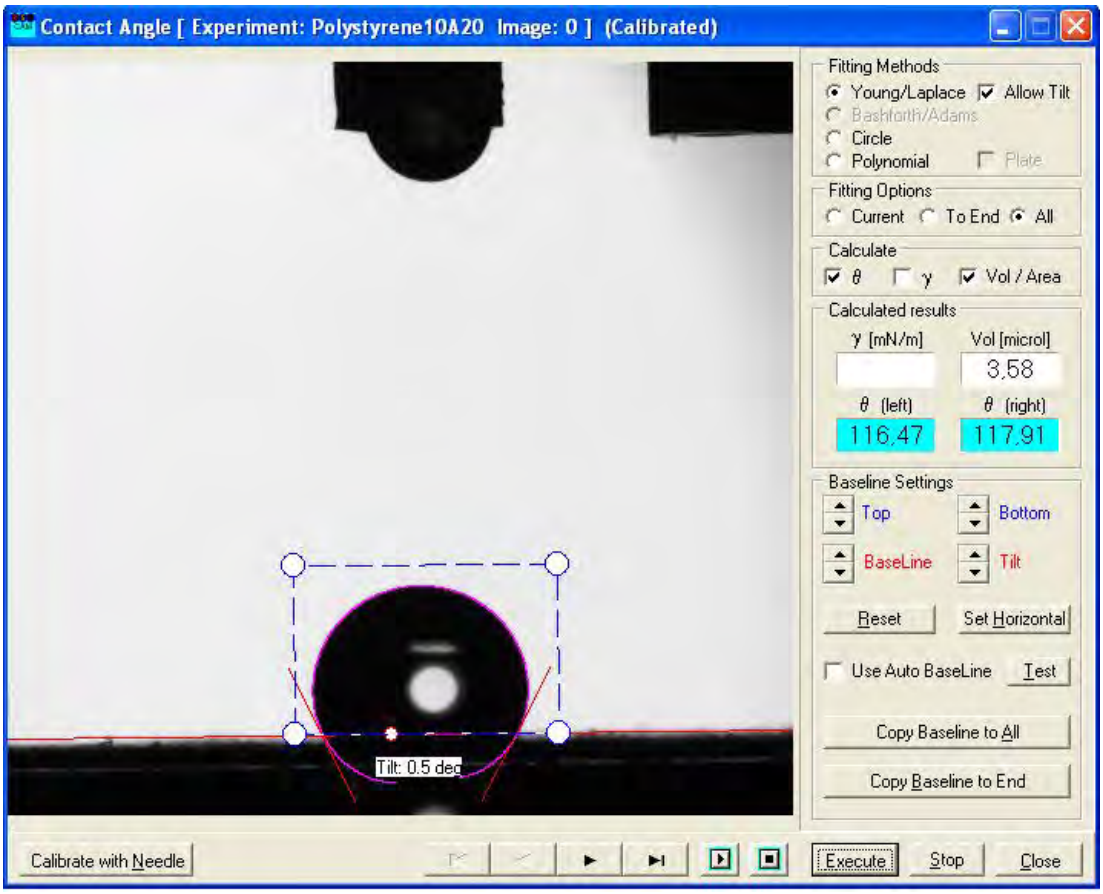

Figure 14. *Contact angle measurement. Test substrate, in this case polystyrene treated filter paper, is shown on the bottom, with measured water drop upon it in the middle. Red lines indicate substrate baseline and contact angles between the drop and the baseline.*

Contact angles are measured by dispersing a drop of given volume of chosen liquid on a surface to be tested. Again the drop is imaged with the digital camera and image analysis software is used to calculate contact angles with help in defining boundaries from the user. Figure 14 shows an example of a completed contact angle measurement.

Measurements are not limited to a single image. The user can take a series of images at chosen time intervals, with a minimum interval of 10 ms, and use these to analyse whether the contact angle is constant or changing as a function of time.

The CAM 200 also comes with an environmental chamber that can be used to conduct tests at higher than ambient temperatures. However, this possibility was not used in this study.

11.3 Dimatix material printer DMP-2831

The printer, a Dimatix material printer DMP-2831 (Fujifilm Dimatix), is a piezo-electric material deposition inkjet printer intended for laboratory research and development work in the field of functional printing. It allows the user to customise and test a variety of printing parameters for inks. The DMP-2831 can hold only one ink cartridge at a time.

The model DMP-2831 can print on a wide variety of flat substrates, with maximum substrate thickness of 25 mm. To ensure that the print head will not make contact with the substrate, the thickness of the substrate needs to be known accurately. The user can also select the distance between the substrate and the print head up to 2.5 mm, though a distance of 1 mm is recommended. Maximum printable area is 210 x 315 mm^2 for thin substrates (up to 500 µm thick), and 210 x 260 mm^2 for thicker substrates. No minimum substrate size is specified, though in practice samples smaller than 50 x 50 mm^2 are likely to be impractical. The substrate is placed on a metal mounting platen that can be either kept at ambient temperature or heated to a selected temperature between 28 and 60 °C. In practice, using ambient temperature setting was found to be a bit problematic in this study, since the platen tended to warm up by 1-2 °C from initial temperature when printer was kept in extended use. The sample mounting platen also comes with a vacuum suction option to help keep samples attached in intimate contact to the plate. However, this vacuum is not sufficient in the case of permeable substrates, which need to be attached via adhesive tape to the platen to keep them secured. [203]

The DMP-2831 can print a wide range of liquids, though hot-melts are not supported. A recommended ideal viscosity range for inks is suggested as 10-12 mPas, though at least liquids within 2-30 mPas range should be jettable with "*limited performance*". For high viscosity liquids, heating the ink chamber up to 70 °C can be used to lower jetting viscosity. A recommended surface tension range is given as 28-42 $mN \cdot m^{-1}$, though again liquids with surface tension up to 60 $mN \cdot m^{-1}$ can be jetted with "*limited performance*". Inks should have slow enough evaporation rate to prevent their drying at the exit to or within the cartridge nozzles, though no numerical values are given for this by the manufacturer. Also, inks should not contain any dissolved gas, since it can hinder jetting. Naturally, any particles suspended within the ink should not agglomerate or settle rapidly. [203]

The printer comes with its own integral pattern editor for designing print patterns. However, this editor requires all patterns to be defined as a set of rectangles, which in practice restricts its usage to relatively simple test patterns. Alternatively, patterns created with other design software can be imported in 1-bit (black-and-white) bit-map (.bmp) image format. While editing or importing images, the user has to specify drop spacing (resolution) to be used for printing. Drop spacing is set in multiples of 5 µm, with 5 µm being the minimum value, and the same spacing is used for both the *x*- and *y*-directions. Drop spacing can also be expressed in terms of resolution, with the 5 µm drop spacing being equal to 5 180 dpi (drops per inch) in resolution. [203]

For jetting purposes, a user can adjust the piezoelectric drive voltage (up to 40 V), frequency (up to 60 kHz) and waveform. A variety of pre-designed waveforms are provided by the manufacturer, but users are also provided with a waveform editor to modify them or design their own from scratch. Other user-adjustable printing parameters are tickle control (stimulates nozzles when not printing, in order to prevent ink from drying at the nozzles) and nozzle meniscus vacuum (prevents ink leaking from non-printing nozzles). Furthermore, the user can specify cleaning cycles to be run on the nozzles before, during and after printing. [203]

For analysing jetting, there is provided a special drop watcher camera that allows the user to observe jetting of droplets from individual nozzles to determine their jettability properties (e.g. presence of satellite droplets). This is not based on any actual high-speed camera system; instead a rather ordinary digital video camera, with high-magnification to catch the droplets, is used in conjunction with a strobe LED to catch images of droplets in specific phases of their flight while the ink is being jetted continuously. The camera system also enables the user to measure droplet velocity by measuring the distance travelled after a chosen time, with 7-9 ms^{-1} being the recommended velocity range. Figure 15 provides an example of a drop watcher camera view, used to evaluate jetting of the polystyrene ink in this study. [203]

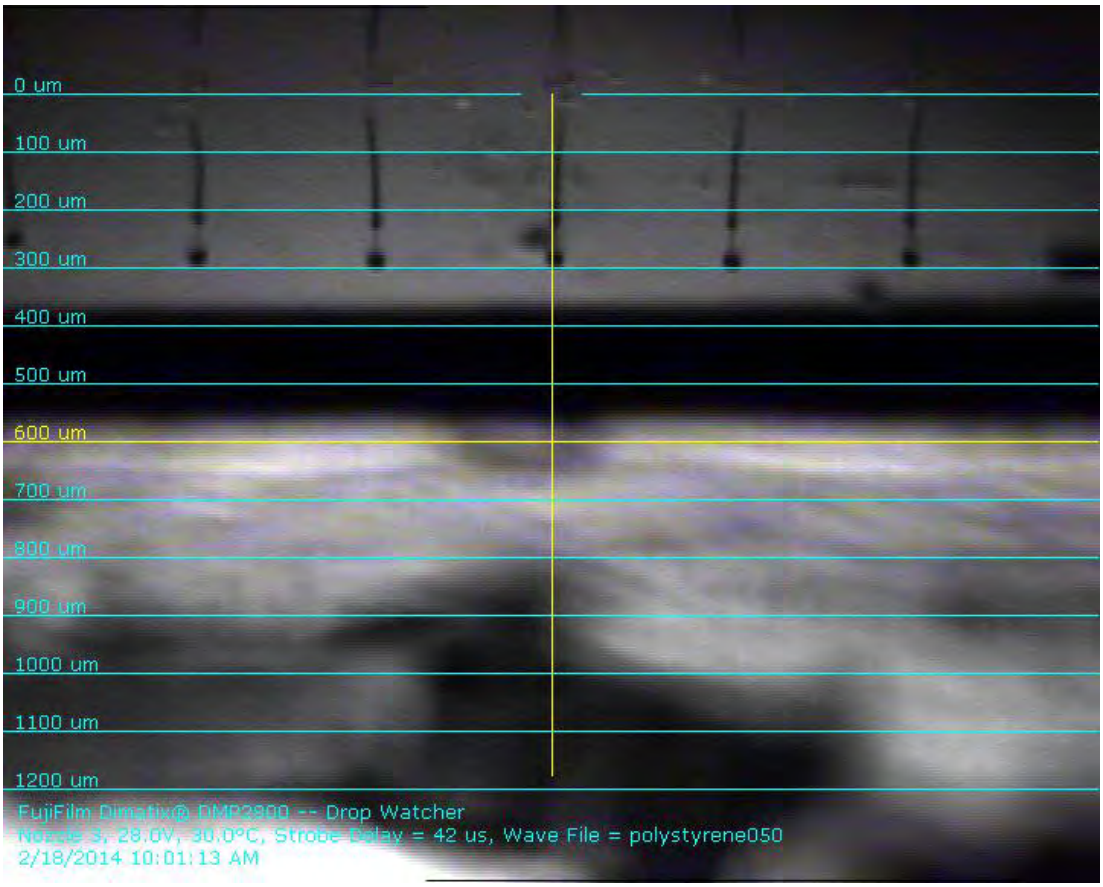

Figure 15. *Example of drop watcher camera view, displaying five drops 42 µs after ejection. Tailing filament is about to separate and form into a satellite droplet.*

Besides measuring velocity, the drop watcher camera could be used to characterise also other aspects of drop behaviour after initial jetting. In some studies similar set-ups have been used for example to measure the time required for a tailing ligament to break free from the nozzle, or the time required for a tailing filament to break into a separate satellite droplet.

The DMP-2831 printer also comes with a tool for measuring drop weight. This is conducted simply by placing a pre-weighted pan within the printer and jetting a specific number of drops into it, with one million drops suggested as a good number. By comparing pan weight before and after printing, the weight of an individual ink drop can be calculated. If ink density is known, actual drop volume can then be calculated. However, in practice this method can be of limited value if significant amounts of ink solvent are likely to evaporate before the pan can be re-measured, though it might still provide a means to measure dry solids weight if all solvent is allowed to evaporate. [203]

The printer also has an option for mounting an integral UV-light, thus allowing for polymerisation of UV-curable inks straight after jetting. However, no such light was installed on the particular printer used in this study.

11.4 Ink cartridges

Printer cartridges are available with two different nominal drop volumes: 1 and 10 pl. For this study DMC-11610 cartridges with 10 pl nominal volume were used. Each cartridge consists of two parts: a fluid module that can contain up to 1.5 cm^3 of ink, and a jetting module that features the actual print head. [203]

The chosen DMC-11610 print head has 16 nozzles, each with a diameter of 21 µm, aligned in a single row with 254 µm spacing between nozzles. In case some of the nozzles are clogged or jetting poorly, the user can choose to print with only a partial set of nozzles, though doing so will increase printing time. To prevent nozzle clogging, maximum recommended particle diameter for inks is 1 % of the nozzle diameter. No covering mechanism is provided to protect the print head and prevent evaporation when the print head is not in use. [203]

According to the manufacturer's instructions, these ink cartridges are intended to be single-use only. However, due to the price and availability of cartridges, in this study they were opened and re-used a multitude of times with no apparent ill-effects in print quality. Still, the jetting module used to print polystyrene ink had to be replaced twice during the study due to several nozzles in the print head becoming clogged, while three fluid modules also had to be replaced as extended exposure to p-xylene caused leaks in the polypropylene ink cartridges used to contain the ink. The latter problem might have been avoidable by using a more chemically resistant (and more expensive) version of the cartridge that replaces polypropylene parts with liquid crystal polymer.

Each cartridge was supplied with a metal syringe tip, used for filling cartridges, and maintenance pad, used with cleaning print heads. These were used as intended.

11.5 Permeance testers

Two different paper permeance testers, based on measuring of air flow, were used in this study to characterise substrates. These were an SE 114 Bendtsen tester (Lorentzen & Wettre) and a Gurley-Hill SPS tester (W. & L.E. Gurley).

The Bendtsen test is based on clamping the sample tightly between two metal rings, and forcing a continuous flow of pressurised air through the centre of the rings. Air flow rate is measured, and the substrate permeance is calculated based on it. Two different measurement heads are available for this tester, with 5 and 10 cm^2 areas for the air flow through the rings, respectively.

The Gurley-Hill SPS test is also based on clamping a test sample between two metal rings and forcing an air flow through it. However, instead of using continuous flow, a specific volume of air (100 cm^3) is forced through the test substrate by a well-lubricated gravity-propelled metal cylinder. The time required for this volume to flow through the sample is measured, and permeance is calculated as

$$S = \frac{128}{t} \tag{23}$$

where S is permeance in terms of $\mu m \cdot Pa^{-1}s^{-1}$ and t is measured time.

11.6 Imaging and image analysis

All imaging of dry samples was carried out with an Epson Expression 1680 (Seiko Epson) flatbed scanner. This scanner has hardware resolution of 3 200 dpi (dots per inch), but image resolution of 12 800 dpi is achievable through software-level interpolation. Full-colour scanning can be conducted in 24 or 48-bit format. Maximum document area is A4 sized, though with high resolution scanning the actual imaging area can be more limited. [204]

Microscopes with integral cameras were initially studied as an alternative imaging tool. However, closer experimentation revealed that the available microscopes, while having excellent resolution, had imaging areas that were too small to capture fully many of the details that would need to be measured from actual samples.

Image analysis was carried out with ImageJ version 1.44p (National Institutes of Health) image processing and analysis software. This is a freely available open source software kit with lots of analysis tools. In this study, only a small group of relatively simple operations was employed, namely image cropping, image conversions into greyscale and binary formats, together with particle area analysis from binary images. [205]

12 Methods

12.1 Preparation of hydrophobic inks

Hydrophobic inks were prepared by measuring a small amount of solvent, typically 10-20 g, into a glass jar and adding the appropriate amount of hydrophobising agent. According to the printer manufacturer's instructions, care should be taken when mixing inks, since any gas entrapped within the ink could cause troubles with jetting [203] [206]. Thus, to avoid any risk of air entrapment, the hydrophobising agent was simply allowed to dissolve and diffuse into the solvent overnight (>16 h) without additional external agitation. This may have been an overtly cautious approach, and is certainly not practical for large scale manufacturing. De-aeration would probably be required.

Four different inks were manufactured from the three available hydrophobising agents. The first three inks consisted of pure paraffin, polystyrene or AKD dissolved in solvent, while the fourth ink consisted of a mixture of polystyrene and AKD in solvent.

Xylene was chosen as a solvent for all inks, since it had been used previously to good effect as a solvent for flexographically printed polystyrene inks [82]. Importantly, it also has surface tension that is within the recommended surface tension range for the DMP-2831 printer (28-42 $mN \cdot m^{-1}$). Xylene is available in three different isomers, with p-xylene chosen for this study due to it being conveniently immediately available.

Paraffin ink consisted of 3 % by weight of paraffin wax dissolved in p-xylene. The dry solids content was limited by poor solubility of paraffin wax in the chosen solvent: higher amounts would simply not dissolve. Even this concentration of paraffin wax dissolved only very slowly, requiring close to 24 hours until the remains of the cut paraffin flakes could no longer be detected by the naked eye. As described previously in the literature study, a good number of prior studies have been carried out to investigate the use of various waxes for hydrophobising porous substrates. However, these have all relied on melting the wax to enable it to spread and absorb. Dissolving wax instead in a solvent, as is done here, which might allow skipping the melting step, was not found in the prior literature studied.

Polystyrene ink (PS ink for short) consisted of 5 % by weight polystyrene dissolved in p-xylene. This is the same mass concentration that produced best results in a prior study where polystyrene ink was applied by flexography and three different concentrations of 2.5 %, 5 % and 10 % by weight were studied [82]. Literature study also suggested that this level of

concentration could be expected to be jettable for polystyrene of the chosen molecular weight [145]. Polystyrene pellets were observed to dissolve rather quickly in p-xylene, with no visible traces remaining after one hour in the solvent.

Alkyl ketene dimer ink (AKD ink for short) consisted of 6 % by weight AKD dissolved in p-xylene. Previously published studies had demonstrated jetting of 2 % [15], 3 % [157] and 5 % [158] by weight concentrations of AKD dissolved in n-heptane. In the current study, p-xylene rather than n-heptane was again chosen as solvent, in order to allow for better comparison with polystyrene ink, for which p-xylene had already been chosen**.** Also, the surface tension of n-heptane is well below the recommended range for the DMP-2831 printer. In any case, AKD pellets were found to dissolve easily in p-xylene, with no visible traces remaining after one hour in solvent.

Combined alkyl ketene dimer and polystyrene ink (AKD-PS ink for short) consisted of 6 % AKD and 2 % polystyrene dissolved in p-xylene. This ink formulation was inspired by an interest to see how small an amount of polystyrene, used as a rheological modifier, would affect jetting and spreading behaviour of a primarily AKD-based ink. On studying prior literature, no studies could be found where two hydrophobising agents of such differing natures were combined together.

12.2 Ink viscosity measurement

Ink viscosities were measured with the MCR 300 rheometer, described previously. The chosen measurement geometry for tests was to use the temperature controlled Peltier base plate and PP50 flat disk spindle with 50 mm diameter. To hold the samples between the surfaces during rotation, a 1 mm measurement gap was used between the spindle top plate and the base plate. This gap could hold approximately 2 cm^3 of the ink liquids. All measurements were conducted with the Peltier plate set to 30 °C.

The viscometer hardware enabled a shear rate range for such setup from $2.618 \cdot 10^{-4}$ to 3 142 s^{-1}. However, for the samples used in this study the practical shear rate range proved to be roughly 20 - 1 000 s^{-1}. If shear rate was increased beyond this range, the rotating movement of the spindle would eventually result in some of the liquid sample escaping from the space between the spindle and the base plate due to the centrifugal effect. On the other hand, at shear rates lower than this range the induced forces were too low for reliable consistent

measurement, to the extent that the system could occasionally even report negative viscosity values!

Samples to be measured were applied to the measurement area using a syringe with a 0.45 µm GHP Acrodisc syringe filter (Pall Corporation) and metal needle tip attached. The purpose of the syringe filter was to remove any large contaminant particles, which should not be present within inkjet ink. Ordinarily, a sample is first placed onto the base plate, the spindle is lowered and excess sample is wiped off. This is a good approach for more viscous samples, but did not work for the inks studied, due to their low surface tension and viscosity resulting in them spreading all over the base plate, which is significantly larger than the spindle. As a workaround to this problem, the spindle was first lowered to the measurement position, and after this the syringe was used to inject a test sample carefully into the 1 mm gap between the two plates. The capillary effect then acts to keep the liquid in place and prevent it from spreading. With some practice and a steady hand, it became possible to fill the gap to match the edge of the spindle, though when this failed excess liquid needed to be carefully wiped away from beyond the edges.

Two different viscosity measurement set-ups were used to characterise different rheological behaviour. These were, respectively, a low shear rate viscosity test, conducted at constant shear rate, and a non-Newtonian behaviour test, conducted at varying shear rates.

Low shear rate viscosity tests were conducted at a constant shear rate of 100 s^{-1}. This was chosen to provide sufficient safety margin at the lower end of the viable measuring range. Preliminary tests also suggested that there was no significant non-Newtonian behaviour to be observed within the 20 – 100 s^{-1} shear rate range. For these tests, 5 samples were taken from each ink. Every sample was placed in the rheometer for 5 min, with viscosity measured 10 times in succession at 30 s intervals. This resulted in a total of 50 measurements per ink.

Non-Newtonian behaviour tests were conducted by ramping up shear rate slowly from 100 to 1 000 s^{-1}. Shear rate was increased steadily by 50 s^{-1} steps at 30 s intervals, with viscosity measured once at every interval, resulting in viscosity being recorded for 19 distinct shear rate values. This measurement was conducted 3 times for each ink.

12.3 Ink surface tension measurement

Surface tension measurements for inks were carried out with the CAM 200 contact angle meter using the pendant drop experiment method. For measuring, a polypropylene pipette tip

was attached to an automatic dispenser, and the tip was then filled with the ink to be tested. All tests were conducted in a laboratory room held at approximately 23 °C and 50 % relative humidity.

Due to their low surface tension, p-xylene based inks proved to be initially tricky to measure with this method. Due to its low surface tension, p-xylene could wet polypropylene and thus drops formed during squeezing liquid out of pipette tended to initially adhere around the pipette tip, rather than form a drop hanging from the tip. In retrospect, this problem could have been avoidable if a pipette tip of lower surface energy material, such as Teflon, had been used. However, with polypropylene tips a workaround was found by slowly dispensing more liquid until gravity would pull the drop down so that it would be hanging from the tip. Care needed to be taken, since applying a bit too much liquid could result in the droplet falling off altogether rather than being left hanging from the tip. Thus, hanging drops were formed in multiple steps.

Initially, 4 liquid doses of 0.4 µl each were dispensed to form the droplet, with short intervals between. These intervals were intended to allow liquid to settle down, resulting in more stable behaviour than if all liquid had been dispensed in one step. This was followed by dispensing 1 to 4 further doses of 0.1 µl each, until a properly hanging drop could be observed. This resulted in drops having total volumes of 1.7 to 2.0 µl. All fluid was dispensed at a rate of 0.75 µl s^{-1}. It is worth pointing out that pendant drops formed in this fashion were not entirely stable, since a strong vibration, such as a door being slammed in a neighbouring room, could sometimes result in a drop climbing up to surround the pipette tip.

Once a pendant drop had been successfully formed, it was imaged 10 times at 1 s intervals. Surface tension was measured from these images using a fitting method to the Young-Laplace expression. For each ink, 10 pendant drops were imaged. This resulted in 100 measurements per ink, with the exception of paraffin ink for which one drop was inadvertently imaged only once, resulting in 91 measurements for that ink.

12.4 Substrate permeance testing

Permeance (permeability) is a substrate property used to describe the flow rate of air, under pressure, through a sheet of permeable substrate in a unit time. It is a sheet property, rather than a constituent material property, and normalised with respect to thickness. [207]

Two different measurement methods were used for evaluating permeance of the filter papers. Firstly, Bendtsen permeance was measured using the SE 114 Bendtsen tester according to ISO 5636-3 standard, with the exception that the 5 cm^2 measurement head was used instead of the regular 10 cm^2 measurement head in order to increase the measurement range. Measurements for each paper type were taken from 10 paper discs, with 4 separate points measured per disc.

Secondly, Gurley permeance was measured with the Gurley-Hill SPS tester according to ISO 5636-5 standard, using regular 100 cm^3 air volume for measurements. For each paper type 10 samples, each cut from a different paper disc, were measured.

12.5 General printing arrangements

All printing in this study was carried out using the DMP-2831 printer with DMC-11610 ink cartridges. Due to the cost and limited availability of these cartridges, a decision was taken to re-use and refill cartridges for as long as they were viable, even though the manufacturer recommends them to be used only once. No instructions were available from the manufacturer as to how to disassemble a cartridge. However, some experimentation showed that this could be done quite easily by pushing two paper clips into openings in the bottom of the jetting module in order to force back arms holding the fluid module and the jetting module together. After this, pushing one end of the jetting module firmly against a hard edge is sufficient to force the two modules apart.

Initial studies also indicated that inks should not be stored within the cartridges, since there was no mechanism present in the print head to prevent evaporation. Such evaporation would lead to increase in dry solids concentration that could seriously affect jetting and printing performance. Evaporation could possibly be limited by covering the nozzle externally with a layer of Parafilm or other impermeable material before storing, though with solvent based inks care should be taken to ensure that such a covering layer would be resistant to solvent vapours. However, rather than experimenting with such external covering, the decision was taken to empty out the fluid modules daily after use, and re-fill them again just before the next printing or jettability studying session.

Filling fluid modules was done as per the printer manufacturer's instructions: a syringe was filled with a few cm^3 of ink, a syringe disc filter was attached to the end of the syringe, and a metal fill tip (supplied with every cartridge) was attached to this. The fluid module was filled

close to the brim in a fume hood, and a jetting module was clipped on and the assembled cartridge was placed right way up so that ink could flow to the print head. In case the nozzle plate of the jetting module did not look clean, it was wiped with a paper hand towel moistened either with p-xylene or ethyl alcohol.

As for the rheological measurement, the purpose of the syringe disc filter is to remove any large particles from the ink that could cause clogging in the print head. While the hydrophobising agents used in this study were not expected to contain any such large particles when in pure form, there was a risk that impurities either contained within the materials or introduced externally during ink manufacturing or handling could be present, and thus the filtering step was employed. The manufacturer's recommendation is to use a filter within a 0.20 to 0.45 µm filtering size range. For this study, 0.45 µm GHP Acrodisc syringe disc filters (Pall Corporation) were chosen, which were readily available.

When printing or jettability testing had been concluded for a day, a jetting module was cleaned by disassembling the ink cartridge, replacing the ink-containing fluid module with another one filled with pure solvent, and jetting this solvent for a while in order to remove any original ink left within the print head. Additionally, the nozzle plate was externally wiped with a hand towel moistened with p-xylene.

After the jetting module had been cleaned, also the ink-containing fluid module was emptied and cleaned. This was done by first shaking the open fluid module to remove as much of the ink as possible, then filling the fluid module with pure solvent, closing the module with a small plastic cap (provided with every module), shaking again to mix solvent with any ink remnant left in the fluid module, and finally opening the cap and emptying out the contents again. This procedure left a little bit of solvent within the fluid module, though this would usually evaporate before the module would be needed again. For safety, all shaking of fluid modules was carried out behind a glass plate within a fume hood, with a paper hand towel used to absorb all of the ink and solvent.

In order to avoid mix-ups, every fluid module was clearly labelled with the intended contents, either type of ink or p-xylene. The jetting modules did not have space for adding extra labels, with most of the free surface area taken by the manufacturer's serial number. Every cartridge with its fluid modules and other supplies was stored in a plastic container, clearly labelled with the name of the ink it was intended to be used with.

Actual printing sessions were started by attaching an ink cartridge to the printer and using the drop watcher camera feature to inspect that all nozzles were jetting properly. If necessary, nozzles were cleaned by wiping externally with a paper hand towel moistened with p-xylene or ethyl alcohol, using printer cleaning cycle features to force nozzles open and/or using pure solvent instead of ink to dissolve blockages. If these operations would not help, poorly or not all jetting nozzles would be marked as not to be used for printing. In case some nozzles were observed to produce too low drop velocities, their drive voltages could be adjusted individually to provide correct velocities.

The laboratory room where printing was conducted was typically at 21 °C, and while the relative humidity conditions for this room were not monitored, it was isolated from draughts etc. with limited infrequently used access. In order to provide good consistency and repeatability for jettability testing, the print head ink chamber temperatures were kept at 30.0 ± 0.2 °C in all studies. The sample mounting platen was originally intended to be kept at ambient temperature, in order to provide slow drying times for the inks. However, monitoring the mounting platen temperatures revealed that during extended printing platen temperatures tended to rise by 1-2 °C from initial conditions, which would have resulted in inconsistency between samples. Therefore, the lowest heating setting of 28.0 ± 0.2 °C was used for the mounting platen to provide consistent conditions. That said, it might have been more sensible to use the same temperature settings for both the ink chamber and the sample mounting platen. It was found that the vacuum pump was not sufficient to hold highly permeable paper substrates in place, and Scotch tape was required to fix them properly to the platen. Nevertheless, the vacuum pump itself was also kept in use during printing. Distance between substrate and print head was set to 1 mm. Manufacturer-provided information (see Table 2) was used for defining the substrate thickness limitation on the print head to sample gap settings. For the meniscus vacuum reading, the default value of "4.0 inches H_2O" was used.

All other printing parameter settings were determined on an ink-by-ink basis as a result of the jettability studies. Chosen values for these parameters will be discussed in more detail later on.

The substrates prior to printing were stored, as previously mentioned, in a room with local climate of 23 °C and 50 % relative humidity. Prior to removal from this room, the filter paper discs were quartered, after which each quarter was marked with an individual three-digit number using a graphite pencil, and finally these numbered quarters were sealed within

plastic Ziploc bags, typically in groups of ten per bag. They were only removed from these bags just prior to being printed upon. Individual three-digit numbers were used to keep track as to the paper type and used print settings (ink, drop spacing and pattern type).

After printing, all samples were allowed to dry long enough for all the visible solvent to evaporate. Drying happened quite quickly, though no actual times were measured. After drying, samples containing AKD needed to be heat-treated, in order for the AKD to react with cellulose. This was carried out by heating these samples for 10 min at 100 °C, either in a Modell 600 drying oven (Memmert) or on a laboratory digital hotplate SD300 (Stuart). Samples that did not contain any AKD were ready to use immediately after drying.

12.6 Ink jettability testing

The purpose of ink jettability testing was to evaluate practical jetting ranges for the studied inks. This was carried out by varying jetting waveform, drive voltage and frequency, while observing drop velocity, jetting stability and satellite droplet formation using the drop watcher feature on the DMP-2831. However, the effect of ink temperature on jetting behaviour was not studied, with all tests being conducted with the ink chamber at 30 °C, as previously mentioned.

Every ink was tested with three pre-defined waveforms provided by the printer manufacturer. These waveforms were named by the manufacturer as follows:

1. Dimatix Model Fluid Waveform
2. Low-viscosity
3. Hi-viscosity Short Polymer

Details of these waveforms can be found in appendix 1.

Each ink and waveform was tested with a range of frequencies, starting with 2 kHz and increasing in 2 kHz intervals as long as stable jetting could be observed. Jetting frequency is an important parameter in mass production, since use of low jetting frequencies will limit production speeds.

Drive voltage was originally intended to be studied for the whole available range, from jetting threshold up to the maximum 40 V value, at 1 V intervals. However, practical experience showed that running the print head at drive voltages close to the jetting threshold could very easily lead to nozzle plate flooding around the observed nozzle. This would stop

jetting and necessitate time consuming cleaning of the nozzle plate. Also, knowing exact jetting threshold was not strictly needed for practical purposes. Therefore, a decision was taken to observe systematically only those nozzles that could produce drops with velocities of 3 $m \cdot s^{-1}$ or more. It is worth keeping in mind that drive voltage here is a device-specific parameter, and reported results are not directly applicable to other manufacturers' print heads.

Velocity itself was measured with the help of the grid lines overlaid on top of the camera picture, as shown previously in Figure 15. Time delay, which could be set up to 200 µs for low frequency jetting, though having a lower maximum for some of the higher jetting frequencies, was adjusted so that the centre of the observed drop was approximately matching alignment with a chosen gridline. Velocity could be then calculated trivially based on time and distance travelled. The manufacturer's recommendation is to use the 1 000 µm line as the reference for measuring velocity, and this was indeed used in the present study whenever possible. However, low velocity drops could not reach this gridline within the available time delay, and these drops needed to be instead measured against the 600, 700, 800 or 900 µm gridline, depending on their velocity. While the set-up is good for measuring velocities in the intended velocity range of 5-10 $m \cdot s^{-1}$, it starts suffering from lack of resolution, i.e. high granularity, when measuring significantly higher velocities, since the minimum increment for time delay in the camera is 1 µs.

Velocity characterisation enables one to find by interpolation a jetting parameter region where good jetting velocities could be found. For this purpose, velocities were recorded only for one nozzle per jetting module, chosen for being relatively representative of the nozzles on a particular cartridge. A more statistically relevant study could have included recording velocities for a larger number of nozzles, preferably over multiple cartridges. It is worth also pointing out that the camera system does not actually measure velocities of single drops. Rather, due to the stroboscopic nature of the system, what is viewed by a user is a continuous feed of images depicting a multitude of individual drops, even though the view can appear very static when jetting is stable.

Satellite droplet formation was evaluated on a simple yes/no scale by visually observing drop behaviour after jetting. The shortcoming of this method is that it did not take into account the variety of forms that satellite droplet production could manifest. The number of satellite droplets, as well as their size and velocity, could vary significantly as jetting parameters were adjusted. That said, while it might be possible to estimate drop volumes from images

taken by this camera, it would be a slow and difficult procedure, and certainly beyond the intended design parameters of the system. A high speed camera with good resolution would be needed to define such behaviour accurately applied to a series of single droplets.

The presence of satellite droplets made estimation of velocity a bit more complex, since instead of a single drop with a single velocity, there was a group of drops with possibly significantly differing velocities. This was solved by considering the first drop to reach the observed gridline as the main drop, for which velocity was recorded. However, sometimes an exception had to be made, when the leading droplet would be very small and thus not representative of the main body of the jetted ink: in these cases the second, larger droplet would be considered as the main print contributing drop.

Jetting stability was also evaluated based on a simple yes/no scale. This tended to be somewhat subjective, since actually during observation there became manifested quite a sliding scale of stability. On one end of the scale, there were settings which produced very stable jetting with consistent velocity for a long time. On the other extremity of the scale, jetting could go out of control and lead to nozzle plate flooding within a couple of seconds. In between there were various states where jetting could take place, but produced velocities were not entirely stable. In a rather arbitrary fashion, some jetting conditions, where there was just slight drop velocity fluctuation but an average velocity could still be easily estimated, were considered stable and their velocities were recorded. If velocity fluctuated significantly as a function of time, jetting parameters were considered unstable, with a notice of instability recorded instead of velocity.

12.7 Contact angle measurements

Surface hydrophobicity of printed and unprinted surfaces was characterised by measuring contact angles between the surfaces and distilled water with the CAM 200 contact angle meter. For this purpose, rectangles measuring 15 x 50 mm^2 were designed using the Dimatix pattern editor and printed. These were then cut down so that only a 5 x 50 mm^2 strip from the middle was left, since measuring with CAM works easiest with narrow strips of material. Before measuring, samples were stored overnight at 23 °C and 50 % relative humidity.

Before any measurements took place, the CAM 200 was calibrated according to the manufacturer's instructions. For measuring, the strip to be measured was attached with Scotch tape to a sample holder, consisting of a metal shoe horn. Measurements were carried

out by placing the sample holder, with a sample attached, under the automatic dispenser unit. Then a 4 µl drop of distilled water was dispensed from the dispenser head and placed upon the sample.

For surfaces expected to be hydrophobic, the drop form was then visually inspected to see if there was surface unevenness around the edges that could disturb measurements; especially stray fibres sticking out of the surface plane could disturb the drop form noticeably. If the drop was rejected, a new one was dispensed instead. If it was accepted, image recording was then triggered manually, and 10 images were taken at 1 s intervals. In the case where the surface was expected to have contact angles below 90°, it was tested with a few pilot drops, and automatic triggering was used instead to start imaging as soon as a drop would touch the substrate. In this case, 12 images were taken with 1 s intervals, though out of these a couple of the first ones needed to be rejected due to the dispenser tip disturbing the drop form, resulting in 9-10 actual good images. Images were then analysed with the integral software using the Young-Laplace fitting method to calculate contact angles on both right and left sides of the drops.

The chosen filter papers absorbed water drops so quickly that contact angle could not be measured even when using the shortest imaging time of 10 ms. Similar situations happened also with some treated substrates, where the water drop got absorbed before it could be imaged. In these cases, a contact angle value of 0° was recorded.

The tested samples were printed with polystyrene ink on Whatman 4 filter paper, with drop spacing values of 10, 15, 20 and 25 µm. For each drop spacing 5 samples were printed. Each sample had contact angle tested first with 4 drops on the printed side, and then, after an overnight of drying, with 4 drops on the reverse side. Thus, a total of 20 drops and approximately 200 images were analysed per side for each drop spacing value.

12.8 Line spreading measurements

In order to measure spreading of inks on substrates, a simple line test pattern was designed with the Dimatix pattern editor and printed. This consisted of 10 parallel lines, each 35 mm long. Nominal line width ranged from 0.1 mm to 1.0 mm, in 0.1 mm increments.

In order to make the hydrophobic printed lines visible, they were visualised in the wicking mode for water. The printed samples were attached to a drying rack with laundry pegs to support them, so that their lower ends were in contact with cyan dyed water, held in plastic

jars below, to act as a liquid super-source. Dyed water was allowed to wick up the hydrophilic areas until it had reached the tops of the lines and they were fully visible. At this point, samples were taken out and left to dry.

Once the samples were dry, they were imaged with the Epson Expression 1680 scanner. A region measuring 5 x 60 mm^2, containing a section of each of the ten lines, was scanned from each sample both from the printed side and the reverse side. Images were scanned in 24-bit RGB format with 3 200 dpi resolution.

Scanned images were analysed with ImageJ software in order to determine the width of the lines. This analysis was implemented by first converting the images automatically into greyscale format, and then further converting them into binary format using manual thresholding. The software functionality setting of *Analyze particles*, with the *Include holes* option, was used to measure the areas of the ten line sections. By dividing these areas with the length of the scanned section, line width was obtained.

Line spread test samples were printed with a variety of settings. With polystyrene ink, they were printed on Whatman 4 filter paper with 10 and 15 µm drop spacing, with 5 samples printed with each drop spacing value. With AKD and AKD-PS inks, they were printed on both Whatman 1 and Whatman 4 filter papers with 20, 30, 40 and 50 µm drop spacing, with 5 samples printed on each paper with each drop spacing value.

12.9 Hydrophobic barrier tests

In order to test how wide hydrophobic barriers would need to be printed on the respective substrates to prevent water from wicking past, a specific barrier test pattern was designed with the Dimatix pattern editor and printed. This consisted of 11 vertical channels in parallel. The first channel was left open as a control channel, while the rest of the channels had a barrier of increasing width placed at their respective entrances. Nominal total width of the test design was 50 mm. The complete device design is presented in Figure 16.

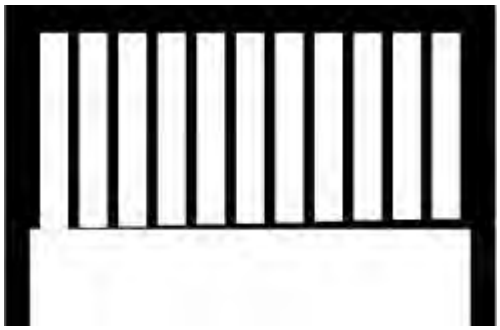

Figure 16*. Barrier test pattern design. Thick hydrophobic columns on the edges provide the device with rigidity when hydrophilic regions are wet.*

Due to differences in line spreading, two slightly different versions of the design were used. In the narrower barrier design, used for inks with significant line spreading (AKD and AKD-PS), barriers had nominal widths ranging from 0.05 to 0.5 mm in 0.05 mm increments, and walls separating parallel channels were nominally 0.5 mm wide. In the wider barrier design, used for inks with more limited line spreading (PS), barriers had nominal widths ranging from 0.1 to 1.0 mm in 0.1 mm increments, and walls separating parallel channels were nominally 1.0 mm wide.

After printing, patterns were cut off and trimmed a little bit from the sides so that they would be able to stand upright in a 50 mm diameter plastic jar. Trimming of the sides was necessary due to the real printed devices being slightly wider than the original design, due to ink spreading. The simple task of cutting off the patterns was slightly complicated by the fact that on a dry sheet the pattern is effectively invisible, as demonstrated in Figure 17. Thus, a moistened fingertip was used to wet the substrate locally around the corners of the printed device. This made the corners temporarily visible, and they were marked with a graphite pencil. After this, the samples were again allowed to dry totally in order to make them easier to cut.

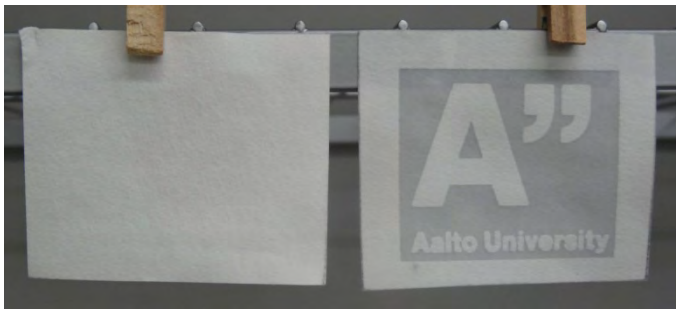

***Figure 17**. Patterns printed with polystyrene or AKD on filter paper are almost invisible when dry, but wetting will cause a visible opacity change on the hydrophilic areas. Displayed here are two Aalto university logos printed with polystyrene ink, shown completely dry (left) and after dipping in a jar of water (right).*

Once samples were cut and trimmed to the correct shape, they were stored overnight in the test room at 23 °C and 50 % relative humidity before proceeding to actual barrier testing. For this test, ten 50 mm diameter polystyrene jars were used, with a 3-4 mm layer of cyan dyed water placed in the bottom of each jar. Then a set of 10 test devices was taken and the devices were dropped into the jars in quick succession. Once a device would reach the bottom of the jar, dyed water would start wicking up from the bottom of the device, trying to find a way past the barriers. This test arrangement is demonstrated in Figure 18. The samples in the jars were observed for 30 min, with a timer started after the last device of the set had been placed in a jar, with results recorded every 5 min.

Barrier penetration was tracked separately for each channel, using a simple yes/no format: if any dyed water could be observed above the barrier line when viewed from the printed side, the barrier was considered penetrated. However, in practice it was soon observed that also a more graded approach might make sense, since the amount of liquid that would wick past the penetrated barrier could vary significantly, indicating that there were significant differences in barrier breaches that let water past.

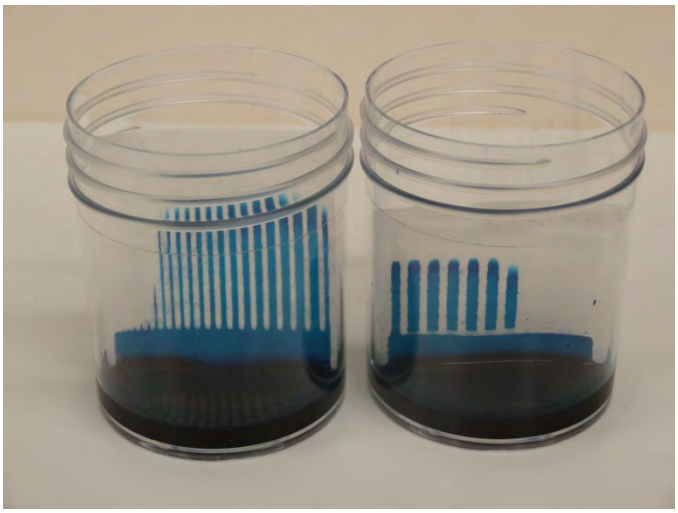

Figure 18. *Experimental set-ups for testing channels (left) and barriers (right).*

After the 30 minute observation period was complete, samples were removed from their jars and placed to dry. After a couple of hours of drying, a few drops of red dyed water were applied with a syringe to each of those channels that had not been penetrated, after which the test devices were dried again.

Once the samples were dry, they were imaged with the Epson Expression 1680 scanner in order to study the dimensions of some of the unpenetrated barriers. One barrier was chosen from each test device, and approximately a 2.5 x 2.5 mm^2 area containing this barrier was scanned from the printed side in 24-bit RGB format with 12 800 dpi resolution. The chosen barrier to be imaged was not selected on only a single device basis, but based on the performance of barriers within a group of 10 identically printed samples: out of these, the lowest nominal width barrier that had not been penetrated on any of the devices was chosen as the one to be imaged for the whole group.

Scanned images were analysed with ImageJ software in order to determine the actual width of the barriers. This analysis was implemented by first cropping the image so that the areas of the barrier closest to the walls were excluded, since on these regions the barriers were wider than in the centre due to merging effects. After this, images were converted automatically into greyscale format, followed by further converting them into binary format using manual thresholding. The *Analyze particles* -functionality, with *Include holes* -option, was again used to measure the area of the imaged barrier. By dividing this area with the length of the scanned section, the barrier width was obtained.

Barrier test samples were printed with a variety of settings. With polystyrene ink, they were printed on both Whatman 1 and Whatman 4 filter papers with 10, 15, 20 and 25 µm drop spacing, with 10 samples printed on each paper with each drop spacing value. With AKD and AKD-PS inks, they were printed on both Whatman 1 and Whatman 4 filter papers with 15, 20, 25, 30, 35, 40, 45 and 50 µm drop spacing, with 10 samples printed on each paper with each drop spacing value.

For paraffin ink, only a small pilot series was printed on Whatman 4 filter paper, consisting of 5 samples with 10, 15, 15, 20 and 20 µm drop spacing.

12.10 Hydrophilic channel tests

In order to test how narrow the working hydrophilic channels could be between the hydrophobic boundaries, a specific channel test pattern was designed with the Dimatix pattern editor and printed. This design consisted of 22 parallel channels with nominal channel widths ranging from 0.5 to 2.6 mm in 0.1 mm increments. Parallel channels were separated from each other by channels of 0.5 mm nominal width. Nominal total width of the test design was 50 mm, while channels themselves were nominally 32 mm long. The complete device design is presented in Figure 19.

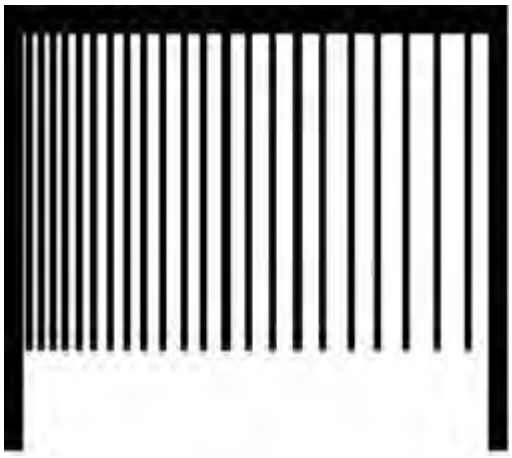

Figure 19. *Test pattern design for channel width tests. Thick hydrophobic columns on the sides provide rigidity and support when hydrophilic regions are wet.*

After printing, test devices were prepared and stored in a similar fashion to those used for barrier tests. The experimental test set-up for testing channels was rather similar to those used for barrier tests, as can be seen from Figure 18 (shown previously). Again, ten 50 mm diameter plastic jars with 3-4 mm of cyan dyed water on the bottom were used. Ten test

devices were dropped into the jars, and dyed water was allowed to wick up the channels for 5 or 10 min. After this, the test devices were taken out of the jars, dried and visually evaluated to determine in which of all channels water had wicked to the top.

Some channels were chosen for more detailed analysis, and these were scanned as before with the Epson Expression 1680 in 24-bit RGB format with 12 800 dpi resolution. Scanned images were analysed with ImageJ software in order to determine the average width of the channels. This analysis was implemented by first cropping off the ends of the channels, which differed slightly in dimensions from the main body of the channel. After this, images were converted automatically into greyscale format, followed by further converting into binary format using manual thresholding. As before, the *Analyze particles* -functionality, with *Include holes* -option, was used to measure the area of the imaged channel. By dividing the area with the length of the scanned section, channel width w was obtained.

Channel test samples were printed with a variety of settings. With polystyrene ink, they were printed on Whatman 4 filter paper, to ensure complete penetration, with 15 µm drop spacing, with 10 samples printed. With AKD and AKD-PS inks, they were printed on both Whatman 1 and Whatman 4 filter papers, since these inks penetrated further, with 30 and 45 µm drop spacing, with 10 samples printed on each paper with each drop spacing value.

13 Results

13.1 General

All results are reported with 95 % confidence intervals whenever possible. In many cases these are relatively high. This is partially due to limited sample sizes, but it is worth noticing that also the studied filter papers are by their very nature rather uneven, with significant local variation in structure on the fine scale. However, detailed characterisation of such variation is beyond the scope of the current study.

13.2 Substrate permeance

Measured air flow and permeance for the filter paper substrates are listed in Table 3. For convenience, also the manufacturer provided air flow information, previously listed in Table 2, is repeated here.

Table 3. Filter paper permeances.

Paper	**Whatman 1**	**Whatman 4**
Air flow, manufacturer (s/100 cm^3/in^2)	10.5	3.7
Air flow, Gurley (s)	4.3 ± 0.7	0.9 ± 0.4
Air flow, Bendtsen (cm^3 min^{-1})	1 430 ± 190	Not measurable
Permeance, Gurley (µm$Pa^{-1}s^{-1}$)	30 ± 5	135 ± 50
Permeance, Bendtsen (µm$Pa^{-1}s^{-1}$)	37.9 ± 3.0	Not measurable

Measuring air flow for Whatman 4 filter paper proved to be problematical. With the Bendtsen test, air flows were beyond the upper limit of the measurement range (3 000 cm^3 min^{-1}) of the test device, even with the small 5 cm^2 measurement head. With the Gurley test, air flow times could be easily measured, but they fall under the reliable measurement range for the instrument, which has a lower limit of 1.3 s. In principle the Gurley measurements could have been conducted with greater air volumes, i.e. 200 or 300 cm^3 instead of the standard 100 cm^3, to obtain results that would fall within the reliable measurement range. However, in practice this was not feasible, since the adjustment was inaccessible. Furthermore, since the sheet volume was so high that it bordered on preventing complete penetration of the ink volumes used this was not pursued further.

With Whatman 1 filter paper, air flows could be easily measured. Permeances calculated from the air flow measurement results differ somewhat between Gurley and Bendtsen measurements, with the Gurley method producing lower results. However, an approximate

value ~ 35 µm ·$Pa^{-1}s^{-1}$ could be considered to fit within the confidence intervals for both measurement methods.

Comparing these experimental results with the information provided by the manufacturer is a not straightforward, since the latter does not explicitly specify the test method used for air flow. However, the given units (s/100 cm^3/in^2) suggest that it has been with Gurley, though with different measurement head geometry than used in this study.

The ratio between the permeances for the two papers, adopting the manufacturer provided information, gives a value of 1:2.8, though no similar ratio can be reliably calculated for the measured Gurley permeances due to unreliable results for Whatman 4. Similarly, an accurate ratio for the Bendtsen method cannot be calculated either, though knowing that Whatman 4 was above the upper limit for air flow measurement range indicates that the air flow ratio would be at least 1:2.1 or more.

13.3 Ink properties

Measured ink properties are presented in Table 4. This Table also includes values of inverse Ohnesorge number *Z* calculated from measured results according to equation 1, presented previously in the literature study. Notice that viscosity has been measured at 30 °C while surface tension has been measured at 23 °C.

Table 4. Ink properties.

Ink	**Viscosity, low shear (mPa·s)**	**Surface tension ($mN \cdot m^{-1}$)**	***Z***
Paraffin	0.61 ± 0.02	28.55 ± 0.12	26.3
AKD	0.63 ± 0.04	28.54 ± 0.21	25.5
AKD-PS	0.90 ± 0.04	28.35 ± 0.12	17.8
PS	1.21 ± 0.07	28.18 ± 0.15	13.2

Attempts to measure exact ink densities failed, due to the low surface tension inks wetting polypropylene pipette tips and making it practically impossible to obtain exact volumes of the inks. This problem might have been avoidable by using pipette tips made of Teflon or some other low surface energy material. In any case, for the purposes of calculating surface tension and *Z*, inks were assumed to have a density close to that of pure xylene at 20 °C, i.e. 0.8611 $kg \cdot dm^{-3}$.

Measured results for surface tension were very close to that of pure p-xylene, which is 28.37 $mN \cdot m^{-1}$ at 20 °C. Thus, the presence of hydrophobising agents in inks does not have any practical effect on surface tension of non-polar solvents. Surface tension of pure solvent itself was not measured as a control, though this would have been good practice if strong deviation from the surface tension from that of p-xylene had been seen for the formulated inks.

With low shear viscosity, also pure p-xylene was tested for comparison, having a value of 0.58 ± 0.04 mPa·s. Paraffin and AKD, with their low molecular weights, resulted in ink viscosities that were only slightly higher than that of pure p-xylene. Polystyrene with its significantly higher molecular weight produced ink with clearly higher viscosity, while PS-AKD ink with its lower polystyrene content fell quite neatly between pure AKD and PS inks in respect to viscosity.

When ink viscosity was further tested as a function of increasing shear rate, all four inks exhibited shear thickening, i.e. their viscosity increased when shear rate was increased. These results are displayed graphically in Figure 20, with numerical values presented in appendix 2. Notice that this behaviour was not tested with pure solvent, so it is not entirely clear from these results whether the shear thickening is purely due to the presence of the dissolved hydrophobising agents, or if the solvent itself also displays noticeable non-Newtonian behaviour. However, a prior study using molecular dynamics modelling indicates that p-xylene, as well as benzene and toluene, is actually a shear thinning liquid [208]. Therefore, it can be assumed that the observed shear thickening behaviour in this study is either due to evaporation and solids rise during shear, or due to polymer entanglement amongst the solved hydrophobising agent. The latter is much more likely, especially since no significant loss of the test sample due to evaporation could be observed visually after any of the tests.

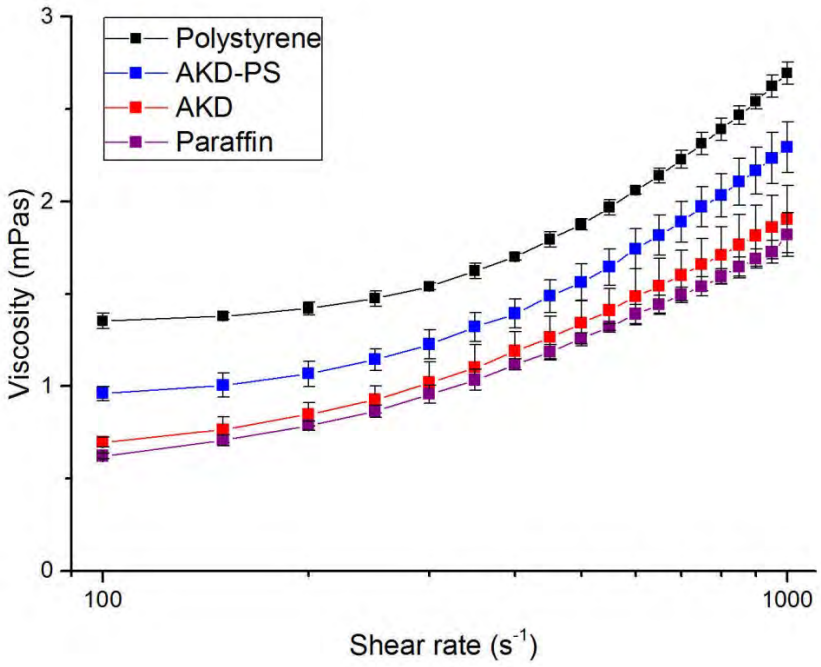

Figure 20. *Rheological behaviour of inks expressed as a function of shear rate. X-axis is on a logarithmic scale.*

While perhaps not immediately apparent from Figure 20, measured viscosities for 100 s^{-1} shear rate in this test were slightly higher than those listed in Table 4. This is presumed to be due to shear thickening tests being conducted significantly later than the original viscosity measurements displayed in Table 4. Thus, between the two tests the ink containers were opened a good number of times in order to obtain small amounts of ink for printing or other tests, and some of the solvent may have escaped each time due to evaporation. Thus, there would have been a slight increase in hydrophobising agent concentration. Therefore, the results displayed in Figure 20 are likely to represent the behaviour of inks with concentrations slightly higher than the nominal concentrations. However, they can still be expected to demonstrate a general shear thickening trend that is likely to be also found in inks with nominal concentrations.

In the case such shifts in concentration have taken place, this may have also had a slight effect on printing results. Rather than preparing a fresh batch of ink for every print run, inks were produced in slightly larger batches of up to 20 cm^3, and these were consumed completely before a new batch was prepared. However, since the effect of such concentration shifts was not considered at the time, it is not easy to estimate what practical effect this may have had on individual print runs.

Finally, *Z* values calculated for the inks, with the exception of PS ink, are higher than 14, indicating according to literature that satellite droplet formation is likely to take place [97]. However, it should be kept in mind that the values for viscosity and surface tension used to calculate *Z* are not exactly those that would be found present in the actual print head. While any difference for surface tension, measured at 23 °C rather than 30 °C used in the print head, would be relatively small, viscosity on the other hand would likely be significantly higher under the high shear rates present in the print head.

13.4 Ink jettability and printing settings

Drop velocities for the inks and pure p-xylene were studied under different combinations of waveform, drive voltage and jetting frequency. Of the three tested waveforms, *Hi-viscosity Short Polymer* ended up producing the best performance, and was chosen as the waveform to be used for actual printing.

Pure p-xylene could be jetted at up to 4 kHz under all three waveforms. Paraffin ink could be also jetted at up to 4 kHz (6 kHz with *Hi-viscosity Short Polymer* waveform), but good velocities were only achievable at 2 kHz frequency.

AKD ink could be jetted at up to 4 kHz, but, as for p-xylene alone, good velocities were only achievable at 2 kHz. AKD-PS ink could be jetted at up to 6 kHz with good velocity, though proved unstable beyond this. PS ink could be jetted at up to 12 kHz with the *Hi-viscosity Short Polymer* waveform, but only at 2 kHz with the other two tested waveforms. However, most stable jetting for PS ink was achieved at 6 kHz.

A practical reminder of the importance of correct frequency settings was had once during pilot printing experiments, when PS ink was printed accidentally at 20 kHz instead of the intended 6 kHz. This resulted in the nozzle plate becoming flooded and individual nozzles starting to become non-jetting almost immediately after printing had commenced, resulting in a very bad print quality. Luckily the error was spotted and corrected quickly.

Satellite droplets were produced with all inks and print settings, regardless of voltage, frequency or waveform. In the light of the high *Z* values for the inks, as mentioned previously, this is not a surprising result. The number of satellite droplets produced under different conditions was not recorded. The size of satellite droplets could also be observed to vary depending on settings, but there was no possibility to quantify their volumes.

Based on ink jettability studies, print settings specified in Table 5 were adopted for different inks for use in printing of the actual test samples.

Table 5. Printing settings.

Ink	**Waveform**	**Drive voltage / V**	**Velocity / ms^{-1}**	**Frequency / kHz**
Paraffin	*Hi-Viscosity Short Polymer*	17	~ 6.9	2.0
AKD	*Hi-Viscosity Short Polymer*	18	~ 8.0	2.0
AKD-PS	*Hi-Viscosity Short Polymer*	16	~ 9.0	6.0
PS	*Hi-Viscosity Short Polymer*	28	~ 8.7	6.0

Approximate velocities as a function of drive voltage at chosen printing frequencies are presented graphically in Figure 21, together with velocities for pure p-xylene jetted at 2 kHz. Numerical values for the velocities are presented in appendix 3. Notice that in Figure 21 no confidence intervals are shown. This is due to velocities having been recorded for only a single nozzle, chosen for being relatively representative of the nozzles on a given cartridge. A proper statistical study of jetting velocities would have involved recording velocities for multiple nozzles on multiple jetting modules.

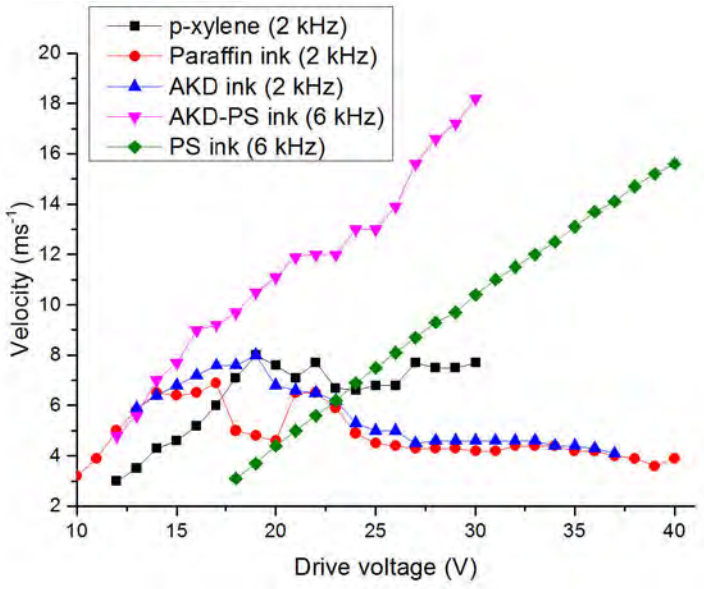

Figure 21. *Stable drop velocities as function of drive voltage at printing frequencies.*

As can be seen from Figure 21, velocities for PS and AKD-PS inks increase continuously as a function of drive voltage, in accordance with a model presented in the literature [100].

However, for p-xylene and the other two inks, velocity peaks quite early at 7-8 ms^{-1} and then reduces. This is probably due to the low viscosity of these fluids.

The final printing settings were completed by selecting the automated print head cleaning settings. There was no clear methodology specified for this, so somewhat arbitrary values were picked, which were tested during pilot studies and found to work well enough to be adopted. The main cleaning cycle used consisted of a 0.1 s purge operation, followed by a 1.0 s delay and a 1.0 s blot operation. This cycle was run for all inks at the beginning and end of printing. Furthermore, the same cleaning cycle was also run regularly during printing, every 60 s or 60 bands (whichever came first) for PS ink, and every 240 s or 240 bands for other inks. In this cleaning cycle the purge operation forces ink out of nozzles with the application of an overpressure, while the blot operation removes ink that has flooded onto the nozzle plate. Gentler or less frequent cleaning settings might have produced equally good results, but their optimisation was not the purpose of this study.

More frequent cleaning, however, was chosen for the polystyrene ink, since when viewing drop watcher camera images it was observed to start behaving in a so-called *bungee jump* manner in nozzles that would stay stationary for some time. This phenomenon results in jetted drops failing to detach from the nozzles, and instead getting pulled back inside. This might be due to local viscosity increase caused by evaporation at the nozzle, though there might also be some viscoelastic build-up taking place, due to the extra amplitude pulse used in the equipment to stimulate non-jetting nozzles.

When the print head was idle, i.e. not printing, a cleaning cycle, consisting of ordinary jetting conducted at 1.5 kHz for 200 ms, was run at 240 s intervals.

13.5 Contact angles

Measured contact angles as a function of drop spacing for PS ink on Whatman 4 filter are shown on Figure 22, both for printed and reverse sides. Numerical values for the same are presented in appendix 4.

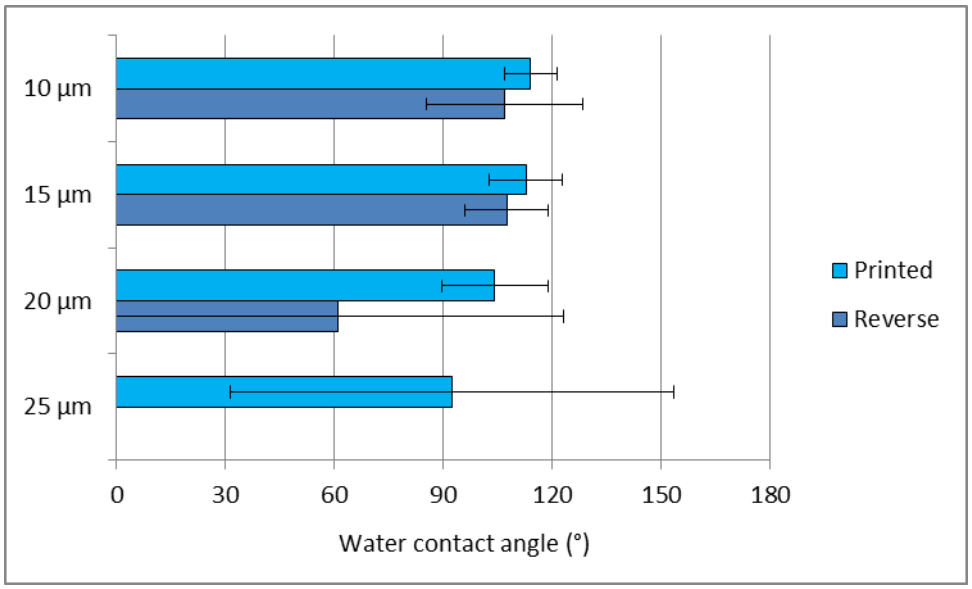

Figure 22. *Contact angle as a function of drop spacing for printed and reverse sides of Whatman 4 filter paper.*

On samples printed with 10 or 15 µm drop spacing, both printed and reverse sides were clearly hydrophobic.

On samples printed with 20 µm drop spacing, the printed side was still clearly hydrophobic, but the reverse side displayed a wide variety of contact angles, from effectively 0° (water got absorbed immediately) to slightly over 90°, with most imaged samples falling somewhere in between. In addition, imaged drops tended to be dynamic, spreading slightly during the imaging period, and contact angles could differ significantly between right and left hand sides of an imaged drop. This all indicates significant local variation in the amount of polystyrene that had managed to reach the reverse sides of the printed samples. In Figure 22 this simply appears as a high confidence interval, which does not fully do justice to the observed variation.

On samples printed with 25 µm drop spacing, the printed side was still mainly hydrophobic, though in 2 cases out of 20 the measured drops got absorbed immediately (contact angle 0°), resulting in a high confidence interval. This phenomenon might have been due to some very local jetting failures on the print head. In any case, on the reverse sides of these samples all drops got absorbed immediately, indicating that very little if any polystyrene ink had managed to reach through to this side of the samples.

13.6 Line spreading of inks

The scanned widths of printed test lines, for both printed and reverse sides, as a function of nominal line width are presented in Figures 23 to 27. Numerical values for the same are presented in appendix 5. Widths are only measured for those cases where a continuous, clearly defined line could be found on all 5 measured samples. For PS ink, width was measured from the middle of the line, while for AKD and AKD-PS inks it was measured from close to the base of the line. Measured lines are expressed in terms of absolute width, rather than in terms of relative spreading compared to nominal width.

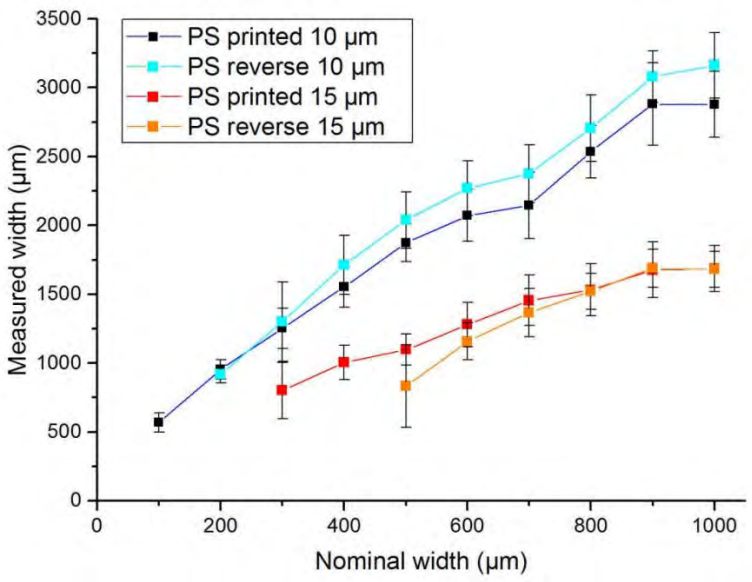

***Figure 23**. Line widths for PS ink printed on Whatman 4 filter paper: drop spacings 10 and 15 µm.*

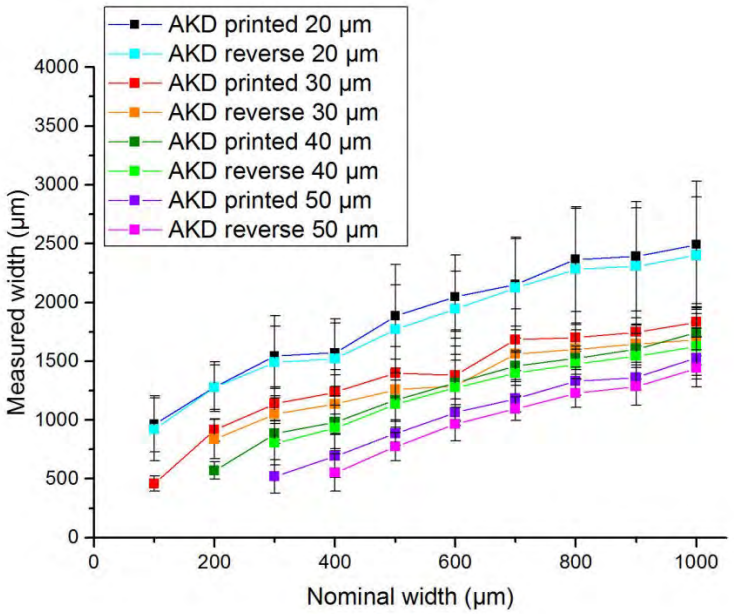

Figure 24. *Line widths for AKD ink printed on Whatman 1 filter paper: drop spacings 20, 30, 40 and 50 µm.*

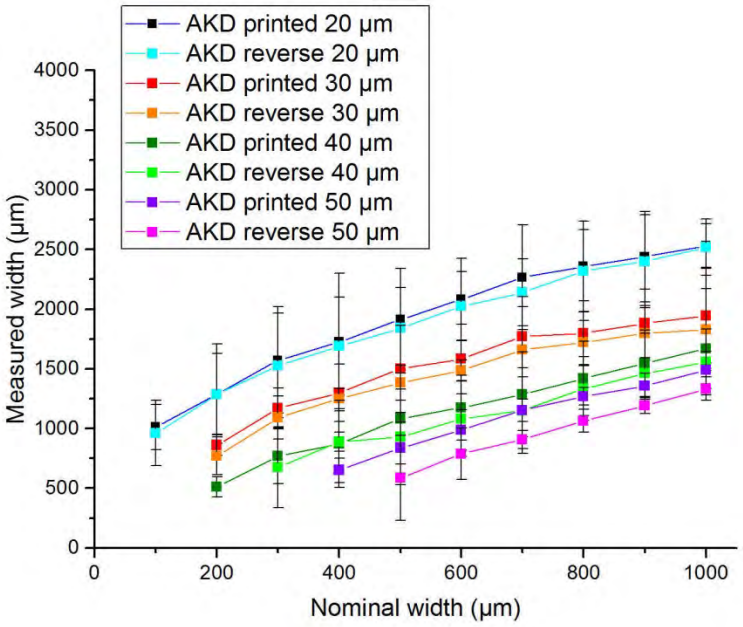

Figure 25. *Line widths for AKD ink printed on Whatman 4 filter paper: drop spacings 20, 30, 40 and 50 µm.*

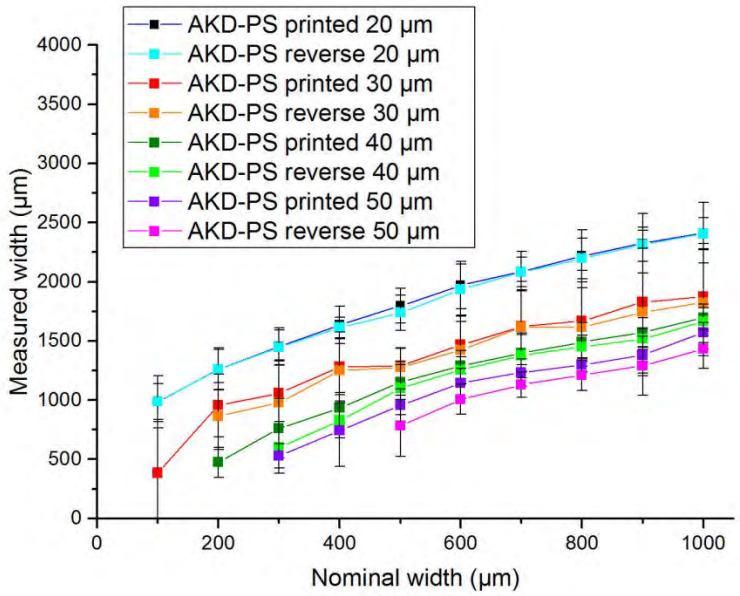

***Figure 26**. Line widths for AKD-PS ink printed on Whatman 1 filter paper: drop spacings 20, 30, 40 and 50 µm.*

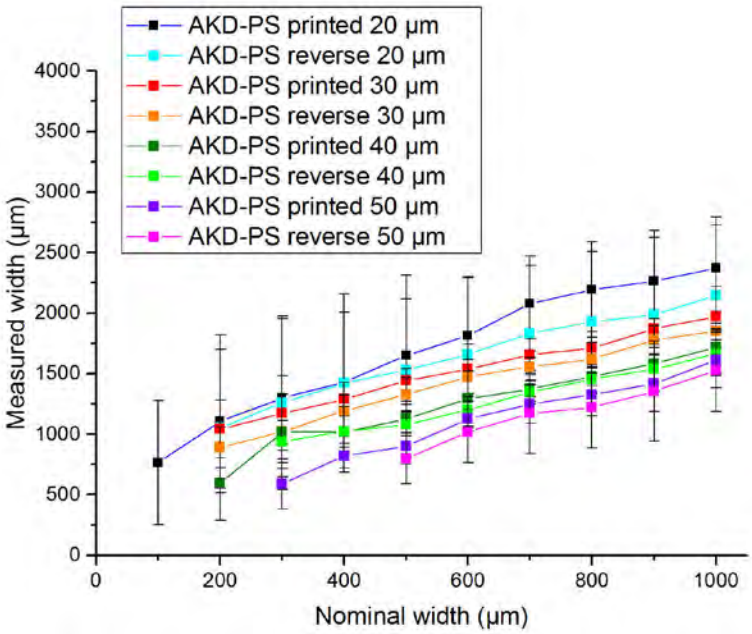

***Figure 27**. Line widths for AKD-PS ink printed on Whatman 4 filter paper: drop spacings 20, 30, 40 and 50 µm.*

The choice of drop spacing was limited by the performance of the inks. With PS ink, line widths could not be measured with 20 µm or greater drop spacing, since that would not result in a satisfactory hydrophobic pattern on the reverse side. Trying to measure AKD or

AKD-PS line widths at 10 µm drop spacing with the chosen test patterns would have resulted in some of the wider lines blending together, making their widths no longer measurable. A slightly different test pattern would have been needed to measure them.

As can be seen from the previous Figures, measured line widths tend to be slightly narrower on the reverse side compared to the printed side. Another noticeable issue is that there are very few measurable lines on either side of the paper that are under 500 µm wide. Lines narrower than this were discontinuous or otherwise too poorly defined to be properly measurable.

13.7 Hydrophobic barriers

Paraffin wax performed catastrophically poorly in producing barriers during pilot tests. It was tested with 5 samples, printed with drop spacing from 10 to 20 µm. When tested, these barriers barely slowed down water wicking at all. Therefore, further barrier testing with paraffin wax was abandoned. The rest of this section deals with barriers created with PS, AKD and AKD-PS inks.

Barrier penetration was observed as a function of time for 30 min at 5 min intervals in order to determine how quickly barrier penetration on substrates happens. An overview of this time-wise behaviour is presented in Figures 28 and 29 for Whatman 1 and for Whatman 4 filter paper, respectively. Numerical values for the same are presented in appendix 6. The results displayed in these Figures are organised by ink and drop spacing, but grouped together for all 10 barriers of different widths on the 10 test samples, resulting in a range of 0-100 for the results.

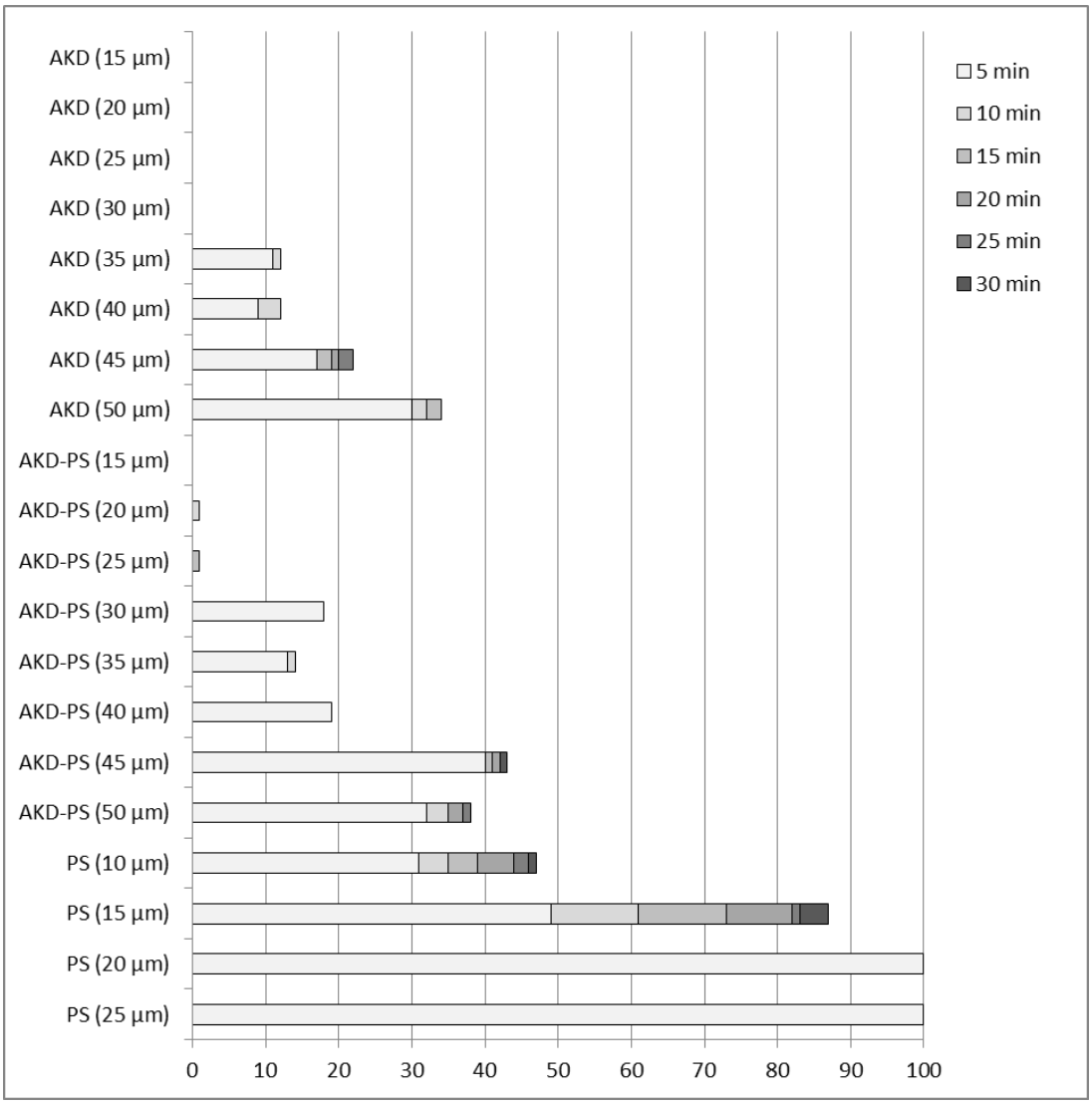

Figure 28. *Number of barriers penetrated on Whatman 1 filter paper as a function of time for different ink and drop spacing combinations: data are shown as cumulative barriers penetrated as the sum over the time segments.*

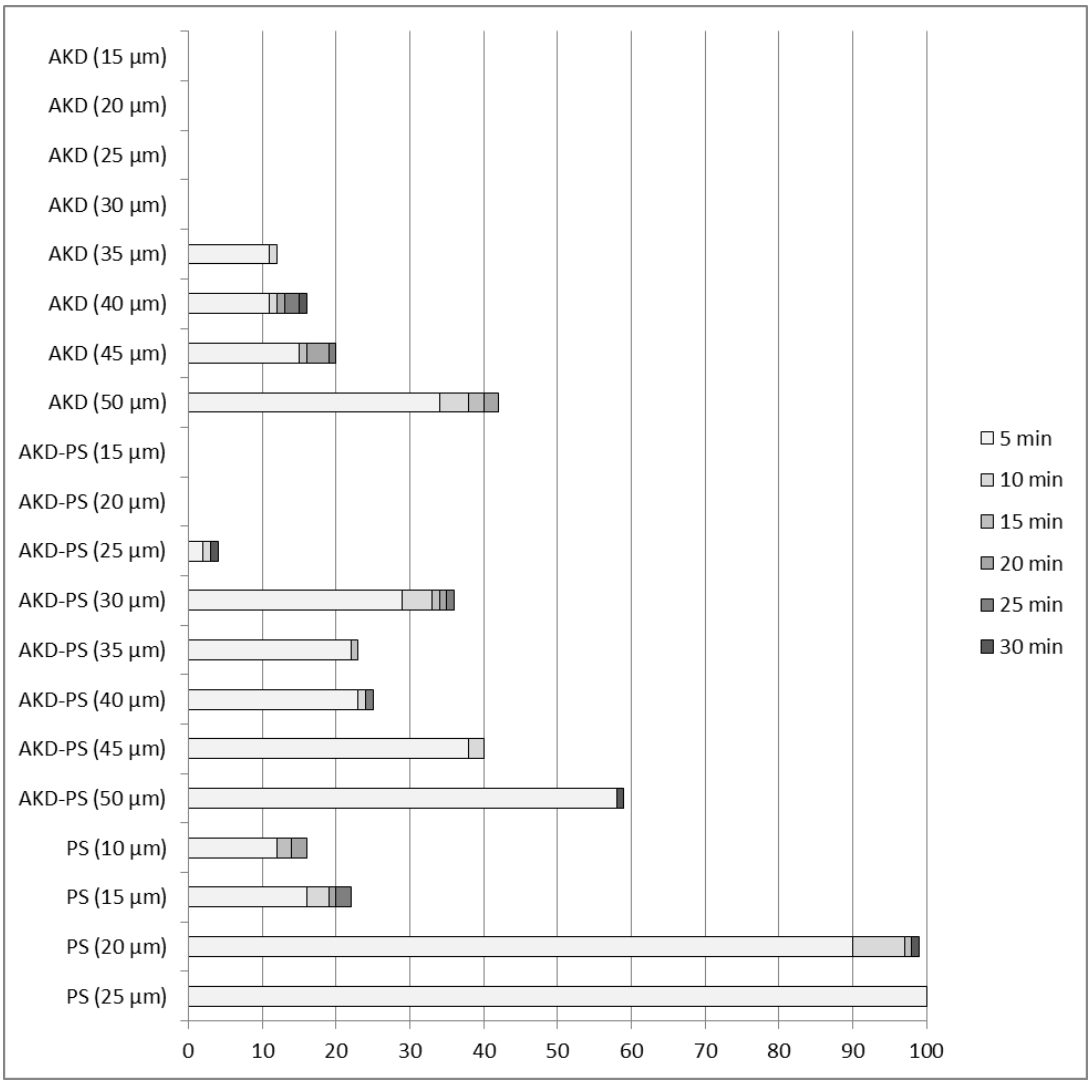

Figure 29. *Number of barriers penetrated on Whatman 4 filter paper as a function of time for different ink and drop spacing combinations: data are shown as cumulative barriers penetrated as the sum over the time segments.*

As can be seen from the Figures above, barrier penetration pre-dominantly occurred during the first 5 minutes, with very little barrier penetration taking place in the remaining 25 minutes. Thus, final results would have largely been quite similar if the barriers had only been tested for 5 min rather than 30 min. One noticeable exception to this behaviour is PS ink on Whatman 1 filter paper with 10 and especially 15 µm drop spacing. This could be taken to indicate that those printing conditions resulted in a number of barriers that could seriously delay wicking, but could not totally prevent it. The rest of this section analyses barriers as they were after 30 min of testing. Any reported barrier widths are for the printed side.

As previously mentioned, the main challenge of producing reliable hydrophobic barriers is in achieving the full depth of penetration and sufficient hydrophobisation of the reverse side. This could also be observed in these tests, where barrier penetration tended to take place clearly from the reverse side. This is illustrated in Figures 30 and 31.

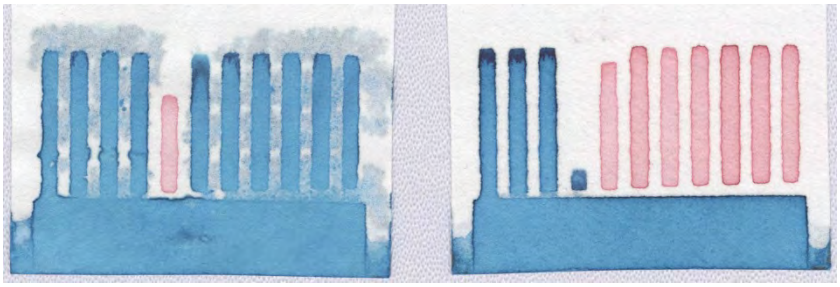

Figure 30. *Examples of barrier tests, printed with polystyrene ink at a drop spacing of 15 µm on Whatman 1 (left) and Whatman 4 (right) filter papers. Cyan-dyed channels are ones where coloured water wicked past the barriers, while magenta-dyed channels mark barriers that were not penetrated.*

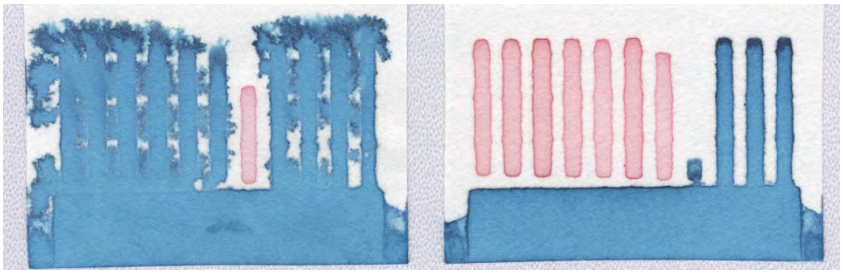

Figure 31. *Reverse side views of the samples shown in the previous Figure 30. On Whatman 1 (left) significant liquid spreading on the reverse side can be observed.*

Samples printed with polystyrene ink showed limited success. For samples printed on Whatman 1 filter paper, no reliable barrier could be produced at any studied drop spacing (10-25 µm), though samples printed with 10 µm drop spacing came close, having 90 % success rate for the two widest barriers.

On Whatman 4 filter paper, no reliable barriers could be produced with 20 or 25 µm drop spacing. However, with 10 µm drop spacing, reliable barriers with nominal width of 300 µm (measured width 996 ± 114 µm) could be produced, while with 15 µm drop spacing reliable barriers needed a nominal width of 400 µm (measured width 883 ± 91 µm). These do not

quite match up with the results from the previous section, where 200 and 500 µm wide lines were required to produce reliably measurable wicking containment lines on the reverse side.

With AKD and AKD-PS inks, reliable barriers could be produced on both filter papers at all tested drop spacing values from 15 µm to 50 µm. However, with short drop spacing value the hydrophilic channel behind the barrier becomes so constricted by the spreading walls that measuring the width of the barrier reliably was not possible. Table 6 lists the minimum nominal barrier width needed to produce a reliable barrier for a given drop spacing, while Figure 32 presents the relationship between drop spacing and measured barrier widths for the same barriers. Numerical values for the information presented in Figure 32 can be found in appendix 7.

Table 6. Nominal barrier width [µm] for narrowest reliable barrier.

Ink	**Paper**	**Drop spacing / µm**							
		15	**20**	**25**	**30**	**35**	**40**	**45**	**50**
AKD	Whatman 1	50	50	50	50	150	250	250	300
AKD	Whatman 4	50	50	50	50	150	250	300	350
AKD-PS	Whatman 1	50	100	150	200	200	150	400	450
AKD-PS	Whatman 4	50	50	100	300	200	300	300	400

As can be seen from Table 6, on samples printed with AKD, the required nominal line width increases clearly as a function of increasing drop spacing, and both papers behave similarly. On samples printed with AKD-PS, there are some anomalies (Whatman 1 with 40 µm drop spacing, Whatman 4 with 30 µm drop spacing) which might suggest some problem with printing conditions when printing these samples.

Also, the required nominal widths to produce a barrier listed here are slightly narrower than those required previously to produce good lines for measuring line spreading. This might be largely explained by differing grading in the test set-ups, since lines were measured at 100 µm intervals, while barriers were tested at 50 µm intervals.

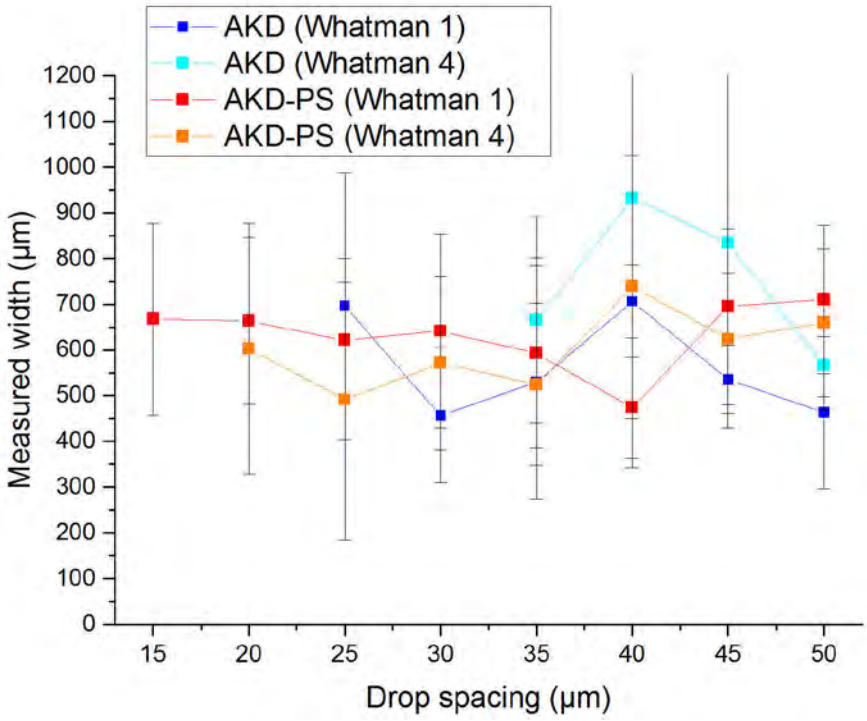

Figure 32. *Measured widths for reliable barriers. Those barriers where a reliable width could not be measured are not shown.*

As can be seen from Figure 32, measured width for the narrowest reliable barrier is approximately the same regardless of drop spacing. Combined with results from Table 6 this indicates that if drop spacing is decreased, a reliable barrier can still be produced by increasing the nominal line width, and due to line spreading the real barrier width is of roughly similar dimensions in both cases. The narrowest barrier shown in this Figure is 463±166 µm (AKD on Whatman 1 at 50 µm drop spacing) while the widest barrier is 932±560 µm (AKD on Whatman 4 at 40 µm drop spacing). The widest barrier is roughly comparable to those reported for PS ink earlier on, though most of the listed barriers are narrower than that.

Furthermore, Figure 32 does not indicate any clear trend between paper or ink type, and required real barrier width for these two inks and papers.

13.8 Hydrophilic channels

Hydrophilic channel test results provided a bit of a surprise. Test samples printed with PS ink on Whatman 4 filter paper at 15 µm drop spacing behaved consistently in the expected manner: dyed water easily wicked the whole length on all but the narrowest channels within

5 min. However, on samples printed with AKD or AKD-PS ink wicking was much slower, with water in none of the channels reaching the top of the channel within the originally allocated time of 5 min. Therefore water was allowed to wick for another five minutes, but still the water would not quite reach the top on any of the channels. Examples of test devices after the tests are displayed in Figure 33.

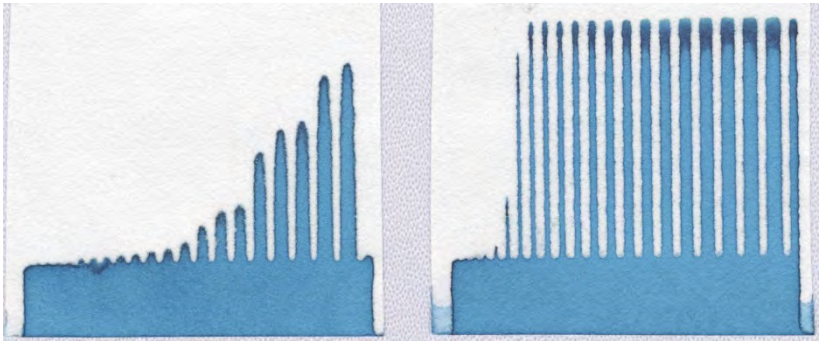

Figure 33. *Examples of channel tests, printed on Whatman 4 filter paper with AKD ink at drop spacing of 45 µm (left) and with polystyrene ink at drop spacing of 15 µm (right).*

Closer examination of the devices printed with AKD or AKD-PS ink revealed that the wicking front within the channel is not roughly flat, as expected, but closer to a tapered round shape. This suggests that water initially advanced along the centre of the channel, and then spread out to the sides. Furthermore, wicking distances seemed to increase as a function of channel width. In any case, all of the channels on AKD or AKD-PS printed samples were considered to have failed the test, and their dimensions were not further characterised. This would suggest that there is a migration of the common hydrophobising agent in the formulations, namely AKD, along the filter paper fibre surfaces, which acts only temporarily to pin the advancing meniscus. Thus in these regions wicking is replaced by diffusional molecular motion.

With patterns printed with PS ink on Whatman 4 filter, channels with nominal widths of 1.2 and 1.3 mm were chosen for closer examination, since they indicated the narrowest channels where water could wick the full length of a channel quite reliably within 5 min. On channels with nominal width of 1.2 mm, water managed to reach the top of the channel in 9 out of 10 tested samples, while on the 10th sample it fell approximately 4 mm short. On all channels with nominal width of 1.3 mm or more water managed to reach the end of the channel with 100 % consistency, while on channels with nominal width of 1.1 mm or less, water did not reach the end of the channel on any of the test samples, being either entirely blocked or

seriously slowed down by chokepoints within the channel. This indicates a relatively sharp shift from consistently well performing to consistently poorly performing channels.

When the actual channel widths were measured from the printed side, nominal channel width of 1.2 mm resulted in a measured width of 540 ± 76 µm and nominal channel width of 1.3 mm in a measured width of 680 ± 80 µm. Channel widths on reverse sides were not measured. Differences between the nominal and measured widths are due to the line spreading of the hydrophobic walls separating the channels from each other. Adjusting the width of the separating wall would affect the relationship between the nominal and measured widths.

Comparing the result of 680 ± 80 µm with those previously published, as listed in Table 1, it is found to be slightly wider than channels reported for flexographically printed polystyrene ink (500 µm), inkjet etching of polystyrene-treated substrate (450 ± 50 µm) or inkjet-printed hot-melt wax (561 ± 45 µm). However, it is comparable to that for inkjet-printed PDMS (700 µm).

From a practical device design perspective, it might be desirable to keep channel dimensions on devices a little bit wider than the narrowest achievable width, in order to provide some extra margin of error in production. Furthermore, very narrow channels may wick liquid slower than wider channels. In a very recently published experimental study, wicking speed was measured on laser-cut paper strips 0.5-2.0 mm wide, with the narrower channels having somewhat slower wicking speeds than wider channels [209]. While no explanation was given for this phenomenon, it might be due to non-uniform structure of paper resulting in random local chokepoints that have a relatively bigger impact on narrower channels, where fewer alternative routes are available.

14 Discussion

14.1 Ink volume versus pore volume

Information provided by the results of the line spreading tests, presented previously, can be used to calculate pore volumes for the regions entirely hydrophobised by printed lines. If a printed line produces a continuous hydrophobic line on both sides of a substrate, then, assuming that the cross-section of the line within the substrate would be wedge-shaped, wide at the print side and narrowing toward the reverse side, the total area of the cross-section, including both pores and solid material, would be

$$A = ½\, h\, (w_\mathrm{p} + w_\mathrm{r}) \tag{24}$$

where h is thickness of the substrate, and w_p and w_r are the line widths on the printed and reverse sides. The total pore volume V_p for a section of uniform line can be defined as

$$V_\mathrm{p} = Al\varepsilon = ½hl\varepsilon\left(w_\mathrm{p} + w_\mathrm{r}\right) \tag{25}$$

where l is the length of the observed line section and ε is substrate porosity.

The above equations are based on the assumption that the cross-section is wedge-shaped, with straight edges. This is a somewhat oversimplified model, since in reality the sides are likely to be slightly curved. Determining the real shape of cross-sections reliably would require microscopic study of cross-sections, which is beyond the scope of the present work.

For comparison, ink volume V_i consumed by a DMP-2831 printer to produce a section of line is dependent according to the selected drop spacing, and can be expressed as

$$V_\mathrm{i} = d^{-2} l V_d w_\mathrm{n} \tag{26}$$

where d is the used drop spacing, w_n is the nominal line width and V_d is the volume of an individual ink drop.

The relative ratio of pore volume to ink volume can then be simply calculated as

$$\frac{V_\mathrm{p}}{V_\mathrm{i}} = \frac{d^2 h\varepsilon(w_\mathrm{p}+w_\mathrm{r})}{2w_\mathrm{n}V_d} \tag{27}$$

with values greater than 1 indicating that the volume of the pores contained within the hydrophobic region is larger than the amount of ink needed to hydrophobise that same region.

Combining equation 27 with previously presented line spreading data for different inks under different conditions, and with substrate properties presented in Table 2, while presuming that ink drops were of the nominal 10 pl volume, ratios of V_p/V_i can be easily calculated for the inks and substrates used in the current study. These ratios are displayed in Figure 34 for Whatman 1 filter paper and in Figure 35 for Whatman 4 filter paper. These values are presented in numerical form in appendix 8.

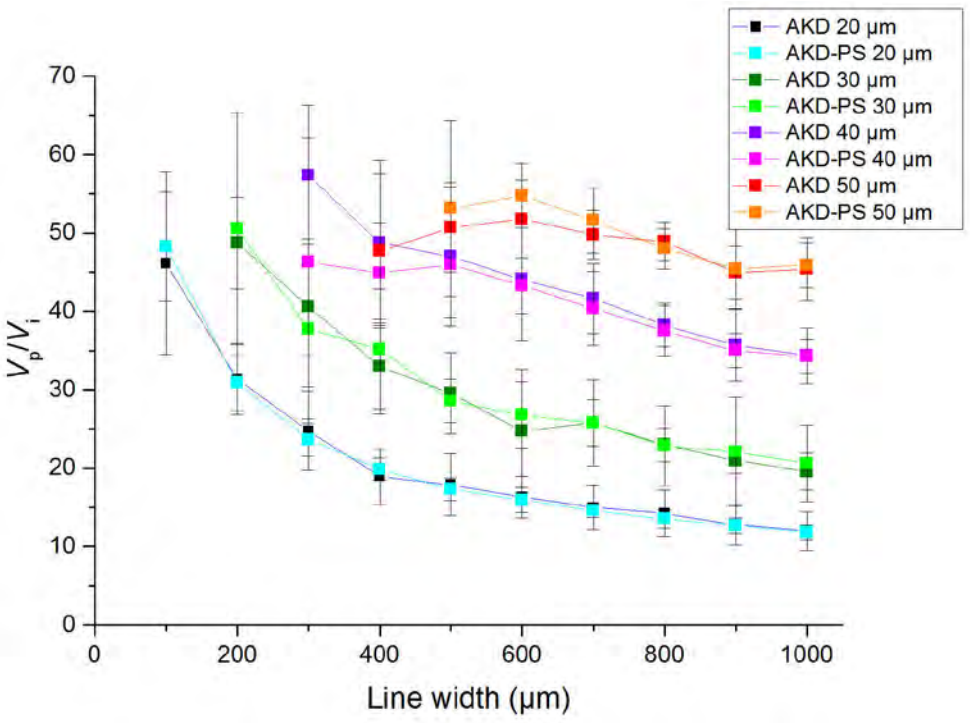

Figure 34. *V_p/V_i ratios for lines printed on Whatman 1 filter paper, as a function of line width for a range of drop spacing.*

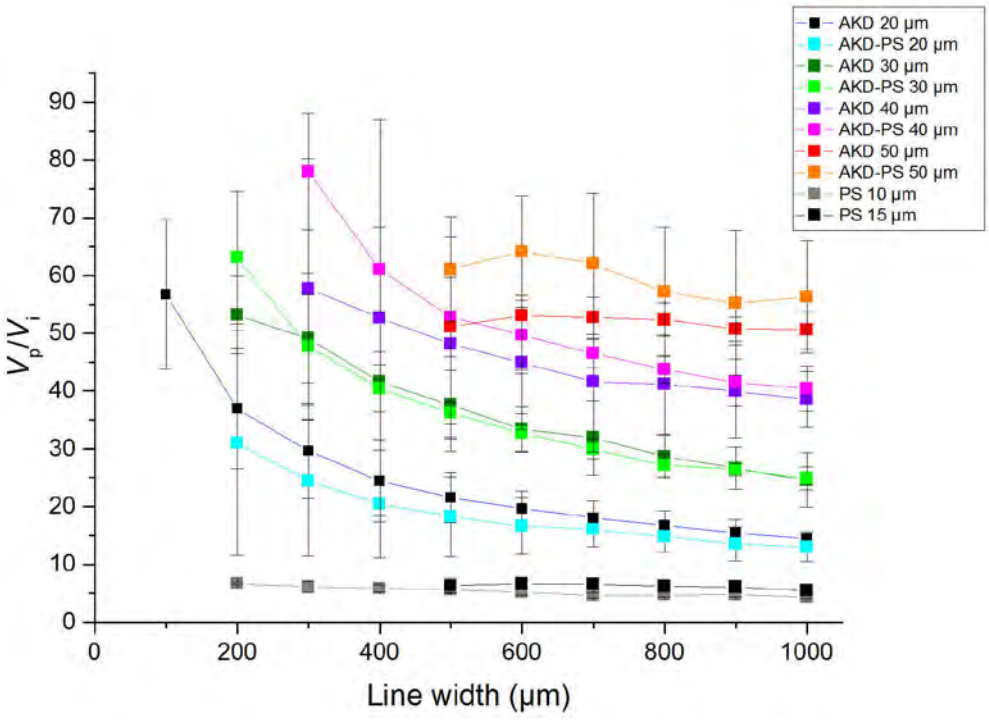

Figure 35. *V_p/V_i ratios for lines printed on Whatman 4 filter paper, as a function of line width for a range of drop spacing.*

Values of V_p/V_i ratio vary quite a bit, from around 5 for polystyrene ink to well over 50 for AKD containing inks with high drop spacing. Comparing the graphs in the Figures, a number of observations can be easily made. Firstly, AKD and AKD-PS inks tend to result in roughly similar volume ratios. Secondly, increase in drop spacing results in an increase in volume ratio. Thirdly, an increase in line width results in a decrease in volume ratio. Fourthly, polystyrene inks seem to have lower volume ratios than AKD containing inks, though different drop spacing values used for these inks limit direct comparison. Finally, lines printed with AKD or AKD-PS ink on Whatman 4 filter paper tend to produce on average around 16 % higher volume ratios than similar lines printed on Whatman 1. Interestingly, this is approximately the same as the pore volume to sheet area ratio for the two papers, which is 17 % higher for Whatman 4 than Whatman 1, and suggests that the level of pore filling in both cases is similar, which in turn suggests that most of the wicking is via a precursor fibre surface film wetting. This must also be the case in general, as all volume ratios are significantly greater than 1, confirming that the spreading of the inks has happened primarily as a film flow along fibre surfaces, rather than the ink front depending on complete filling of pores in order to advance. There simply would not have been anywhere near enough ink to completely fill all of the pores with hydrophobised regions.

That said, some local pore filling may still have taken place, especially in the proximity of the printed surface.

Previously, initial advance of a water front on un-sized paper has been shown to be similarly driven by surface film flow [188]. The findings above indicate that p-xylene, a non-polar solvent, spreads in a similar fashion.

14.2 Regimes of hydrophobicity

In an ideal hydrophobically patterned device, hydrophobic areas are highly and uniformly hydrophobic, while hydrophilic areas are highly and uniformly hydrophilic. However, the real world is a more complex place, and patterned devices can display a number of intermediate regimes between these two ideal extremes. In this work, a number of such regimes were manifest.

The first occurrence an intermediate regime can be seen in the results for contact angle measurements with polystyrene. In most cases these were clearly hydrophobic where printed, or highly hydrophilic (water absorbed immediately) where not printed. However, when contact angles were measured for the reverse sides of the substrates printed with 20 µm drop spacing, results were somewhere in between – drops spread on the surface, but did not get absorbed quickly. This indicates that some ink managed to reach the reverse side of the substrates, but not enough to fully hydrophobise them. Furthermore, there was highly local variation in contact angles, even for left and right hand sides of the same water drop, indicating that the amounts of ink that reached the reverse varied locally. This would suggest that the uneven nature of the substrate resulted in faster access to the reverse side on some areas. This in the printing world is known as strike through. Contact angle measurements do not directly tell how much polystyrene had managed to reached the reverse side. To better quantify these amounts would likely require some more advanced surface analysis technique, such as X-ray photoelectron spectrometry (XPS).

A second occurrence can be seen with line spreading test patterns printed with AKD or AKD-PS inks. When these test patterns were placed into contact with dyed water at one edge, to allow water to wick up the hydrophilic regions, the final line edges did not immediately become visible. Rather, the line looked slightly club-shaped, with the end that had just come in contact with water appearing wider. This is illustrated with Figure 36, taken from a dried sample.

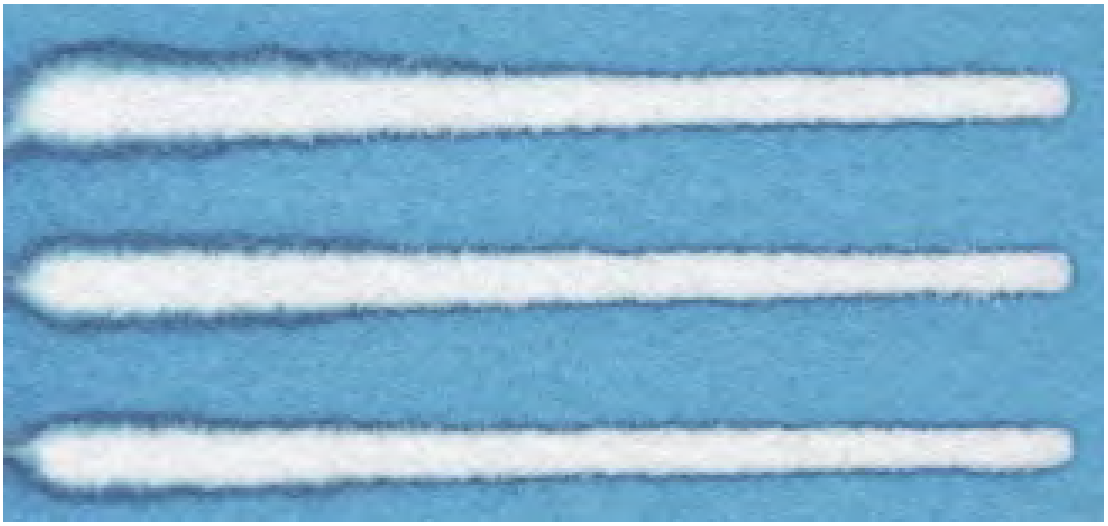

Figure 36. *Lines printed with AKD ink on Whatman 4 filter paper at 40 µm drop spacing, seen from the printed side. Water (cyan) has wicked from right to left, resulting in a slightly club-shaped form to the hydrophobic region. Enlarged image, displayed lines are actually 35-36 mm long.*

On the right hand side of Figure 36, where water has been longest in contact with the hydrophilic-hydrophobic interface line, a sharp edge is visible, indicating that here the dyed water had reached the edge of the fully hydrophobic region. However, on the left hand side, which had remained exposed to dyed water for a shorter time (test pattern was taken to dry soon after water reached this far), the edge region is less clearly defined. There is a light cyan region, suggesting limited presence of dyed water close to the edge of the supposed fully hydrophobised region, and a darker, wider line beyond this where significantly more dye has dried.

A similar effect could also be observed with channel test patterns printed with AKD-containing inks, as described previously. In those cases it manifested by the wicking front initially advancing along the centre of the channel, and then spreading to the sides. With channels, this is a very unwelcome situation, since it slows down the advance of the liquid flow along the channel, with regions on the sides of the channel drawing away liquid from the centre of the channel.

This suggests that surrounding the fully hydrophobised region, there is a wider region which has become slightly hydrophobic, so that water advances very slowly in this region, compared to the fully hydrophilic regions. No such region is observable on samples printed

with polystyrene, indicating that this might be related to properties of AKD and its known hydrolysis and migration properties on cellulose fibres.

In a paper machine wet-end, there is an interaction between cationic AKD-particles and anionically charged fibres [155]. This promotes retention of AKD, which is highly beneficial from the paper-making perspective. Similar interaction might have taken place here when AKD-containing inks migrated along the fibre surfaces after the solvent was removed, or part of the AKD molecules may have become separated from the ink by this attraction, actually resulting in a reduction of AKD concentration, partially counteracted by evaporation, as the ink advanced further away from the original printed region. This could then result in the ink at the farthest reaches having too little AKD left to result in full hydrophobisation. If this is the case, there would be a gradient in AKD (or AKD reacted cellulose) concentration when viewed from the original printed region towards edges. Verifying such a gradient would require some quantitative surface analysis methods, such as Raman mapping.

Besides initial spreading of the ink, AKD can possibly spread further out during the curing step, where it is heated well over the melting point. A number of possible spreading mechanisms for heated AKD have been presented, including capillary wicking along fibre gaps, vaporisation followed by re-deposition, and fibre wetting by autophobic monolayer pre-cursor, as well as low-temperature spreading after curing [15] [210].

Surface diffusion of AKD on typical paper fibre matrix has been shown to occur, with diffusion coefficient being of the order 10^{-11} m^2s^{-1}, and increasing linearly with temperature [210]. Such diffusion resulting in AKD spreading beyond the original printed pattern might occur during the curing process. However, the distance that can be diffused within the scope of the 10 min curing phase is rather short.

Vaporising followed by re-deposition by condensation could result in transport of non-reacted AKD within or between paper sheets [210]. In the present study, samples cured in the oven were exposed to air circulation during the process, and this would have likely carried away any evaporated AKD leaving the original sheet. On the other hand, samples cured on the laboratory hot plate were covered with blotting paper sheets to prevent any air draughts from blowing them off the plate, and thus evaporated AKD could have re-deposited within the original sheet or transferred to the blotting paper.

If the melted AKD could spread significantly, this could affect the AKD concentrations close to the edges. However, if there is a strong affinity between fibre and AKD, it should also restrict the spreading of melted AKD. Since the printed AKD patterns on paper are effectively invisible to the naked eye, and not properly hydrophobic before the curing step has been carried out, estimating the amount of spreading during or after curing would require some advanced instrumentation. For example, Raman mapping carried out before and after the curing step could help to diagnose the amount of line spreading resulting from the heating.

Another possible explanation for such a phenomenon could be simply poor printing quality. As mentioned previously, all of the inks resulted in satellite droplets, which could end up somewhere else than the main drop. However, when line spread patterns were printed, the printing unit travelled in the direction of the lines. Thus, any satellite droplet that had too high or low speed would still end up on the intended printing region. For ink to be jetted seriously away from the intended line region, some of the nozzles would have needed to have started jetting significantly to the side. Indeed, such a phenomenon could be observed very occasionally during drop watch tests. However, such random error could not explain the magnitude of the effect shown here, visible on 40 samples printed with 2 different jetting modules, and thus has to be dismissed.

In previous studies reporting inkjet printing of AKD-based solutions [15] [157] [158], no such uneven edge region was reported. Those studies also used as solvent n-heptane, chosen specifically due to being a fast evaporating solvent, and it has a higher vapour pressure than p-xylene [200]. Thus, n-heptane based ink could be expected to have less time to spread. However, n-heptane also differs from p-xylene in having lower surface tension, with n-heptane based ink reported as having a surface tension of 19.90 $mN \cdot m^{-1}$ at 25 ºC [158]. Lower surface tension also reduces the amount of spreading that would take place in a given amount of time. These difference in solvent properties between observed and previously reported is a likely explanation for the uneven edge region reported in this study. However, simply substituting p-xylene for heptane might also bring new challenges regarding jettability, since the low surface tension of heptane-based inks is well below the recommended minimum surface tension level for the DMP-2831 printer, and this could result in nozzle plate flooding or other problems.

Another approach to look at these edge regions is to consider transport mechanisms for liquid inside paper. In the literature, four different mechanisms have been identified [155]:

1. Capillary penetration
2. Surface diffusion on fibres
3. Diffusion through fibres
4. Vapour phase transport

Capillary transport has been previously discussed extensively, and it has been assumed to be the only significant method of transport for samples in paperfluidic devices. However, AKD works through spot hydrophobisation, where individual and relatively small AKD molecules substitute hydroxyl groups by reaction with the cellulose surface. While spot hydrophobisation can relatively easily stop capillary wicking by pinning the advancing meniscus, there may remain enough space between hydrophobised spots to allow small amounts of water to slowly diffuse past them. If such diffusion takes place, then two different regimes could be proposed to exist and correlate with observation: the fully hydrophobised region, where water cannot advance at all, and a partially hydrophobised region, where water can diffuse but cannot advance as surface or capillary flow.

The third and rarest occurrence could be observed in barrier test samples printed with polystyrene on Whatman 1 filter paper at 15 µm drop spacing. While these test patterns did not demonstrate reliable enough barriers, some of the hydrophobic barriers demonstrated interesting properties. On 3 of the 10 tested devices, coloured dye managed to break initially into the barrier region, but on some areas it could not break further into the hydrophilic channel on the other side – instead, it continued to wick along the hydrophobic wall separating the two channels! An example of this phenomenon is displayed in Figure 37.

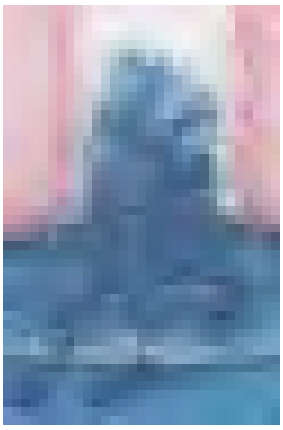

Figure 37. *Enlarged picture from the reverse side of a barrier test pattern printed on Whatman 1 filter paper with polystyrene ink at 15 µm drop spacing. Cyan dyed water has penetrated initial barrier, visible as a darker line in the bottom, and continued wicking along the hydrophobised region, but has failed to break back into the hydrophilic channels (marked with magenta dyed water afterwards).*

This result looks odd – surely the preferred path for liquid should be via the hydrophilic channel, rather than along the poorly wicking wall separating the two channels. In order to stop the liquid from passing into the hydrophilic channel, the border region of the wall has to be more hydrophobic than the bulk of the wall itself. However, this border region is actually farther away from the original printed line than the bulk of the wall.

One way to explain this observation is by the coffee stain effect. This is a phenomenon where a small amount of liquid dries on a surface, and dissolved solids are concentrated to the edge due to convections caused by evaporation. Indeed, such a phenomenon can also take place within a thin porous medium, as demonstrated in a previous study where hydrophilic channels were etched into polystyrene-treated paper in order to re-deposit the polystyrene [110]. While that study used a different solvent, toluene, it would not be unreasonable to expect that the same could also take place with p-xylene. This could be simply verified by repeating the inkjet etching study with p-xylene as a solvent instead of toluene. Alternatively, the coffee stain effect could also be evaluated by applying a drop of PS ink on a smooth glass slide, allowing the ink to dry and then evaluating the surface profile in some fashion – the coffee stain effect should result in a roughly doughnut shaped outline after drying. For more advanced analysis methods, Raman mapping could be used to analyse polystyrene concentrations around the edges of the barriers, to see if the edge area has higher concentration than the bulk.

The coffee stain effect would be very beneficial for paperfluidic devices. Deposition of higher concentrations of hydrophobising material at the barrier edges would result in more clearly defined edges, with a sharp contrast between the hydrophilic and hydrophobic regions.

14.3 Contact angles versus barrier tests

In this research, contact angles were studied for polystyrene printed on Whatman 4 filter paper in order to see how this test method would correlate with the results of the barrier test studies. This ink/paper combination was chosen because it displayed a rapid shift in barrier performance when drop spacing was increased. Contact angle of the printed side did not give reliable indication to the expected performance of barriers. However, when the contact angles for the reverse sides were measured, good correlation existed: on samples printed at 10 or 15 µm drop spacing, the reverse side was clearly hydrophobic and reliable barriers could be produced. When drop spacing was increased to 20 or 25 µm, the reverse sides remained partially or fully hydrophilic, and no reliable barriers could be produced anymore.

For comparison, it might have been interesting to conduct a similar contact angle study also for polystyrene printed on Whatman 1 filter paper at 10, 15 and 20 µm drop spacing. With these conditions, no reliable barriers could be produced.

AKD-containing inks used in this study could produce reliable barriers with all used drop spacing values, up to 50 µm. Therefore, measuring their contact angles was not considered particularly interesting, since they could all be expected to be clearly hydrophobic on the reverse side. However, if drop spacing would be further increased beyond this, at some point the reverse sides could also be expected to start featuring lower contact angles. Studying performance of AKD-containing inks with drop spacing in the 55-75 µm range might provide more insight into their behaviour.

14.4 Substrate properties

Only two different substrates were examined in this study, and these were quite close in their properties when it comes to thickness, basis weight or porosity. As regards raw material, they are both made of cotton cellulose.

AKD-containing inks managed to penetrate the full depth of both substrates, to produce reliable barriers. However, the more viscous PS ink could produce reliable barriers only on

Whatman 4, indicating that it could easier penetrate through this substrate, even though Whatman 4 is actually slightly thicker than Whatman 1.

There are two aspects where these two papers differ from each other, particle retention rating and permeance. Whatman 4 has larger particle retention rating, which indicates that it has more large pores through which large particles can pass through. These large pores also explain why Whatman 4 also has higher permeance, with air more easily able to pass through the large pores.

However, previous findings indicate that polystyrene ink actually travelled through the substrate mainly by surface flow along fibre surfaces, which is different to a path taken by flowing air through the pores. Also, internal friction of liquids makes their flow properties quite different from gases, and a porous medium behaves differently as a flow resistor for the two, resulting in different kinds of preferred paths through it [175]. Thus, while permeance seems to correlate with quick penetration, it cannot truly explain it. Perhaps the path travelled on Whatman 1 from printed to reverse side was more tortuous than on Whatman 4?

In a very recently published experimental study, fibre thicknesses of various Whatman filter and chromatography papers were studied using scanning electron microscopy. Based on analysis of 20 fibres per paper type, imaged from the paper surface, fibres on Whatman 1 were reported to be 19 ± 1 µm thick, while those on Whatman 4 were reported to be 20 ± 4 µm thick, indicating no major difference between the two papers in this aspect. [209]

When dyed water wicked along the filter papers, such as in the control channel used in barrier tests, it could be observed to travel somewhat faster on Whatman 4 when compared to Whatman 1. However, no effort was taken here to measure exact wicking speeds for water, since it was not the purpose of this particular study. However, it might have been useful to conduct a similar wicking test for p-xylene, to see if the same difference could be observed for this non-polar solvent. As can be seen from the results of line spread tests, p-xylene certainly spreads well on a cellulose substrate.

In any case, if a substrate was to be designed for easy patterning of hydrophobic barriers with solvent-based inks, there are two other aspects that should be taken into particular consideration: thickness and uniformity of structure. Thickness is quite obvious, since together with tortuosity it determines the length of path that the ink needs to travel to penetrate the full depth of the substrate. The thinner the substrate, the easier it is to produce

barriers. However, too thin substrates would also be lacking in mechanical strength. One alternative could be to use a composite structure consisting of a thin, easily hydrophobically patterned wicking layer attached to a thicker, impermeable backing layer providing mechanical strength.

Uniformity of structure could be viewed from several different angles. One of these is uniformity in the respective *x*, *y* and *z* dimensions. On paper, fibres are oriented primarily in the plane of the sheet, and a path traversed along fibre surfaces in the *z* direction might thus appear quite different from one traversed in the plane of the sheet. Furthermore, due to manufacturing procedure and resulting fibre orientation, paths travelled in the *x* and *y* directions (machine and cross-machine directions) may also appear different. On the other hand, in a porous medium consisting of spherical particles bound to each other, the traversed path could be expected to be similar regardless of chosen direction.

Uniformity could also be seen in terms of microscale variations in traverse times between parallel paths in a given direction. Filter paper is a rather rough material that displays limited uniformity, affecting all inks used to pattern it, not just polystyrene. An example of the problems caused by the lack of uniformity in the *z* direction can be seen in Figure 38.

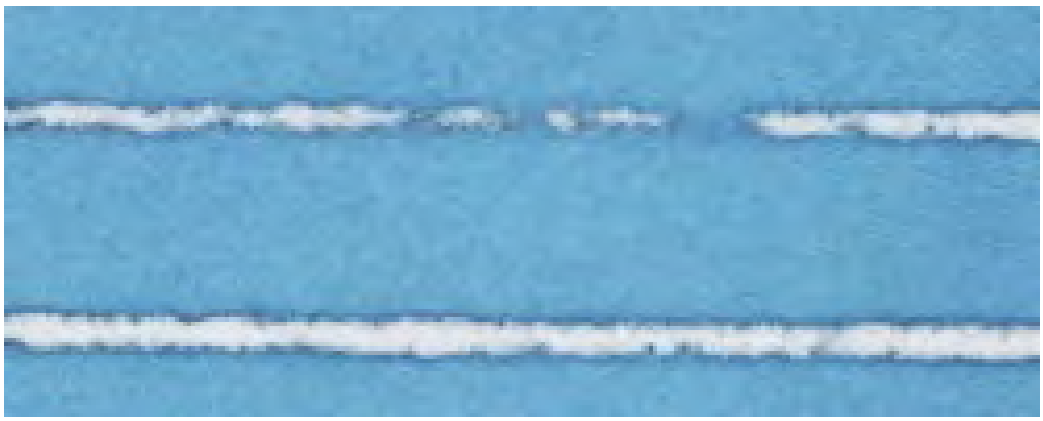

Figure 38. *Lines printed on Whatman 4 filter paper with polystyrene ink at 15 µm drop spacing, viewed from the reverse side. Top line is nominally 0.3 mm and bottom line 0.4 mm wide.*

As can be seen from Figure 38, a continuous line printed on one side of the paper has resulted in a discontinuous line (upper one in Figure 38) on the reverse side. That is to say, in some local areas the path between the separate sides was short enough for the ink to reach

the other side before drying, while in others it was not. Increasing the width of the printed line resulted in a continuous line (lower one), though in this case the lack of uniformity still manifests itself as a rather ragged outline. Better uniformity would allow for better resolution, i.e. narrower barriers and channels.

14.5 Hydrophobic ink properties

Desirable ink properties for hydrophobic inkjet inks can be summarised as follows:

1. Stable jetting at sufficiently high jetting frequencies
2. Sufficient depth penetration
3. Sufficient dry solid content to produce barriers
4. Sharply defined edges for printed patterns

Achieving a good overall performance is something of a compromise due to the way these properties interact with viscosity. Achieving good jetting (1) requires moderate viscosity, while best depth penetration (2) is achieved with low viscosity. Increasing dry solid content (3) results in an increase in viscosity. However, the controlling viscosity of ink during the printing process tends to be dynamic rather than just the static value.

Complex (non-Newtonian) fluids can display shear thickening, such as all the inks in this study, resulting in higher viscosity when exposed to high shear rates, such as those encountered in inkjet print heads. This can be used to an advantage by formulating inks that that have high viscosity within the print head (high shear rate) but low viscosity when spreading on a substrate (low shear rate). However, actually measuring viscosities at shear rates close to those encountered in print heads is something of a technical challenge at the moment.

Another dynamic phenomenon affecting ink viscosity is drying. As solvent evaporates from ink during drying, relative dry solids content and thus ink viscosity increases. However, within this study, there was no effort taken to study such drying effects and the resulting viscosity increase as a function of time.

Furthermore, temperature increase can be used to decrease viscosity. It might be a tempting idea to heat up the substrate to decrease ink viscosity and thus increase penetration. However, such an approach might backfire due to increased temperature resulting in faster solvent evaporation. In this study, all tests were conducted at constant temperatures, though

printer settings would have enabled testing the effect of higher ink chamber and mounting platen temperatures on ink penetration.

In the rest of this section, the hydrophobic inks used in this study are evaluated in the light of the four criteria (1-4) mentioned at the beginning.

Paraffin wax based ink performed very poorly. It had limited jetting frequency (2 kHz), due to low viscosity. More importantly, it could not produce effective barriers, with all 5 pilot barrier test patterns getting penetrated very fast. Initially, this was speculated to have been due to part of the solid content being not entirely dissolved and thus getting removed by the filtering step. However, when viscosities of filtered and unfiltered paraffin wax ink were compared, there was no noticeable difference. Finally, barrier properties of the ink were tested by allowing unfiltered ink to wick directly into filter paper strips from a container, thus effectively saturating the pores in the region that it would cover. After drying, cyan dyed water was allowed to wick along the paper starting from the reverse, still hydrophilic, end. When the wicking water front reached the edge of the paraffin treated region, it stopped for a while, but eventually it started slowly penetrating into the paraffin treated region. Thus, no full hydrophobisation could be reached with this ink, even when pores were effectively saturated with it, indicating too low dry solid content. However, due to poor solubility of paraffin wax in p-xylene this could not be increased any further. Still, it might be possible to produce hydrophobic regions with paraffin wax, if a solvent with better solubilising could be found, or alternatively by using pure paraffin wax as an ink in itself in hot-melt inkjet printing.

AKD ink also suffered from limited jetting frequency (2 kHz) due to low viscosity. However, it could easily penetrate the full depth of both tested substrates and produce reliable barriers, even with relatively large drop spacing. Low viscosity presumably helped in achieving good penetration. The reactive nature of AKD, replacing hydroxyl groups rather than just adsorbing on the fibre surface, probably makes it a very good hydrophobising agent, and small molecular size probably results in a good coverage. However, edge definition was poor, with a partially hydrophobised edge region surrounding the fully hydrophobised core region. This poor edge definition may have been due to the choice of solvent used in this work or due to the well-known hydrolysing and migrating effect of AKD on fibres.

AKD-PS ink, with some polystyrene added as a rheological modifier, demonstrated improved jetting frequency (6 vs. 2 kHz) when compared to plain AKD ink. This is presumably due to the increased viscosity and possibly viscoelasticity imparted by the polystyrene molecules to the ink. However, in all other aspects AKD-PS ink behaved very similarly to AKD ink, and the increased viscosity did not seem to have a major effect on the depth penetration.

Polystyrene ink featured good printing frequency (6 kHz), due to its higher viscosity and viscoelastic nature. However, it also required more maintenance effort, due to bungee jump phenomena manifested on idle nozzles, and due to risks of drying ink clogging nozzles. Also, it showed limited depth penetration, being able to penetrate reliably only Whatman 4 filter paper and that only at 10 or 15 µm drop spacing. This again might be due to the higher viscosity of PS ink. However, those areas that were treated by the ink were fully hydrophobised, indicating a sufficient dry solid content. Furthermore, produced edge regions were relatively sharp, possibly due to the coffee stain effect during drying.

However, the polystyrene ink still achieved superior penetration compared to that previously used for flexographic printing [82]. Both of these featured similar inks, with 5 % polystyrene dissolved in xylene. However, there was a significant difference in the molecular weight of used polystyrenes (35 vs. 290 kDa), resulting in a significant difference in viscosity (1.2 vs. 6 mPa·s). This resulted in the literature reported flexography printed polystyrene ink managing to achieve only partial penetration, necessitating printing on both sides to produce proper barriers. If the flexography printing study had been conducted using a polystyrene with lower molecular weight and viscosity, better penetration depth might have been achievable. However, there may have also been a difference in the ink volumes transferred to papers, though unfortunately the published study did not mention details of the chosen anilox rollers, which makes it difficult to estimate those volumes. When it comes to volumes, inkjet provides users with the possibility to deposit very high volumes simply by adjusting spatial frequency of jetted drops. Furthermore, inkjet does not suffer problems from only partial transfer of ink, say, from rollers to substrate.

Neither AKD nor PS ink displayed ideal behaviour. However, their performance might be improvable. In the case of PS ink, even lower molecular weight polymer would help to reduce viscosity and improve penetration. In case of AKD ink, faster evaporating solvent could improve edge definition. Furthermore, adding polystyrene to AKD ink as a rheological

modifier showed clear improvement in jetting frequency. No known previously published studies had demonstrated combining multiple hydrophobising agents within a single ink.

14.6 Health and environmental aspects

Within the scope of this study, solvent emissions from printing were not an issue, due to the small size of test samples and relatively small jetting speed of the DMP-2831 printer. In a well-ventilated room, the odour of solvent could not be noticed when samples were printed, even when standing next to the printer.

However, in a large scale production environment solvent emissions would be a problem that would need to be managed. Due to the need to achieve full depth penetration of the porous substrate, quite large volumes of ink are required to hydrophobise a given area. For example, with the 5 % by weight polystyrene ink used in this study, 1 dm^3 of inkjet-printed ink would fully hydrophobise only around 30 m^2 of Whatman 4 filter paper. While commercial solutions are readily available for managing solvent emissions, in some cases it might be desirable to avoid them altogether. In this case, there are two other previously mentioned inkjet technologies that could be used instead, namely UV-curing polymers and hot-melt wax.

14.7 Evaporation from reverse side

One important aspect of the experimental set-up that has not been discussed previously is the way that solvent evaporation from substrates could take place. Since substrates were held fastened to the mounting plate during printing, no solvent evaporation could take place through the reverse side, with the exception of those areas where the vacuum holes are located. These holes can potentially lead to some local variation in evaporation behaviour, especially when the vacuum pump is turned on and pulls air through the substrate above. In retrospect, the effect of vacuum holes could have been eliminated by placing a plastic film beneath the printed substrate to cover the holes.

However, whether the holes are covered or not, this kind of set-up is not really representative of conditions that would be found in a roll-to-roll production environment, where a paper web is most of the time suspended in air and evaporation from a high-permeance substrate can take place from both sides. Simulating such an environment might be achievable by suspending substrates on some sort of mesh frame that would allow for air to flow freely beneath.

15 Conclusions of experimental part

In this experimental work, inkjet printing of hydrophobic patterns on porous substrates was studied with four different inks, made of three different hydrophobising agents dissolved in p-xylene and inkjet-printed on two different filter papers.

Of the tested inks, paraffin wax based ink was found to be ineffective, due to poor solubility limiting achievable dry solid content. Polystyrene-based ink achieved better depth penetration than a higher molecular weight version printed in the prior art with flexography, being able to produce full-depth barriers with a single inkjet-printed layer. AKD-containing inks achieved good penetration, even with large drop spacing, but suffered from limited jetting frequency and from poor edge definition of printed shapes, a phenomenon not previously reported in literature. This difference in AKD edge definition between printed samples and literature descriptions was most likely due to a difference in solvent properties and/or the hydrolysis and migration properties of AKD on cellulose fibres. Addition of some polystyrene to AKD ink as a rheological modifier improved maximum jetting frequency, but had no major effect on properties of the actual printed patterns.

A clear difference could be seen in substrate properties between Whatman 1 and Whatman 4 filter papers when barriers were patterned with polystyrene ink. Sufficient penetration depth to produce reliable barriers could only be achieved on Whatman 4, even though this substrate is actually slightly thicker than Whatman 1. Exact mechanisms that could explain this difference in behaviour remain unexplained, but tortuosity is strongly suspected. With AKD-containing inks, both substrates could be penetrated to full depth.

Regarding resolution for polystyrene ink, reliable channels 680 ± 80 µm wide and barriers 883 ± 91 µm wide could be produced on Whatman 4 filter paper when printing at 15 µm drop spacing. For AKD based inks, somewhat narrower barriers could be produced, with narrowest reliable barriers measuring 457 ± 147 µm wide. However, good channels could not be produced with AKD or AKD-PS based inks due to poor definition of channel edges.

Penetration of hydrophobic ink into filter paper was found to take place as film flow rather than through complete filling of pores. This could be deduced from observations that a given ink volume hydrophobised a significantly larger pore volume region than its own volume could occupy.

16 Future work

Many suggestions for future improvements and studies have been mentioned throughout the text. The most important ones amongst them are gathered here.

As regards test methodology, a significant restriction in this study was that the produced hydrophobic patterns were not directly visible to the naked eye, necessitating dyeing of hydrophilic regions to outline hydrophobic areas. This also meant that areas would need to be arbitrarily classified either as fully hydrophilic or fully hydrophobic, though in reality both hydrophilic and hydrophobic regions could vary in their intensity. This limitation in test methodology could be circumvented by using more advanced instrumental analytical methods to characterise differences in chemical concentrations in different regions of a substrate. For example, Raman mapping, which can easily detect polystyrene on cellulose substrate, could be used to analyse polystyrene concentrations at the edges of hydrophobised regions to evaluate how sharp the shifts in concentration are, and if the coffee-stain effect really takes place when patterns printed with polystyrene ink dry. Other quantitative methods, such as X-ray Photoelectron Spectroscopy (XPS) could be used to compare hydrophobising agent concentrations between the printed and reverse sides, to complement information obtainable by contact angle measurements.

Reasons behind the poor edge definition of AKD printed patterns, possibly due to solvent properties and/or migration on cellulose, could be examined in more detail to find out the dominating mechanism(s). Also, it could be useful to study with Raman mapping if the curing phase results in the AKD printed pattern spreading further out beyond the original limits of ink spreading.

The effect of substrate properties in facilitating ink depth penetration could also be further studied, possibly with a wider range of substrates. Cross-section studies of printed patterns could help to characterise ink spreading in different directions.

Finally, tested inks could be systematically tested against other alternatives, including hot-melt wax, to study their relative merits. Results of such cross-comparisons should be helpful for anyone considering a hydrophobising technique for actual production.

References

[1] D.R. Ballerini, X. Li, and W. Shen, "Patterned paper and alternative materials as substrates for low-cost microfluidic diagnostics", *Microfluidics and Nanofluidics*, vol. 13, no. 5, pp. 769-787, 2012.

[2] M.L .Kovarik, P.C. Gach, D.M. Ornoff, Y. Wang, J. Balowski, L. Farrag, and N.L. Allbritton, "Micro Total Analysis Systems for Cell Biology and Biochemical Assays", *Analytical Chemistry*, vol. 84, no. 2, pp. 516-540, 2012.

[3] A.W. Martinez, S.T. Phillips, and G.M. Whitesides, "Diagnostics for the Developing World: Microfluidic Paper-Based Analytical Devices", *Analytical Chemistry*, vol. 82, no. 1, pp. 3-10, 2010.

[4] A.W. Martinez, M.J. Butte, G.M. Whitesides, and S.T. Phillips, "Patterned Paper as Platform for Inexpensive, Low-Volume, Portable Bioassays", *Angewandte Chemie (International ed.)*, vol. 46, no. 8, pp. 1318-1320, 2007.

[5] X. Li, D. Ballerini, and W. Shen, "A perspective on paper-based microfluidics: Current status and future trends", *Biomicrofluidics*, vol. 6, no. 1, pp. 011301-1-011301-13, 2012.

[6] R. Pelton, "Bioactive paper provides a low-cost platform for diagnostics", *Trends in Analytical Chemistry*, vol. 28, no. 8, pp. 925-942, 2009.

[7] A.W. Martinez, "Microfluidic paper-based analytical devices: from POCKET to paper-based ELISA", *Bioanalysis*, vol. 3, no. 23, pp. 2589-2592, 2011.

[8] C. Fellers, "The structure of Paper and its Modelling", in *Paper Products Physics and Technology*. Berlin: Walter de Gruyter GmbH, 2009, pp. 1-24.

[9] D.D. Liana, B. Raguse, J.J. Gooding, and E. Chow, "Recent Advances in Paper-based Sensors", *Sensors*, vol. 12, no. 9, pp. 11505-11526, 2012.

[10] P. Lisowski and P.K. Zarzycki, "Microfluidic Paper-Based Analytical Devices (μPADs) and Micro Total Analysis Systems (μTAS): Development, Applications and

Future Trends", *Chromatographia*, vol. 76, no. 19-20, pp. 1201-1214, 2013.

[11] E.W. Nery and L.T. Kubota, "Sensing approaches on paper-based devices: a review", *Analytical and Bioanalytical Chemistry*, vol. 405, no. 24, pp. 7573-7595, 2013.

[12] N.R. Pollock, S. McGray, D.J. Colby, F. Noubary, H. Nguyen, T.A. Nguyen, S. Khormaee, S. Jain, K. Hawkins, S. Kumar, J.P. Rolland, P.D. Beattie, N.V. Chau, V.M. Quang, C. Barfield, K. Tietje, M. Steele, and B.H. Weigl, "Field Evaluation of a Prototype Paper-Based Point-of-Care Fingerstick Transaminase Test", *PloS One*, vol. 8, no. 9, 2013.

[13] C.D. Chin, V. Linder, and S.K. Sia, "Commercialization of microfluidic point-of-care diagnostic devices", *Lab on a chip*, vol. 12, no. 12, pp. 2118–2134, 2012.

[14] S. Dharmaraja, L. Lafleur, S. Byrnes, P. Kauffman, J. Buser, B. Toley, E. Fu, P. Yager, and B. Luatz, "Programming paper networks for point of care diagnostics", in *Proc. SPIE 8615, Microfluidics, BioMEMS, and Medical Microsystems XI*, San Francisco, 2013.

[15] X. Li, J. Tian, and W. Shen, "Progress in patterned paper sizing for fabrication of paper-based microfluidic sensors", *Cellulose*, vol. 17, no. 3, pp. 649-659, 2010.

[16] A.W. Martinez, S.T. Phillips, and G.M. Whitesides, "Three-dimensional microfluidic devices fabricated in layered paper and tape", *Proceedings of the National Academy of Sciences of the United States of America*, vol. 105, no. 50, pp. 19606-19611, 2008.

[17] H. Liu and R.M. Crooks, "Three-Dimensional Paper Microfluidic Devices Assembled Using the Principles of Origami", *Journal of the American Chemical Society*, vol. 133, no. 44, pp. 17564–17566, 2011.

[18] G.G. Lewis, M.J. DiTucci, M.S. Baker, and S.T. Phillips, "High throughput method for prototyping three-dimensional, paper-based microfluidic devices", *Lab on a Chip*, vol. 12, no. 15, pp. 2630-2633, 2012.

[19] N.R. Pollock, J.P. Rolland, S. Kumar, P.D. Beattie, S. Jain, F. Noubary, V.L. Wong, R.A. Pohlmann, U.S. Ryan, and G.M. Whitesides, "A Paper-Based Multiplexed

Transaminase Test for Low-Cost, Point-of-Care Liver Function Testing", *Science Translational Medicine*, vol. 4, no. 152, pp. 1-10, 2012.

[20] L. Xiao, X. Liu, R. Zhong, K. Zhang, X. Zhang, X. Zhou, B. Lin, and Y. Du, "A rapid, straightforward, and print house compatible mass fabrication method for integrating 3D paper-based microfluidics", *Electrophoresis*, vol. 34, no. 20-21, pp. 3003-3007, 2013.

[21] H. Liu, X. Li, and R.M. Crooks, "Paper-Based SlipPAD for High-Throughput Chemical Sensing", *Analytical Chemistry*, vol. 85, no. 9, pp. 4263-4267, 2013.

[22] E. Fu, T. Liang, P. Spicar-Mihalic, J. Houghtaling, S. Ramachandran, and P. Yager, "Two-Dimensional Paper Network Format That Enables Simple Multistep Assays for Use in Low-Resource Settings in the Context of Malaria Antigen Detection", *Analytical Chemistry*, vol. 84, no. 10, pp. 4574-4579, 2012.

[23] Srinivasan V., V.K. Pamula, and R.B. Fair, "Droplet-based microfluidic lab-on-a-chip for glucose detection", *Analytica Chimica Acta*, vol. 507, no. 1, pp. 145-150, 2003.

[24] S. Di Risio and N. Yan, "Bioactive Paper Through Inkjet Printing", *Journal of Adhesion Science and Technology*, vol. 24, no. 3, pp. 661-684, 2010.

[25] J.T. Delaney, P.J. Smith, and U.S. Schubert, "Inkjet printing of proteins", *Soft Matter*, vol. 5, no. 24, pp. 4866-4877, 2009.

[26] G. Arrabito, C. Musumeci, V. Aiello, S. Libertino, G. Compagnini, and B. Pignataro, "On the Relationship between Jetted Inks and Printed Biopatterns: Molecular-Thin Functional Microarrays of Glucose Oxidase", *Langmuir*, vol. 25, no. 11, pp. 6312-6318, 2009.

[27] C.O. Phillips, S. Govindarajan, S.M. Hamblyn, R.S. Conlan, D.T. Gethin, and T.C. Claypole, "Patterning of Antibodies Using Flexographic Printing", *Langmuir*, vol. 28, no. 25, pp. 9878-9884, 2012.

[28] C. Sicard and J.D. Brennan, "Bioactive Paper: Biomolecule Immobilization Methods and Applications in Environmental Monitoring", *MRS Bulletin*, vol. 38, no. 4, pp.

331-334, 2013.

[29] Z. Zhao, J. Tian, Z. Wu, J. Liu, D. Zhao, W. Shen, and L. He, "Enhancing enzymatic stability of bioactive papers by implanting enzyme-immobilized mesoporous silica nanorods into paper", *Journal of Materials Chemistry B*, vol. 1, no. 37, pp. 4719-4722, 2013.

[30] S.M.Z. Hossain, R.E. Luckham, A.M. Smith, J.M. Lebert, L.M. Davies, R.H. Pelton, C.D.M. Filipe, and J.D. Brennan, "Development of Bioactive Paper Sensor for Detection of Neurotoxins Using Piezoelectric Inkjet Printing of Sol-gel Derived Bioinks", *Analytical chemistry*, vol. 81, no. 13, pp. 5474-5483, 2009.

[31] H. Koivula, R. Pelton, J.D. Brennan, J. Grenon, and T. Manfred, "Flexographic printability of sol-gel precursor dispersions for bioactive paper", *Nordic Pulp & Paper Research Journal*, vol. 28, no. 3, pp. 450-457, 2013.

[32] C. Rozand, "Paper-based analytical devices for point-of-care infectious disease testing", *European Journal of Clinical Microbiology and Infectious Diseases*, vol. 33, no. 2, pp. 147-156, 2014.

[33] A.V. Kuznetsov, "Modeling Bioconvection in Porous Media", in *Handbook of Porous Media*, K. Vafai, Ed. Boca Raton: CRC Press, 2005, pp. 645-686.

[34] J.C. Jokerst, J.A. Adkins, B. Bisha, M.M. Mentele, L.D. Goodridge, and C.S. Henry, "Development of a Paper-Based Analytical Device for Colorimetric Detection of Select Foodborne Pathogens", *Analytical Chemistry*, vol. 84, no. 6, pp. 2900-2807, 2012.

[35] S.M.Z. Hossain, C. Ozimok, C. Sicard, S.D. Aguirre, M.M. Ali, Y. Li, and J.D. Brennan, "Multiplexed paper test strip for quantitative bacterial detection", *Analytical and Bioanalytical Chemistry*, vol. 403, no. 6, pp. 1567-1576, 2012.

[36] F. Deiss, M.E. Funes-Huacca, J. Bal, K. Thjung, and R. Derda, "Antimicrobial susceptibility assays in paper-based portable culture devices", *Lab on a Chip*, vol. 14, no. 1, pp. 167-171, 2014.

[37] P. Rattanarat, W. Dungchai, D.M. Cate, W. Siangproh, J. Volckens, O. Chailapakul, and C.S. Henry, "A microfluidic paper-based analytical device for rapid quantification of particulate chromium", *Analytica Chimica Acta*, vol. 800, pp. 50-55, 2013.

[38] R.V. Taudte, A. Beavis, L. Wilson-Wilde, C. Roux, P. Doble, and L. Blanes, "A portable explosive detector based on fluorescence quenching of pyrene deposited on coloured wax-printed microPADs", *Lab on a Chip*, vol. 13, no. 21, pp. 4164-4172, 2013.

[39] B.M. Jayawardane, I.D. McKelvie, and S.D. Kolev, "A paper-based device for measurement of reactive phosphate in water", *Talanta*, vol. 100, pp. 454-460, 2012.

[40] L. Feng, H. Li, L-Y. Niu, Y, Guan, C. Duan, Y-F. Guan, C. Tung, and Q. Yang, "A fluorometric paper-based sensor array for the discrimination of heavy-metal ions", *Talanta*, vol. 108, pp. 103-108, 2013.

[41] M. Vaher and M. Kaljurand, "The development of paper microzone-based green analytical chemistry methods for determining the quality of wines", *Analytical and bioanalytical chemistry*, vol. 404, no. 3, pp. 627-633, 2012.

[42] J.R. Tortora and B. Derrickson, *Principles of Anatomy and Physiology, 13th edition, Volume 2*. Hoboken: John Wiley & Sons, 2011.

[43] X. Yang, O. Forouzan, T.P. Brown, and S.S. Shevkoplyas, "Integrated separation of blood plasma from whole blood for microfluidic paper-based analytical devices", *Lab on a chip*, vol. 12, no. 2, pp. 274-280, 2012.

[44] J. Noiphung, T. Songjaroen, W. Dungchai, C.S. Henry, O. Chailapakul, and W. Laiwattanapaisal, "Electrochemical detection of glucose from whole blood using paper-based microfluidic devices", *Analytica Chimica Acta*, vol. 788, pp. 39-45, 2013.

[45] X. Yang, J. Kanter, N.Z. Piety, M.S. Benton, S.M. Vignes, and S.S. Shevkoplyas, "A simple, rapid, low-cost diagnostic test for sickle cell disease", *Lab on a Chip*, vol. 13, no. 8, pp. 1464-1467, 2013.

[46] M. Li, T. Junfei, M. Al-Tamimi, and S. Wei, "Paper-Based Blood Typing Device That Reports Patient's Blood Type “in Writing“", *Angewandte Chemie international edition*, vol. 51, no. 22, pp. 5497-5501, 2012.

[47] J. Su, M. Al-Tamimi, and G. Garnier, "Engineering paper as a substrate for blood typing bio-diagnostics", *Cellulose*, vol. 19, no. 5, pp. 1749-1758, 2012.

[48] J.R. Tortora and B. Derrickson, *Principles of Anatomy and Physiology, 13th edition, Volume 1*. Hoboken: John Wiley & Sons, 2011.

[49] H. Kim and H. Noh, "Quantifying the Fluid Volumes in Paper Microfluidic Devices for Dry Eye Test", *Macromolecular Research*, vol. 21, no. 7, pp. 788-792, 2012.

[50] S.A. Klasner, A.K. Price, K.W. Hoeman, R.S. Wilson, K.J. Bell, and C.T. Culbertson, "Paper-based microfluidic devices for analysis of clinically relevant analytes present in urine and saliva", *Analytical and Bioanalytical Chemistry*, vol. 397, no. 5, pp. 1821-1829, 2010.

[51] C.L. Cassano and Z.H. Fan, "Laminated paper-based analytical devices (LPAD): fabrication, characterisation, and assays", *Microfluidics and Nanofluidics*, vol. 15, no. 2, pp. 173-181, 2013.

[52] D.M. Cate, W. Dungchai, J.C. Cunningham, J. Volckens, and C.S. Henry, "Simple, distance-based measurement for paper analytical devices", *Lab on a Chip*, vol. 13, no. 12, pp. 2397-2404, 2013.

[53] W.W. Yu and I.M. White, "Inkjet-printed paper-based SERS dipsticks and swabs for trace chemical detection", *Analyst*, vol. 138, no. 4, pp. 1020-1025, 2013.

[54] W. Dungchai, O. Chailapakul, and C.S. Henry, "Electrochemical Detection for Paper-based Microfluidics", *Analytical Chemistry*, vol. 81, no. 14, pp. 5821-5826, 2009.

[55] K. Maejima, T. Enomae, A. Isogai, K. Suzuki, and D. Citterio, "All-inkjet-printed "lab-on-paper" with Electrodes and Microchannels", in *NIP28: International Conference on Digital Printing Technologies and Digital Fabrication 2012,*

Technical Program and Proceedings, Quebec, 2012, pp. 554-556.

[56] H. Chen, J. Cogswell, C. Anagnostopoulos, and M. Faghri, "A fluidic diode, valves, and a sequential-loading circuit fabricated on layered paper", *Lab on a Chip*, vol. 12, no. 16, pp. 2909-2913, 2012.

[57] E. Fu, B. Lutz, P. Kauffman, and P. Yager, "Controlled reagent transport in disposable 2D paper networks", *Lab on a Chip*, vol. 10, no. 7, pp. 918-920, 2010.

[58] B. Lutz, T. Liang, E. Fu, S. Ramachandran, P. Kauffman, and P. Yager, "Dissolvable fluidic time delays for programming multistep assays in instrument-free paper diagnostics", *Lab on a Chip*, vol. 13, no. 14, pp. 2840-2847, 2013.

[59] G.G. Lewis, J.S. Robbins, and S.T. Phillips, "Point-of-Care Assay Platform for Quantifying Active Enzymes to Femtomolar Levels Using Measurements of Time as the Readout", *Analytical Chemistry*, vol. 85, no. 21, pp. 10432-10439, 2013.

[60] G.G. Lewis, M.J. DiTucci, and S.T. Phillips, "Quantifying Analytes in Paper-Based Microfluidic Devices Without Using External Electronic Readers", *Angewandte Chemie*, vol. 124, no. 51, pp. 12879 –12882, 2012.

[61] X. Li, J. Tian, T. Nguyen, and W. Shen, "Paper-based Microfluidic Devices by Plasma Treatment", *Analytical Chemistry*, vol. 80, no. 23, pp. 9131-9134, 2008.

[62] Z.W. Zhong, Z.P. Wang, and G.X.D. Huang, "Investigation of wax and paper materials for the fabrication of paper-based microfluidic devices", *Microsystem technologies*, vol. 18, no. 5, pp. 649-659, 2012.

[63] A.W. Martinez, S.T. Phillips, Z. Nie, C. Cheng, E. Carrilho, B.J. Wiley, and G.M. Whitesides, "Programmable diagnostic devices made from paper and tape", *Lab on a Chip*, vol. 10, no. 19, pp. 2499-2504, 2010.

[64] H. Noh and S.T. Phillips, "Metering the Capillary-Driven Flow of Fluids in Paper-Based Microfluidic Devices", *Analytical chemistry*, vol. 82, no. 10, pp. 4181-4187, 2010.

[65] N.K. Thom, K. Yeung, M. Pillion, and S.T. Phillips, "Fluidic batteries as low-cost sources of power in paper-based microfluidic devices", *Lab on a Chip*, vol. 12, no. 10, pp. 1768-1770, 2012.

[66] K.M. Schilling, A.L. Lepore, J.A. Kurian, and A.W. Martinez, "Fully Enclosed Microfluidic Paper-Based Analytical Devices", *Analytical Chemistry*, vol. 84, no. 3, pp. 1579-1585, 2012.

[67] K. Maejima, S. Tomikawa, K. Suzuki, and D. Citterio, "Inkjet printing: An integrated and green chemical approach to microfluidic paper-based analytical devices", *RSC advances*, vol. 3, no. 24, pp. 9258-9263, 2013.

[68] S. Liu and J.H. Masliyah, "Dispersion in Porous Media", in *Handbook of Porous Media, 2nd edition*, K. Vafai, Ed. Boca Raton: CRC Press, 2005, pp. 81-140.

[69] F. Civan and V. Nguyen, "Modeling Particle Migration and Deposition in Porous Media by Parallel Pathways with Exchange", in *Handbook of Porous Media*, K. Vafai, Ed. Boca Raton: CRC Press, 2005, pp. 457-484.

[70] H. Orelma, I. Filpponen, L. Johansson, J. Laine, and O.J. Rojas, "Modification of Cellulose Films by Adsorption of CMC and Chitosan for Controlled Attachment of Biomolecules", *Biomacromolecules*, vol. 12, no. 12, pp. 4311-4318, 2011.

[71] A.K. Yetisen, M.S. Akram, and C.R. Lowe, "Paper-based microfluidic point-of-care diagnostic devices", *Lab on a Chip*, vol. 13, no. 12, pp. 2210-2251, 2013.

[72] P.O. Meinander, "Specialty papers", in *Paper and board grades*, H. Paulapuro, Ed. Helsinki: Fapet Oy, 2000, pp. 99-130.

[73] Whatman Ltd. Qualitative Filter Papers - Standard Grades. [Online]. http://www.whatman.com/QualitativeFilterPapersStandardGrades.aspx

[74] B.G. Exposito, "Paper-based microfluidic sensing devices fabricated by inkjet printing technology", Keio University, Master's thesis 2012.

[75] Y. Lu, W. Shi, J. Qin, and B. Lin, "Fabrication and Characterization of Paper-Based

Microfluidics Prepared in Nitrocellulose Membrane by Wax Printing", *Analytical Chemistry*, vol. 82, no. 1, pp. 329-335, 2010.

[76] A. Apilux, Y. Ukita, M. Chikae, O. Chailapakul, and Y. Takamura, "Development of automated paper-based devices for sequential multistep sandwich enzyme-linked immunosorbent assays using inkjet printing", *Lab on a Chip*, vol. 13, no. 1, pp. 126-135, 2013.

[77] Y. Lu, W. Shi, L. Jiang, J. Qin, and B. Lin, "Rapid prototyping of paper-based microfluidics with wax for low-cost, portable bioassay", *Electrophoresis*, vol. 30, no. 9, pp. 1497-1500, 2009.

[78] D.A. Bruzewicz, M. Reches, and G.M. Whitesides, "Low-Cost Printing of Poly(dimethylsiloxane) Barriers to Define Microchannels in Paper," *Analytical Chemistry*, vol. 80, no. 9, pp. 3387-3392, 2008.

[79] A. Määttänen, D. Fors, S. Wang, D. Valtakari, P. Ihalainen, and J. Pelkonen, "Paper-based planar reaction arrays for printed diagnostics", *Sensors and Actuators B: Chemical*, vol. 160, no. 1, pp. 1404–1412, 2011.

[80] E. Lehtinen, J. Paltakari, and O. Imppola, "Introduction to pigment coating and surface sizing of paper and board", in *Pigment coating and surface sizing of paper*, Jouni Paltakari, Ed. Helsinki: Paperi ja Puu Oy, 2009, pp. 11-28.

[81] P. Gustafsson, S. Grönqvist, M. Smolander, T. Erho, M. Toivakka, and J. Peltonen, "Bioactive pigment coatings comprising enzymes", in *Proceedings for the 7th International Paper and Coating Chemistry Symposium*, Hamilton, 2009, pp. 171-175.

[82] J. Olkkonen, K. Lehtinen, and T. Erho, "Flexographically Printed Fluidic Structures in Paper", *Analytical Chemistry*, vol. 82, no. 24, pp. 10246-10250, 2011.

[83] A.W. Martinez, S.T. Phillips, B.J. Wiley, M. Gupta, and G.M. Whitesides, "FLASH: A rapid method for prototyping paper-based microfluidic devices", *Lab on a Chip*, vol. 8, no. 12, pp. 2146-2150, 2008.

[84] E. Carrilho, S.T. Phillips, S.J. Vella, A.W. Martinez, and G.M. Whitesides, "Paper Microzone Plates", *Analytical Chemistry*, vol. 81, no. 15, pp. 5990-5998, 2009.

[85] G. Chitnis, Z. Ding, C. Chang, C.A. Savran, and B. Ziaie, "Laser-treated hydrophobic paper: an inexpensive microfluidic platform", *Lab on a Chip*, vol. 11, no. 6, pp. 1161-1165, 2011.

[86] A. Qi, S.P. Hoo, J. Friend, L. Yeo, Z. Yue, and P.P.Y. Chan, "Hydroxypropyl Cellulose Methacrylate as a Photo-Patternable and Biodegradable Hybrid Paper Substrate for Cell Culture and Other Bioapplications", *Advanced Healthcare Materials (early view)*, 2013.

[87] X. Fang, H. Chen, X. Jiang, and J. Kong, "Microfluidic Devices Constructed by a Marker Pen on a Silica Gel Plate for Multiplex Assays", *Analytical Chemistry*, vol. 83, no. 9, pp. 3596-3599, 2011.

[88] S.J. Reinholt, A. Sonnenfeldt, A. Naik, M.W. Frey, and A.J. Baeumner, "Developing new materials for paper-based diagnostics using electrospun nanofibers", *Analytical & Bioanalytical Chemistry (advance article)*, 2013.

[89] S. Xing, J. Jiang, and T. Pan, "Interfacial microfluidic transport on micropatterned superhydrophobic textile", *Lab on a Chip*, vol. 13, no. 10, pp. 1937-1947, 2013.

[90] A. Nilghaz, D.H.B. Wicaksono, D. Gustiono, F.A.A. Majid, E. Supriyanto, and M.R.A. Kadir, "Flexible microfluidic cloth-based analytical devices using a low-cost wax patterning technique", *Lab on a Chip*, vol. 12, no. 1, pp. 209-218, 2012.

[91] H. Kipphan, *Handbook of Print Media*. Berlin: Springer, 2001.

[92] W.J. Wnek, M.A. Andreottola, P.F. Doll, and S.M. Kelly, "Ink Jet Ink Technology", in *Handbook of Imaging Materials, Second Edition*, A.S. Diamond and D.S. Weiss, Eds. New York: Marcel Dekker, 2002, pp. 531-602.

[93] M. Singh, H.M. Haverinen, P. Dhagat, and G.E. Jabbour, "Inkjet Printing - Process and Its Applications", *Advanced Materials*, vol. 22, no. 6, pp. 673-685, 2010.

[94] B. de Gans, P.C. Duineveld, and U.S. Schubert, "Inkjet Printing of Polymers: State of the Art and Future Developments", *Advanced Materials*, vol. 16, no. 3, pp. 203-213, 2004.

[95] P. Calvert, "Inkjet Printing for Materials and Devices", *Chemistry of Materials*, vol. 13, no. 10, pp. 3299-3305, 2001.

[96] S.D. Hoath, S. Jung, and I.M. Hutchings, "A simple criterion for filament break-up in drop-on-demand inkjet printing", *Physics of Fluids*, vol. 25, no. 2, pp. 021701-1-021701-5, 2013.

[97] D. Jang, D. Kim, and J. Moon, "Influence of Fluid Physical Properties on Ink-Jet Printability", *Langmuir*, vol. 25, no. 5, pp. 2629-2635, 2009.

[98] S.D. Hoath, J.R. Castrejon-Pita, W. Hsiao, S. Jung, G.D. Martin, I.M. Hutchings, T.R. Tuladhar, D.C. Vadillo, S.A. Butler, M.R. Mackley, C. McIlroy, N.F. Morrison, O.G. Harlen, and H.N. Yow, "Jetting of Complex Fluids", *Journal of Imaging Science and Technology*, vol. 57, no. 4, pp. 040403-1-040403-10, 2013.

[99] N.F. Morrison and O.G. Harlen, "Drop-on-demand printing of complex liquids", in *29th International Conference on Digital Printing Technologies (NIP29)*, Seattle, 2013, pp. 271-276.

[100] S.D. Hoath, W. Hsiao, S. Jung, G.D. Martin, I.M. Hutchings, N.F. Morrison, and O.G. Harlen, "Drop Speeds from Drop-on-Demand Ink-Jet Print Heads", *Journal of Imaging Science and Technology*, vol. 57, no. 1, pp. 10503-1-10503-11, 2013.

[101] X. Yan, "Drop-on-demand Inkjet Drop Formation of Dilute Polymer Solutions", Georgia Institute of Technology, Atlanta, Doctoral dissertation 2010.

[102] Y. Liu, M. Tsai, Y. Pai, and W. Hwang, "Control of droplet formation by operating waveform for inks with various viscosities in piezoelectric inkjet printing", *Applied Physics A: Materials Science & Processing*, vol. 111, no. 2, pp. 509-516, 2013.

[103] I.W. Hamley, *Introduction to Soft Matter: Synthetic and Biological Self-Assembling*

Materials, Revised ed. Chicester: John Wiley & Sons, 2007.

[104] D. Xu, V. Sanchez-Romaguera, S. Barbosa, W. Travis, J. de Wit, P. Swan, and S.G. Yeates, "Inkjet printing of polymer solutions and the role of chain entanglement", *Journal of Materials Chemistry*, vol. 17, no. 46, pp. 4902-4907, 2007.

[105] K. A-Alamry, K. Nixon, R. Hindley, J.A. Odel, and S.G. Yeates, "Flow-Induced Polymer Degradation During Ink-Jet Printing", *Macromolecular Rapid Communications*, vol. 32, no. 3, pp. 316-320, 2011.

[106] C. McIlroy, O.G. Harlen, and N.F. Morrison, "Modelling the jetting of dilute polymer solutions in drop-on-demand inkjet printing," *Journal of Non-Newtonian Fluid Mechanics*, vol. 201, pp. 17-28, 2013.

[107] J. Perelaer, J.S. Smith, M.M.P. Wijnen, E. van den Bosch, R. Eckardt, P.H.J.M. Ketelaars, and U.S. Schubert, "Droplet Tailoring Using Evaporative Inkjet Printing", *Macromolecular Chemistry and Physics*, vol. 210, no. 5, pp. 387-393, 2009.

[108] T. Kawase, H. Sirringhaus, R.H. Friend, and T. Shimoda, "Inkjet Printed Via-Hole Interconnections and Resistors for All-Polymer Transistor Circuits", *Advanced Materials*, vol. 13, no. 21, pp. 1601-1605, 2001.

[109] B. de Gans, S. Hoeppener, and U.S. Schubert, "Polymer relief microstructures by inkjet etching", *Journal of Materials Chemistry*, vol. 17, no. 29, pp. 3045-3050, 2007.

[110] K. Abe, K. Suzuki, and D. Citterio, "Inkjet-Printed Microfluidic Multianalyte Chemical Sensing Paper", *Analytical Chemistry*, vol. 80, no. 18, pp. 6928-6934, 2008.

[111] S. Franssila, *Introduction to Microfabrication*. Chichester: John Wiley & Sons, 2004.

[112] M. Pykönen, "Influence of Plasma Modification on Surface Properties and Offset Printability of Coated Paper", Åbo Akademi, Turku, Doctoral dissertation 2010.

[113] L. Cernakova, P. Stahel, D. Kovacik, K. Johansson, and M. Cernak, "Low Cost High-Speed Plasma Treatment of Paper Surfaces", in *Proceedings of 9th TAPPI Advanced Coating Fundamentals Symposium*, Turku, 2006, pp. 7-17.

[114] M. Cernak, J. Rahel, D. Kovacik, M. Simor, A. Brablec, and P. Slavicek, "Generation of Thin Surface Plasma Layers for Atmospheric-Pressure Surface Treatments", *Contributions to Plasma Physics*, vol. 44, no. 5-6, pp. 492-495, 2004.

[115] M.H.A. van Dongen, R.O.F. Verkuijlen, and J.P.C. Bernards, "Wettability and Aging of Polymer Substrates after Atmospheric Dielectrical Barrier Discharge Plasma on Demand Treatment", *Journal of Imaging Science and Technology*, vol. 57, no. 3, pp. 030503-1-030503-5, 2013.

[116] J. Tian., P. Jarujamrus, L. Li, M. Li, and W. Shen, "Strategy to Enhance the Wettability of Bioactive Paper-based Sensors", *Applied Materials & Interfaces*, vol. 4, no. 12, p. 6573−6578, 2012.

[117] J. Lawrence and L. Li, *Laser Modification of the Wettability Characteristics of Engineering Materials*. London: Professional Engineering Publishing, 2001.

[118] J.F. Ready, *Industrial Applications of Lasers*, 2nd ed. San Diego: Academic Press, 1997.

[119] P. Pouli, A. Selimis, S. Georgiou, and C. Fotakis, "Recent Studies of Laser Science in Paintings Conservation and Research", *Accounts of Chemical research*, vol. 43, no. 6, pp. 771-781, 2010.

[120] A. Kaminska, M. Sawczak, M. Cieplinski, G. Sliwinski, and B. Kosmowski, "Colorimetric study of the post-processing effect due to pulsed laser cleaning of paper", *Optica Applicata*, vol. 34, no. 1, pp. 121-132, 2004.

[121] H.M. Szczepanowska and W.R. Moomaw, "Laser Stain Removal of Fungus-induced Stains from Paper", *Journal of the American Institute for Conservation*, vol. 33, no. 1, pp. 25-32, 1994.

[122] A. Kaminska, M. Sawczak, B. Komar, and G. Sliwinski, "Application of the laser ablation for conservation of historical paper documents", *Applied Surface Science*, vol. 253, no. 19, pp. 7860-7864, 2007.

[123] D.R. Leal-Ayalal, J.M. Allwood, and T.A.M. Counsell, "Paper un-printing: using lasers to remove toner-print in order to reuse office paper", *Applied Physics A: Material Sciences and Processing*, vol. 105, no. 4, pp. 801-818, 2011.

[124] D.R. Leal-Ayala, J.M. Allwood, M. Schmidt, and I. Alexeev, "Toner-print removal from paper by long and ultrashort pulsed lasers", *Proceedings of the Royal Society A*, vol. 468, no. 2144, pp. 2272-2293, 2012.

[125] P.A.C. Gane, M. Buri, D.C. Spielmann, B. Neuenschwander, H. Scheidiger, and D. Bättig, "Mechanism of post-print laser marking on coated substrates: Factors controlling", *Journal of Graphic Technology*, vol. 1, no. 1, pp. 37-48, 2003.

[126] J. Nie, Y. Zhang, L. Lin, C. Zhou, S. Li, L. Zhang, and J. Li, "Low-Cost Fabrication of Paper-Based Microfluidic Devices by One-Step Plotting," *Analytical Chemistry*, vol. 84, no. 15, p. 6331−6335, 2012.

[127] M. Vaittinen, "Oriented antibody biointerfaces on nanofibrillated cellulose materials", Aalto university, Espoo, Master's thesis 2013.

[128] V.F. Curto, N. Lopez-Ruiz, L.F. Capitan-Vallvey, A.J. Palma, F. Benito-Lopez, and D. Diamond, "Fast prototyping of paper-based microfluidic devices by contact stamping using indelible ink", *RSC Advances*, vol. 3, no. 41, pp. 18811-18816, 2013.

[129] T. Songjaroen, W. Dungchai, O. Chailapakul, and W. Laiwattanapaisal, "Novel, simple and low-cost alternative method for fabrication of paper-based microfluidics by wax dipping", *Talanta*, vol. 85, no. 5, pp. 2587–2593, 2011.

[130] E.M. Fenton, M.R. Mascarenas, G.P. Lopez, and S.S. Sibbett, "Multiplex Lateral-Flow Test Strips Fabricated by Two-Dimensional Shaping", *Applied Materials & Interfaces*, vol. 1, no. 1, pp. 124-129, 2009.

[131] G.T. Barnes and I.R. Gentle, *Interfacial science: an introduction, second edition*. Oxford: Oxford University Press, 2011.

[132] J. Song and O.J. Rojas, "Approaching super-hydrophobicity from cellulosic materials:

a review", *Nordic Pulp & Paper Research Journal*, vol. 28, no. 2, pp. 216-238, 2013.

[133] M.P. Sousa and J.F. Mano, "Superhydrophobic Paper in the Development of Disposable Labware and Lab-on-Paper devices", *Applied Materials & Interfaces*, vol. 5, no. 9, pp. 3731-3737, 2013.

[134] S. Tuomikoski, "Fabrication of SU-8 microstructures for analytical microfluidic applications", Helsinki University of Technology, Espoo, Doctoral dissertation 2007.

[135] K. Punpattanakul, A. Pimpin, and W. Srituravanich, "Fabrication of paper-based lab-on-a-chip by printing SU-8 polymer", in *The Second TSME International Conference on Mechanical Engineering*, Krabi, 2011.

[136] G. Odian, *Principles of Polymerization, 4th edition*. Hoboken: John Wiley & Sons, 2004.

[137] J.A. Semlyen, "Cyclic Siloxane Polymers", in *Siloxane Polymers*, S.J. Clarson and J.A. Semlyen, Eds. Englewood Cliffs: PTR Prentice Hall, 1993, pp. 135-192.

[138] Dow Corning, "Silicones in industrial applications", 2009.

[139] R.A. Pethrick, *Polymer Science and Technology for Engineers and Scientists*. Dunbeath: Whittles Publishing, 2010.

[140] S. Hemmilä, J.V. Cauich-Rodriguez, J. Kreutzer, and P. Kallio, "Rapid, simple, and cost-effective treatments to achieve long-term hydrophilic PDMS surfaces", *Applied Surface Science*, vol. 258, no. 24, pp. 9864-9875, 2012.

[141] D. Zhang, S.M. Dougal, and M.S. Yeganeh, "Effects of UV Irradiation and Plasma Treatment on a Polystyrene Surface Studied by IR-Visible Sum Frequency Generation Spectroscopy", *Langmuir*, vol. 16, no. 10, pp. 4528-4532, 2000.

[142] D. Geuskens, D. Baeyens-Volant, G. Delaunois, Q. Lu-Vinh, W. Piret, and C. David, "A quantitative study of the chemical reactions resulting from irradiation of polystyrene at 253.7 nm in the presence of oxygen", *Europen Polymer Journal*, vol. 14, no. 4, pp. 291-297, 1978.

[143] K. Abe, K. Kotera, K. Suzuki, and D. Citterio, "Inkjet-printed paperfluidic immuno-chemical sensing device", *Analytical and Bioanalytical Chemistry*, vol. 398, no. 2, pp. 885-893, 2010.

[144] de Gans, B., E. Kazancioglu, W. Meyer, and U.S. Schubert, "Ink-jet Printing Polymers and Polymer Libraries Using Micropipettes", *Macromolecular Rapid Communications*, vol. 25, no. 1, pp. 292-296, 2004.

[145] S.D. Hoath, I.M. Hutchings, and G.D. Martin, "Links Between Ink Rheology, Drop-on-Demand Jet Formation, and Printability", *Journal of Imaging Science and Technology*, vol. 53, no. 4, pp. 041208-1-041208-8, 2009.

[146] S. Jung, S.D. Hoath, and I.M. Hutchings, "The role of viscoelasticity in drop impact and spreading for inkjet printing of polymer solution on a wettable surface", *Microfluidics and Naonofluidics*, vol. 14, no. 1-2, pp. 163-169, 2013.

[147] W. Dungchai, O. Chailapakul, and C.S. Henry, "A low-cost, simple and rapid fabrication method for paper-based microfluidics using wax screen-printing", *Analyst*, vol. 136, no. 1, pp. 77-82, 2011.

[148] A. Zhang and Y. Zha, "Fabrication of paper-based microfluidic device using printed circuit technology", *AIP Advances*, vol. 2, no. 2, pp. 022171-1-022171-6, 2012.

[149] E. Carrilho, A.W. Martinez, and G.M. Whitesides, "Understanding Wax Printing: A Simple Micro-patterning process for paper-based microfluidics", *Analytical Chemistry*, vol. 81, no. 16, pp. 7091-7096, 2009.

[150] K. Govindasamy, S. Potgieter, K. Land, and E. Muzenda, "Fabrication of Paper Based Microfluidic Devices", in *Proceedings of the World Congress on Engineering 2012 Vol III*, London, 2012.

[151] Z. Li, L. Hou, W. Zhang, and L. Zhu, "Preparation of paper micro-fluidic devices used in Bio-assay based on drop-on-demand wax droplet generation", *Analytical Methods*, vol. 6, no. 3, pp. 878-885, 2014.

[152] D. Johnson, "Sizing in acid, neutral and alkaline conditions", in *Applications of Wet-end Paper Chemistry*, I. Thorn and C.O. Au, Eds.: Springer, 2009, pp. 139-171.

[153] J. Roberts, *Neutral sizing*. Leatherhead: Pira International, 1992.

[154] T. Lindström and P.T. Larsson, "Alkyl ketene dimer (AKD) sizing - a review", *Nordic Pulp and Paper Research Journal*, vol. 23, no. 2, pp. 202-209, 2008.

[155] T. Lindström, "Sizing", in *Paper Chemistry and Technology*, M. Ek, G. Gellerstedt, and G. Henriksson, Eds. Berlin: de Gruyter, 2009, ch. 14, pp. 275-318.

[156] A. Vesel, M. Mozetic, A. Hladnik, J. Dolenc, J. Zule, S. Milosevic, N. Krstulovic, M. Klanjsek-Gunde, and N. Hauptmann, "Modification of ink-jet paper by oxygen-plasma treatment", *Journal of Physics D: applied physics*, vol. 40, no. 12, pp. 3689-3696, 2007.

[157] X. Li, J. Tian, G. Garnier, and W. Shen, "Fabrication of paper-based microfluidic sensors by printing", *Colloids and Surfaces B: Biointerfaces*, vol. 76, no. 2, pp. 564-570, 2010.

[158] X. Li, J. Tian, and W. Shen, "Quantitative biomarker assay with microfluidic paper-based analytical devices", *Analytical and Bioanalytical Chemistry*, vol. 396, no. 1, pp. 495-501, 2010.

[159] T. Nurak, N. Praphairaksit, and O. Chailapakul, "Fabrication of paper-based devices by lacquer spraying method for the determination of nickel (II) ion in waste water", *Talanta*, vol. 114, pp. 291-296, 2013.

[160] B. Thompson, *Printing Materials Science and Technology, 2nd edition*. Leatherhead: Pira International, 2004.

[161] D. Citterio, K. Maejima, and K. Suzuki, "VOC-free inkjet patterning method for the fabrication of "paperfluidic" sensing devices", in *15th International Conference on Miniaturized Systems for Chemistry and Life Sciences*, Seattle, 2011, pp. 2099-2101.

[162] Q. He, C. Ma, X. Hu, and H. Chen, "Method for Fabrication of Paper-Based

Microfluidic Devices by Alkylsilane Self-Assembling and UV/O3 patterning", *Analytical Chemistry*, vol. 85, no. 3, pp. 1327-1331, 2013.

[163] P.D. Haller, C.A. Flowers, and M. Gupta, "Three-dimensional patterning of porous materials using vapor phase polymerization", *Soft Matter*, vol. 7, no. 6, pp. 2428-2432, 2011.

[164] P. Kwong and M. Gupta, "Vapor Phase Deposition of Functional Polymers onto Paper-Based Microfluidic Devices for Advanced Unit Operations", *Analytical Chemistry*, vol. 84, no. 22, pp. 10129-10135, 2012.

[165] W.W. Yu and I.M. White, "Inkjet Printed Surface Enhanced Raman Spectroscopy Array on Cellulose Paper", *Analytical Chemistry*, vol. 82, no. 23, pp. 9626-9630, 2010.

[166] M.P. Sousa and J.F. Mano, "Patterned superhydrophobic paper for microfluidic devices obtained by writing and printing", *Cellulose*, vol. 20, no. 5, pp. 2185-2190, 2013.

[167] S.H. Maron and J.B. Lando, *Fundamentals of Physical Chemistry*. New York: Macmillan publishing co, 1974.

[168] A. Marmur, "Kinetics of Penetration into Uniform Porous Media: Testing the Equivalent-Capillary Concept", *Langmuir*, vol. 19, no. 14, pp. 5956-5959, 2003.

[169] R.N. Wenzel, "Resistance of Solid Surfaces to Wetting by Water", *Industrial and Engineering Chemistry*, vol. 28, no. 8, pp. 988-994, 1936.

[170] A. Marmur, "Hydro- hygro- oleo- omni-phobic? Terminology of wettability classification", *Soft Matter*, vol. 8, no. 26, pp. 6867-6870, 2012.

[171] A.B.D. Cassie, "Contact Angles", *Discussions of the Faraday Society*, vol. 3, no. 1, pp. 11-16, 1948.

[172] C.J. Ridgway, P.A.C. Gane, and J. Schoelkopf, "Effect of capillary element aspect ratio on the dynamic imbibition with porous networks", *Journal of Colloid and*

Interface Science, vol. 252, no. 2, pp. 373-382, 2002.

[173] H.V. Tafreshi and T.M. Bucher, "Modeling Fluid Absorption in Anisotropic Fibrous Porous Media", in *Wicking in Porous Materials*, R. Masoodi and K.M. Pillai, Eds. Boca Raton: CRC Press, 2013, ch. 6, pp. 131-159.

[174] K.M. Pillai and K. Hooman, "An Introduction to Modeling Flows in Porous Media", in *Wicking in Porous Materials*, R. Masoodi and K.M. Pillai, Eds. Boca Ration: CRC Press, 2013, ch. 4, pp. 55-95.

[175] M. Leskelä and S. Simula, "Transport phenomena", in *Paper Physics*, K. Niskanen, Ed. Helsinki: Fapet Oy, 1998, pp. 284-317.

[176] R. Masoodi and K.M. Pillai, "Traditional Theories of Wicking: Capillary Models", in *Wicking in Porous Materials*. Boca Raton: CRC Press, 2013, p. 368.

[177] P. Salminen, "Studies of water transport in paper during short contact times", Åbo Akademi, Turku, Doctoral dissertation 1988.

[178] W.D. Carrier, "Goodbye, Hazen; Hello, Kozeny-Carman", *Journal of Geotechnical and Geoenvironmental Engineering*, vol. 129, no. 11, pp. 1054-1056, 2003.

[179] R. Masoodi and K.M. Pillai, "Introduction to Wicking in Porous Media", in *Wicking in Porous Materials*, R. Masoodi and K.M. Pillai, Eds. Boca Raton: CRC Press, 2013, ch. 1, pp. 1-12.

[180] E.W. Washburn, "The dynamics of capillary flow", *The Physical Review*, vol. 17, no. 3, pp. 273-283, 1921.

[181] M. Stange, M.E. Dreyer, and H.J. Rath, "Capillary driven flow in circular cylindrical tubes", *Physics of Fluids*, vol. 15, no. 9, pp. 2587-2601, 2003.

[182] A. Marmur and R.D. Cohen, "Characterization of Porous Media by the Kinetics of Liquid Penetration: The Vertical Capillaries Model", *Journal of Colloid and Interface Science*, vol. 189, no. 2, pp. 299-304, 1997.

[183] C.H. Bosanquet, "On the flow of liquids into capillary tubes", *The London, Edinburgh and Dublin Philosophical Magazine and Journal of Science*, vol. 45, no. 267, pp. 525-531, 1923.

[184] J. Schoelkopf, P.A.C. Gane, and C.J. Ridgway, "Influence of Inertia on Liquid Absorption into Paper Coating Structures", *Nordic Pulp and Paper research Journal*, vol. 15, no. 5, pp. 422-430, 2000.

[185] D. Ma, R.D. Carter, J. Laine, and P. Stenius, "Gibbs energy analysis of ink oil imbibition during ink setting", *Nordic Pulp and Paper Research Journal*, vol. 22, no. 4, pp. 523-528, 2007.

[186] V. Joekar-Niasar and S.M. Hassanizadeh, "Pore-Network Modeling of Wicking: a Two-Phase Flow Approach", in *Wicking in Porous Materials*, R. Masoodi and K.M. Pillai, Eds. Boca Raton: CRC Press, 2013, ch. 9, pp. 237-262.

[187] J. Schoelkopf, P.A.C. Gane, C.J. Ridgway, and G.P. Matthews, "Practical observation of deviation from Lucas–Washburn scaling in porous media", *Colloids and Surfaces A: Physicochemical and Engineering Aspects*, vol. 206, no. 1-3, pp. 445-454, 2002.

[188] R.J. Roberts, T.J. Senden, M.A. Knackstedt, and M.B. Lyne, "Spreading of Aqueous Liquids in Unsized Papers is by Film Flow", *Journal of Pulp and Paper Science*, vol. 29, no. 4, pp. 123-131, 2003.

[189] E. Fu, S.A. Ramsey, P. Kauffman, B. Lutz, and P. Yager, "Transport in two-dimensional paper networks", *Microfluidics and nanofluidics*, vol. 10, no. 1, pp. 29-35, 2011.

[190] P. Kauffman, E. Fu, B. Lutz, and P. Yager, "Visualisation and measurement of flow in two-dimensional paper networks", *Lab on a Chip*, vol. 10, no. 19, pp. 2614-2517, 2010.

[191] H. Hwang, S. Kim, T. Kim, J. Park, and Y. Cho, "Paper on a disc: balancing the capillary-driven flow with a centrifugal force", *Lab on a Chip*, vol. 11, no. 20, pp. 3404-3406, 2011.

[192] N. Godino, E. Comaskey, R. Gorkin, and J. Ducree, "Centrifugally enhanced paper microfluidics", in *IEEE 25th International Conference on Micro Electro Mechanical Systems (MEMS)*, Paris, 2012, pp. 1017-1020.

[193] E. Vereshchagina, K. Bourke, L. Meehan, C. Dixit, D. McClade, and J. Ducree, "Multi-material paper-disc devices for low cost biomedical diagnostics", in *IEEE 26th International Conference on Micro Electro Mechanical Systems (MEMS)*, Taipei, 2013, pp. 1049-1052.

[194] P. Mandal, R. Dey, and S. Chakraborty, "Electrokinetics with ‘‘paper-and-pencil’’ devices", *Lab on a Chip*, vol. 12, no. 20, pp. 4026-4028, 2012.

[195] A.R. Rezg, A. Qi, J.R. Friend, W.H. Li, and L.Y. Yeo, "Uniform mixing in paper-based microfluidic systems using surface acoustic waves", *Lab on a Chip*, vol. 12, no. 4, pp. 773-779, 2012.

[196] S. Veran-Tissoires, S. Geoffroy, M. Marcoux, and M. Prat, "Evaporation and Wicking", in *Wicking in Porous Materials*, R. Masoodi and K.M. Pillai, Eds. Boca Raton: CRC Press, 2013, ch. 8, pp. 201-236.

[197] N. Fries, K. Odic, M. Conrath, and M. Dreyer, "The effect of evaporation on the wicking of liquids into a metallic weave", *Journal of Colloid and Interface Science*, vol. 321, no. 1, pp. 118-129, 2008.

[198] D.A. Barry, J.-Y. Parlange, D.A. Lockington, and L. Wissmeier, "Comment on “The effect of evaporation on the wicking of liquids into a metallic weave” by N. Fries, K. Odic, M. Conrath and M. Dreyer", *Journal of Colloid and Interface Science*, vol. 336, no. 1, pp. 374-375, 2009.

[199] S. Jahanshahi-Anbuhi, P. Chavan, C. Sicard, V. Leung, S.M.Z. Hossain, R. Pelton, J.D. Brennan, and C.M.D. Filipe, "Creating fast flow channels in paper fluidic devices to control timing of sequential reactions", *Lab on a Chip*, vol. 12, no. 23, pp. 5079-5085, 2012.

[200] CRC Press, *CRC Handbook of Chemistry and Physics*, 71st ed., D.R. Lide, Ed. Boca

Raton: CRC Press, 1990.

[201] G. Langenbacher and M. Bernzen, Modular compact rheometer MCR 300 operating instruction, 2000, Technical manual.

[202] KSV Instruments, *Operation Manual CAM Revision 1.2*. Helsinki: KSV Instruments.

[203] Fujifilm Dimatix, *Fujifilm Dimatix Materials Printer DMP-2800 Series User Manual*. Santa Clara: Fujifilm Dimatix, 2010.

[204] Seiko Epson Corporation, *Epson Expression 1680 User's Guide.* Nagano: Seiko Epson Corporation, 2000.

[205] W.S. Rasband. (1997-2014) ImageJ. [Online]. http://imagej.nih.gov/ij/

[206] Fujifilm Dimatix, "Drop Formation Tuning and Fluid Characteristics", Fujifilm Dimatix, Santa Clara, Application note 2006.

[207] A. Bristow, "The Surface of Paper", in *Paper Products Physics and Technology*, M. Ek, G. Gellerstedt, and G. Henriksson, Eds. Berlin: de Gruyter, 2009, ch. 8, pp. 209-232.

[208] S.H. Lee, "Shear Viscosity of Benzene, Toluene, and p-Xylene by Non-equilibrium Molecular Dynamics Simulations", *Bulletin of the Korean Chemical Society*, vol. 25, no. 2, pp. 321-324, 2004.

[209] E. Evans, E.F.M. Gabriel, W.K.T. Coltro, and C.D. Garcia, "Rational selection of substrates to improve color intensity and uniformity on microfluidic paper-based analytical devices", *Analyst (advance article)*, 2014.

[210] R. Seppänen, "On the internal sizing mechanisms of paper with AKD and ASA related to surface chemistry, wettability and friction", Kungliga Tekniska Högskolan, Stockholm, Doctoral dissertation 2007.

Appendix 1

Jetting waveforms

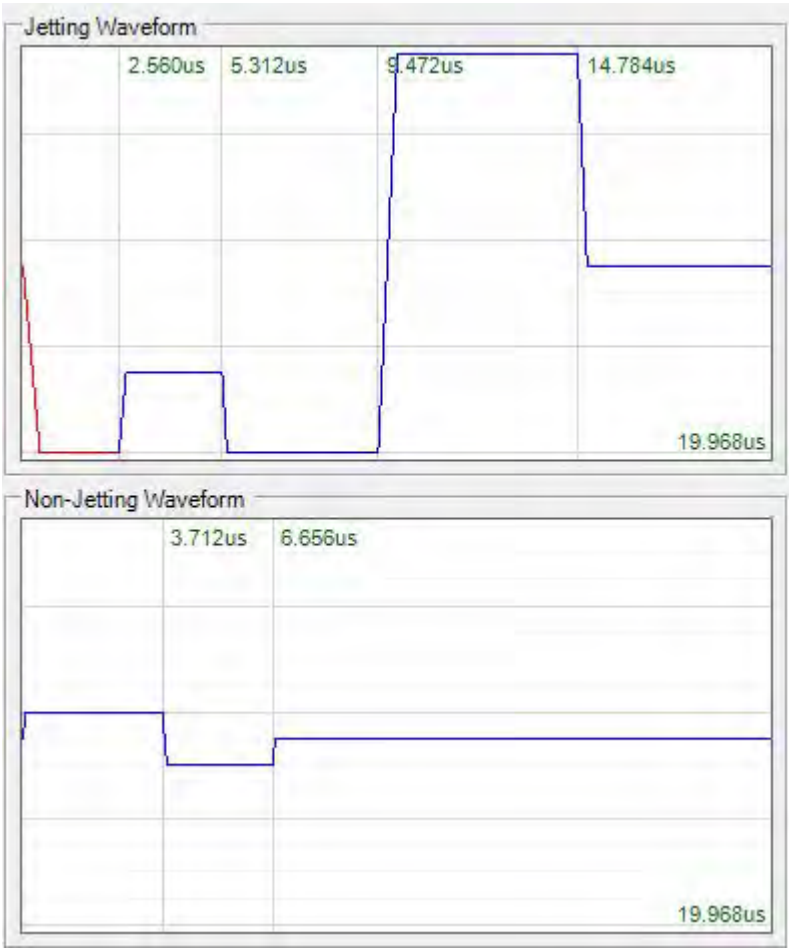

Figure 39. *Low-Viscosity waveform: x-axis represents time, y-axis represents relative intensity of the jetting pulse.*

Figure 40. *Dimatix Model Fluid waveform: x and y-axes as in Figure 39.*

Figure 41. *Hi-Viscosity Short Polymer waveform: x and y-axes as in Figure 39.*

Appendix 2

Viscosity as a function of shear rate

Table 7. Mean μ and standard deviation σ for ink viscosity as a function of shear rate.

Shear rate [s^{-1}]	Viscosity [mPa·s]							
	Paraffin ink		AKD ink		AKD-PS ink		PS ink	
	μ	σ	μ	σ	μ	σ	μ	σ
100	0.622	0.008	0.696	0.013	0.960	0.020	1.353	0.021
150	0.707	0.015	0.764	0.036	1.004	0.033	1.380	0.010
200	0.786	0.013	0.847	0.032	1.067	0.035	1.420	0.017
250	0.864	0.016	0.927	0.038	1.143	0.031	1.473	0.021
300	0.957	0.025	1.019	0.057	1.227	0.040	1.540	0.010
350	1.033	0.029	1.100	0.062	1.320	0.040	1.623	0.021
400	1.117	0.015	1.190	0.053	1.393	0.040	1.700	0.010
450	1.183	0.021	1.263	0.059	1.487	0.045	1.793	0.021
500	1.257	0.015	1.340	0.062	1.563	0.050	1.877	0.015
550	1.320	0.010	1.410	0.061	1.643	0.050	1.967	0.021
600	1.390	0.026	1.483	0.078	1.743	0.055	2.060	0.010
650	1.440	0.026	1.543	0.076	1.817	0.055	2.140	0.020
700	1.493	0.021	1.600	0.070	1.890	0.056	2.227	0.025
750	1.540	0.026	1.657	0.072	1.970	0.056	2.313	0.031
800	1.593	0.021	1.710	0.078	2.033	0.060	2.390	0.030
850	1.643	0.029	1.763	0.085	2.107	0.065	2.467	0.025
900	1.690	0.026	1.813	0.085	2.167	0.065	2.540	0.020
950	1.727	0.032	1.860	0.087	2.233	0.070	2.623	0.031
1 000	1.820	0.061	1.903	0.093	2.293	0.070	2.693	0.031

Appendix 3

Ink velocity

Table 8. Ink velocity as a function of drive voltage using *Hi-Viscosity Short Polymer* waveform. N/A indicates either too low velocity or unstable jetting.

Drive voltage [V]	Velocity [ms^{-1}]				
	p-Xylene (2 kHz)	**Paraffin ink (2 kHz)**	**AKD ink (2 kHz)**	**AKD-PS ink (6 kHz)**	**PS ink (6 kHz)**
10	N/A	3.2	N/A	N/A	N/A
11	N/A	3.9	N/A	N/A	N/A
12	3.0	5.0	N/A	4.8	N/A
13	3.5	5.8	5.9	5.6	N/A
14	4.3	6.5	6.4	7.0	N/A
15	4.6	6.4	6.8	7.7	N/A
16	5.2	6.5	7.2	9.0	N/A
17	6.0	6.9	7.6	9.2	N/A
18	7.1	5.0	7.6	9.7	3.1
19	8.0	4.8	8.0	10.5	3.7
20	7.6	4.6	6.8	11.1	4.4
21	7.1	6.5	6.6	11.9	5.0
22	7.7	6.5	6.5	12.0	5.6
23	6.7	5.9	6.2	12.0	6.2
24	6.6	4.9	5.3	13.0	6.9
25	6.8	4.5	5.0	13.0	7.5
26	6.8	4.4	5.0	13.9	8.1
27	7.7	4.3	4.5	15.6	8.7
28	7.5	4.3	4.6	16.6	9.3
29	7.5	4.3	4.6	17.2	9.7
30	7.7	4.2	4.6	18.2	10.4
31	N/A	4.2	4.6	N/A	11.0
32	N/A	4.4	4.6	N/A	11.5
33	N/A	4.4	4.6	N/A	12.0
34	N/A	4.4	4.4	N/A	12.5
35	N/A	4.2	4.4	N/A	13.1
36	N/A	4.2	4.3	N/A	13.7
37	N/A	4.0	4.1	N/A	14.1
38	N/A	3.9	N/A	N/A	14.7
39	N/A	3.6	N/A	N/A	15.2
40	N/A	3.9	N/A	N/A	15.6

Appendix 4

Contact angles

Table 9. Mean μ and standard deviation σ for contact angle as function of drop spacing, for polystyrene ink printed on Whatman 4 filter paper.

Drop spacing [μm]	Printed side contact angle [°]		Reverse side contact angle [°]	
	μ	σ	μ	σ
10	114.1	3.7	107.0	11.0
15	112.8	5.2	107.6	5.9
20	104.3	7.5	61.1	31.7
25	92.4	31.2	~ 0	~ 0

Appendix 5

Line spreading

Table 10. Mean μ and standard deviation σ for measured line width for AKD ink printed lines as a function of nominal width and drop spacing (DS) on Whatman 1 filter paper on printed side.

Nominal width [μm]	Measured line width [μm]							
	20 μm DS		30 μm DS		40 μm DS		50 μm DS	
	μ	σ	μ	σ	μ	σ	μ	σ
100	965	122	459	33	N/A	N/A	N/A	N/A
200	1 284	107	914	49	571	38	N/A	N/A
300	1 546	174	1 140	73	884	43	519	72
400	1 573	147	1 237	96	981	114	694	93
500	1 884	225	1 398	115	1 171	118	885	53
600	2 047	181	1 378	199	1 317	97	1 065	57
700	2 153	198	1 681	134	1 460	59	1 180	58
800	2 367	228	1 699	58	1 527	51	1 329	62
900	2 392	239	1 747	62	1 605	108	1 361	54
1 000	2 491	274	1 834	65	1 742	102	1 527	91

Table 11. Mean μ and standard deviation σ for measured line width for AKD ink printed lines as a function of nominal width and drop spacing (DS) on Whatman 1 filter paper on reverse side.

Nominal width [μm]	Measured line width [μm]							
	20 μm DS		30 μm DS		40 μm DS		50 μm DS	
	μ	σ	μ	σ	μ	σ	μ	σ
100	920	136	N/A	N/A	N/A	N/A	N/A	N/A
200	1 279	96	837	85	N/A	N/A	N/A	N/A
300	1 491	156	1 051	112	805	96	N/A	N/A
400	1 523	154	1 134	127	931	99	554	80
500	1 769	192	1 257	132	1 133	106	772	61
600	1 946	162	1 290	237	1 276	143	966	73
700	2 125	220	1 562	120	1 397	98	1 096	51
800	2 282	264	1 604	112	1 475	66	1 229	63
900	2 310	252	1 647	81	1 543	99	1 284	81
1 000	2 400	253	1 682	156	1 625	80	1 440	80

Table 12. Mean μ and standard deviation σ for measured line width for AKD-PS ink printed lines as a function of nominal width and drop spacing (DS) on Whatman 1 filter paper on printed side.

Nominal width [μm]	**Measured line width [μm]**							
	20 μm DS		**30 μm DS**		**40 μm DS**		**50 μm DS**	
	μ	**σ**	**μ**	**σ**	**μ**	**σ**	**μ**	**σ**
100	986	112	384	222	N/A	N/A	N/A	N/A
200	1 263	91	954	134	474	65	N/A	N/A
300	1 453	81	1 057	144	762	128	529	52
400	1 635	81	1 283	150	932	66	742	155
500	1 797	76	1 289	75	1 151	75	955	72
600	1 971	103	1 466	123	1 290	66	1 142	64
700	2 088	85	1 625	193	1 395	81	1 233	59
800	2 219	113	1 666	219	1 490	84	1 299	29
900	2 325	128	1 830	307	1 571	62	1 381	34
1 000	2 413	131	1 874	229	1 696	58	1 569	43

Table 13. Mean μ and standard deviation σ for measured line width for AKD-PS ink printed lines as a function of nominal width and drop spacing (DS) on Whatman 1 filter paper on reverse side.

Nominal width [μm]	**Measured line width [μm]**							
	20 μm DS		**30 μm DS**		**40 μm DS**		**50 μm DS**	
	μ	**σ**	**μ**	**σ**	**μ**	**σ**	**μ**	**σ**
100	987	76	N/A	N/A	N/A	N/A	N/A	N/A
200	1 261	86	865	143	N/A	N/A	N/A	N/A
300	1 447	76	979	179	599	111	N/A	N/A
400	1 613	44	1 248	138	829	76	N/A	N/A
500	1 738	77	1 278	82	1 101	115	782	131
600	1 933	110	1 422	123	1 256	58	1 006	65
700	2 082	64	1 617	161	1 377	97	1 129	55
800	2 197	88	1 617	170	1 452	48	1 211	65
900	2 315	73	1 743	275	1 516	46	1 291	128
1 000	2 404	70	1 826	230	1 664	58	1 433	84

Table 14. Mean μ and standard σ deviation for measured line width for AKD ink printed lines as a function of nominal width and drop spacing (DS) on Whatman 4 filter paper on printed side.

Nominal width [μm]	**Measured line width [μm]**							
	20 μm DS		**30 μm DS**		**40 μm DS**		**50 μm DS**	
	μ	**σ**	**μ**	**σ**	**μ**	**σ**	**μ**	**σ**
100	1 013	96	N/A	N/A	N/A	N/A	N/A	N/A
200	1 290	213	860	43	510	44	N/A	N/A
300	1 573	227	1 167	88	771	118	N/A	N/A
400	1 724	294	1 300	122	872	187	651	52
500	1 914	218	1 500	187	1 083	195	838	112
600	2 082	175	1 583	148	1 175	139	987	86
700	2 267	223	1 769	172	1 285	182	1 152	48
800	2 358	194	1 799	139	1 419	159	1 269	38
900	2 439	193	1 879	146	1 546	141	1 356	56
1 000	2 532	92	1 945	201	1 668	85	1 490	78

Table 15. Mean μ and standard deviation σ for measured line width for AKD ink printed lines as a function of nominal width and drop spacing (DS) on Whatman 4 filter paper on reverse side.

Nominal width [μm]	**Measured line width [μm]**							
	20 μm DS		**30 μm DS**		**40 μm DS**		**50 μm DS**	
	μ	**σ**	**μ**	**σ**	**μ**	**σ**	**μ**	**σ**
100	962	139	N/A	N/A	N/A	N/A	N/A	N/A
200	1 288	173	770	81	N/A	N/A	N/A	N/A
300	1 528	223	1 091	91	677	172	N/A	N/A
400	1 689	211	1 251	44	889	41	N/A	N/A
500	1 841	174	1 384	75	931	204	587	182
600	2 024	148	1 488	44	1 080	162	788	110
700	2 140	142	1 659	184	1 151	182	906	38
800	2 321	176	1 719	93	1 335	137	1 066	49
900	2 400	199	1 800	117	1 462	173	1 191	34
1 000	2 517	120	1 827	174	1 556	141	1 332	50

Table 16. Mean μ and standard deviation σ for measured line width for AKD-PS ink printed lines as a function of nominal width and drop spacing (DS) on Whatman 4 filter paper on printed side.

Nominal width [μm]	**Measured line width [μm]**							
	20 μm DS		**30 μm DS**		**40 μm DS**		**50 μm DS**	
	μ	**σ**	**μ**	**σ**	**μ**	**σ**	**μ**	**σ**
100	765	261	N/A	N/A	N/A	N/A	N/A	N/A
200	1 107	302	1 045	122	595	19	N/A	N/A
300	1 300	333	1 173	157	1 016	51	588	107
400	1 428	295	1 289	70	1 019	65	822	53
500	1 651	240	1 445	51	1 129	59	900	44
600	1 817	247	1 539	104	1 293	116	1 127	37
700	2 079	200	1 656	67	1 374	33	1 249	81
800	2 195	201	1 710	69	1 475	37	1 327	90
900	2 264	213	1 870	43	1 583	81	1 418	118
1 000	2 371	181	1 971	127	1 718	77	1 613	117

Table 17. Mean μ and standard deviation σ for measured line width for AKD-PS ink printed lines as a function of nominal width and drop spacing (DS) on Whatman 4 filter paper on reverse side.

Nominal width [μm]	**Measured line width [μm]**							
	20 μm DS		**30 μm DS**		**40 μm DS**		**50 μm DS**	
	μ	**σ**	**μ**	**σ**	**μ**	**σ**	**μ**	**σ**
100	N/A	N/A	N/A	N/A	N/A	N/A	N/A	N/A
200	1 054	391	891	86	N/A	N/A	N/A	N/A
300	1 259	365	1 022	157	939	89	N/A	N/A
400	1 421	377	1 193	69	1 024	104	N/A	N/A
500	1 533	399	1 329	71	1 079	98	802	107
600	1 657	324	1 474	74	1 201	56	1 019	130
700	1 833	285	1 560	37	1 348	51	1 172	169
800	1 928	297	1 621	69	1 455	61	1 221	173
900	1 987	327	1 779	60	1 537	91	1 355	212
1 000	2 149	330	1 850	35	1 665	94	1 526	173

Table 18. Mean μ and standard deviation σ for measured line width for PS ink printed lines as a function of nominal width and drop spacing (DS) on Whatman 4 filter paper on printed side.

Nominal width [μm]	Measured line width [μm]			
	10 μm DS		15 μm DS	
	μ	σ	μ	σ
100	568	36	N/A	N/A
200	953	35	N/A	N/A
300	1 252	75	800	104
400	1 554	75	1 004	64
500	1 872	70	1 097	58
600	2 072	97	1 280	82
700	2 146	123	1 455	94
800	2 535	98	1 531	97
900	2 883	153	1 677	103
1 000	2 880	123	1 686	85

Table 19. Mean μ and standard deviation σ for measured line width for PS ink printed lines as a function of nominal width and drop spacing (DS) on Whatman 4 filter paper on reverse side.

Nominal width [μm]	Measured line width [μm]			
	10 μm DS		15 μm DS	
	μ	σ	μ	σ
100	N/A	N/A	N/A	N/A
200	920	32	N/A	N/A
300	1 301	147	N/A	N/A
400	1 712	110	N/A	N/A
500	2 040	104	833	152
600	2 270	102	1 157	68
700	2 375	108	1 367	90
800	2 708	123	1 521	66
900	3 079	95	1 687	71
1 000	3 163	122	1 680	67

Appendix 6

Barrier penetration as a function of time

Table 20. Number of barriers penetrated as a function of time on Whatman 1 filter paper. Maximum value possible is 100.

Substrate	Ink	Drop spacing [µm]	Barriers penetrated over time					
			5 min	10 min	15 min	20 min	25 min	30 min
Whatman 1	AKD	15	0	0	0	0	0	0
Whatman 1	AKD	20	0	0	0	0	0	0
Whatman 1	AKD	25	0	0	0	0	0	0
Whatman 1	AKD	30	0	0	0	0	0	0
Whatman 1	AKD	35	11	12	12	12	12	12
Whatman 1	AKD	40	9	12	12	12	12	12
Whatman 1	AKD	45	17	17	19	20	22	22
Whatman 1	AKD	50	30	32	34	34	34	34
Whatman 1	AKD-PS	15	0	0	0	0	0	0
Whatman 1	AKD-PS	20	0	1	1	1	1	1
Whatman 1	AKD-PS	25	0	0	1	1	1	1
Whatman 1	AKD-PS	30	18	18	18	18	18	18
Whatman 1	AKD-PS	35	13	14	14	14	14	14
Whatman 1	AKD-PS	40	19	19	19	19	19	19
Whatman 1	AKD-PS	45	40	40	41	42	42	43
Whatman 1	AKD-PS	50	32	35	35	37	38	38
Whatman 1	PS	10	31	35	39	44	46	47
Whatman 1	PS	15	49	61	73	82	83	87
Whatman 1	PS	20	100	100	100	100	100	100
Whatman 1	PS	25	100	100	100	100	100	100

Table 21. Number of barriers penetrated as a function of time on Whatman 4 filter paper. Maximum value possible is 100.

Substrate	Ink	Drop spacing [µm]	Barriers penetrated over time					
			5 min	10 min	15 min	20 min	25 min	30 min
Whatman 4	AKD	15	0	0	0	0	0	0
Whatman 4	AKD	20	0	0	0	0	0	0
Whatman 4	AKD	25	0	0	0	0	0	0
Whatman 4	AKD	30	0	0	0	0	0	0
Whatman 4	AKD	35	11	12	12	12	12	12
Whatman 4	AKD	40	11	12	12	13	15	16
Whatman 4	AKD	45	15	15	16	19	20	20
Whatman 4	AKD	50	34	38	40	42	42	42
Whatman 4	AKD-PS	15	0	0	0	0	0	0
Whatman 4	AKD-PS	20	0	0	0	0	0	0
Whatman 4	AKD-PS	25	2	3	3	3	3	4
Whatman 4	AKD-PS	30	29	33	34	35	36	36
Whatman 4	AKD-PS	35	22	22	23	23	23	23
Whatman 4	AKD-PS	40	23	24	24	24	25	25
Whatman 4	AKD-PS	45	38	40	40	40	40	40
Whatman 4	AKD-PS	50	58	58	58	58	58	59
Whatman 4	PS	10	12	12	14	16	16	16
Whatman 4	PS	15	16	19	19	20	22	22
Whatman 4	PS	20	90	97	98	98	98	99
Whatman 4	PS	25	100	100	100	100	100	100

Appendix 7

Barrier width

Table 22. Mean μ and standard deviation σ of measured barrier width for the narrowest reliable barrier printed with AKD and AKD-PS inks. N/A indicates that the barrier width could not be reliably measured.

Drop spacing [μm]	Barrier width [μm]							
	AKD ink (Whatman 1)		AKD ink (Whatman 4)		AKD-PS ink (Whatman 1)		AKD-PS ink (Whatman 4)	
	μ	σ	μ	σ	μ	σ	μ	σ
15	N/A	N/A	N/A	N/A	668	107	N/A	N/A
20	N/A	N/A	N/A	N/A	663	93	603	140
25	697	149	N/A	N/A	621	65	491	157
30	457	75	N/A	N/A	641	108	571	97
35	529	130	666	115	593	106	525	90
40	706	41	932	301	474	56	739	147
45	536	38	834	206	695	87	624	73

Appendix 8

Pore volume to ink volume ratios

The following Tables list ratios between hydrophobised pore volumes and used ink volumes, as described previously in section 14.1. N/A (not applicable) indicates that hydrophobised pore volume could not be calculated for given settings, due to lack of continuous line on the reverse side.

Table 23. Mean μ and standard deviation σ of V_p/V_i for AKD ink printed lines as a function of nominal width and drop spacing (DS) on Whatman 1 filter paper.

Nominal width [μm]	**V_p/V_i**							
	20 μm DS		**30 μm DS**		**40 μm DS**		**50 μm DS**	
	μ	**σ**	**μ**	**σ**	**μ**	**σ**	**μ**	**σ**
100	46.2	6.0	N/A	N/A	N/A	N/A	N/A	N/A
200	31.4	2.3	48.7	3.0	N/A	N/A	N/A	N/A
300	24.8	2.6	40.6	3.2	57.4	4.5	N/A	N/A
400	18.9	1.8	33.0	3.1	48.8	5.4	47.7	5.0
500	17.9	2.0	29.5	2.6	47.0	4.5	50.7	2.9
600	16.3	1.3	24.7	4.0	44.1	4.0	51.8	2.5
700	15.0	1.5	25.8	1,5	41.6	2.3	49.8	1.6
800	14.2	1.5	23.0	1.1	38.3	1.4	48.9	1.3
900	12.8	1.3	21.0	0.9	35.7	2.3	45.0	1.7
1 000	12.0	1.3	19.6	1.2	34.3	1.8	45.4	2.1

Table 24. Mean μ and standard deviation σ of V_p/V_i for AKD-PS ink printed lines as a function of nominal width and drop spacing (DS) on Whatman 1 filter paper.

Nominal width [μm]	***V*p/*V*i**							
	20 μm DS		**30 μm DS**		**40 μm DS**		**50 μm DS**	
	μ	**σ**	**μ**	**σ**	**μ**	**σ**	**μ**	**σ**
100	48.3	3.6	N/A	N/A	N/A	N/A	N/A	N/A
200	30.9	1.8	50.6	7.5	N/A	N/A	N/A	N/A
300	23.7	1.1	37.8	5.9	46.3	8.1	N/A	N/A
400	19.9	0.7	35.2	3.9	44.9	3.2	N/A	N/A
500	17.3	0.7	28.6	1.4	45.9	3.4	53.2	5.7
600	15.9	0.8	26.8	2.1	43.3	1.8	54.8	2.1
700	14.6	0.4	25.8	2.8	40.4	2.4	51.6	2.1
800	13.5	0.6	22.8	2.6	37.5	1.6	48.0	1.3
900	12.6	0.5	22.1	3.5	35.0	1.1	45.4	2.6
1 000	11.8	0.5	20.6	2.5	34.3	1.1	45.9	1.5

Table 25. Mean μ and standard deviation σ of V_p/V_i for AKD ink printed lines as a function of nominal width and drop spacing (DS) on Whatman 4 filter paper.

Nominal width [μm]	***Vp/Vi***							
	20 μm DS		**30 μm DS**		**40 μm DS**		**50 μm DS**	
	μ	**σ**	**μ**	**σ**	**μ**	**σ**	**μ**	**σ**
100	56.7	6.6	N/A	N/A	N/A	N/A	N/A	N/A
200	37.0	5.3	53.2	3.4	N/A	N/A	N/A	N/A
300	29.7	4.2	49.1	3.9	57.7	11.5	N/A	N/A
400	24.5	3.6	41.6	2.7	52.7	17.5	N/A	N/A
500	21.6	2.2	37.6	3.0	48.1	9.5	51.1	9.7
600	19.6	1.5	33.4	2.0	44.9	5.9	53.1	5.1
700	18.1	1.5	31.9	3.3	41.6	6.2	52.7	1.8
800	16.8	1.3	28.7	1.9	41.2	4.4	52.3	1.5
900	15.4	1.2	26.7	1.9	40.0	4.1	50.8	1.1
1 000	14.5	0.6	24.6	2.4	38.6	2.5	50.6	1.6

Table 26. Mean μ and standard deviation σ of V_p/V_i for AKD-PS ink printed lines as a function of nominal width and drop spacing (DS) on Whatman 4 filter paper.

Nominal width [μm]	***Vp/Vi***							
	20 μm DS		**30 μm DS**		**40 μm DS**		**50 μm DS**	
	μ	**σ**	**μ**	**σ**	**μ**	**σ**	**μ**	**σ**
100	N/A	N/A	N/A	N/A	N/A	N/A	N/A	N/A
200	31.0	9.9	63.1	5.9	N/A	N/A	N/A	N/A
300	24.5	6.6	47.7	6.5	78.0	5.1	N/A	N/A
400	20.4	4.8	40.5	2.1	61.1	3.7	N/A	N/A
500	18.3	3.5	36.2	1.0	52.8	3.5	61.0	4.6
600	16.6	2.5	32.7	1.7	49.7	3.0	64.2	4.9
700	16.0	1.5	30.0	0.9	46.5	1.3	62.0	6.2
800	14.8	1.3	27.2	1.0	43.8	1.2	57.1	5.7
900	13.6	1.5	26.4	0.5	41.5	2.1	55.3	6.4
1 000	13.0	1.3	24.9	1.0	40.5	2.0	56.3	5.0

Table 27. Mean μ and standard deviation σ of V_p/V_i for PS ink printed lines as a function of nominal width and drop spacing on Whatman 4 filter paper.

Nominal width [μm]	***Vp/Vi***			
	10 μm DS		**15 μm DS**	
	μ	**σ**	**μ**	**σ**
100	N/A	N/A	N/A	N/A
200	6.72	0.13	N/A	N/A
300	6.11	0.49	N/A	N/A
400	5.86	0.32	N/A	N/A
500	5.61	0.24	6.30	0.67
600	5.19	0.23	6.62	0.37
700	4.63	0.23	6.57	0.41
800	4.70	0.18	6.22	0.30
900	4.75	0.19	6.10	0.30
1 000	4.34	0.17	5.49	0.23